

A STUDY OF VEHICLE PROPERTIES THAT INFLUENCE ROLLOVER
AND THEIR EFFECT ON ELECTRONIC STABILITY CONTROLLERS

Except where reference is made to the work of others, the work described in this thesis is my own or was done in collaboration with my advisory committee. This thesis does not include proprietary or classified information.

Kenneth D. Lambert

Certificate of Approval:

George T. Flowers
Alumni Professor
Mechanical Engineering

David M. Bevly, Chair
Associate Professor
Mechanical Engineering

David Beale
Professor
Mechanical Engineering

Joe F. Pittman
Interim Dean
Graduate School

A STUDY OF VEHICLE PROPERTIES THAT INFLUENCE ROLLOVER
AND THEIR EFFECT ON ELECTRONIC STABILITY CONTROLLERS

Kenneth D. Lambert

A Thesis
Submitted to
the Graduate Faculty of
Auburn University
in Partial Fulfillment of the
Requirements for the
Degree of
Master of Science

Auburn, Alabama
December 17, 2007

A STUDY OF VEHICLE PROPERTIES THAT INFLUENCE ROLLOVER
AND THEIR EFFECT ON ELECTRONIC STABILITY CONTROLLERS

Kenneth D. Lambert

Permission is granted to Auburn University to make copies of this thesis at its discretion, upon the request of individuals or institutions and at their expense. The author reserves all publication rights.

Signature of Author

Date of Graduation

VITA

Kenneth was born July 19, 1983, the second child of Karen and Jon Lambert and brother to Christopher. Born and raised in Birmingham, Alabama, he attended Cherokee Bend Elementary School, Mountain Brook Junior High School, and Mountain Brook High School, after which, he decided to follow in his brother's footsteps and attend Auburn University, resulting in many wonderful friends, fond memories, and a Bachelor of Science degree in Mechanical Engineering. As an undergraduate, Kenneth learned from his experience designing and building mechanical components for the 2005 Solar Car. After his undergraduate studies were completed, he continued his education by staying at Auburn University and working on his Masters of Science degree in Mechanical Engineering, under Dr. David Bevly in the GPS and Vehicle Dynamics Lab (Gavlab).

THESIS ABSTRACT

A STUDY OF VEHICLE PROPERTIES THAT INFLUENCE ROLLOVER
AND THEIR EFFECT ON ELECTRONIC STABILITY CONTROLLERS

Kenneth D. Lambert

Master of Science, December 17, 2007
(B.S.M.E., Auburn University, 2005)

147 Typed Pages

Directed by David M. Bevly

In this thesis, the vehicle properties that most influence rollover are investigated, and methods to improve stability are examined. Every year, vehicle rollover is the cause of thousands of fatalities on US highways. Electronic Stability Controllers (ESC) have been proven to reduce the incidence of rollover; however, improvement is still possible and necessary. With the development of a detailed vehicle model that includes roll and individual wheel dynamics, research has been done to investigate the properties that most affect rollover. Using these key vehicle properties, equations are developed to estimate the maximum lateral acceleration and velocity allowed before rollover. With a good knowledge of the stability limits, ESC systems are developed in simulation, and testing is done to investigate how these controllers can be optimized to greater ensure stability during evasive maneuvers. Results prove that stability can be improved and that rollover can be averted with correct execution of ESC limits and outputs.

ACKNOWLEDGMENTS

Without the support of family and friends throughout the last few years, this thesis would not have been possible. I must first give thanks to God for all that He has done and will continue to do in my life. I feel as if the journey is just beginning.

I would like to thank my parents for the emotional and monetary support that they have given me over the last 24 years. Without their continuous love and guidance, I would not be the person I am today. I would also like to thank my brother Chris for always being a phone call away when I needed a break from work.

I would like to thank Dr. David M. Bevly, my graduate adviser for challenging me in my undergraduate years and sparking my interest in vehicle dynamics. His motivation has helped me to realize my potential.

I would also like to thank everyone in the GAVLAB for their help with my graduate work, especially all of the guys who I got to share the L-2 office (The Deuce) with. Thanks for letting me be your test driver when one was needed. I now know what 1 g of braking from 80 mph feels like.

Finally, the completion of my Masters degree would have been a daunting task without the love and support of my best friend and soon-to-be wife Chameé. I am forever indebted to her for the sacrifices she has made over the last two and a half years.

Style manual or journal used Journal of Approximation Theory (together with the style known as “aums”). Bibliography follows the IEEE Transactions format.

Computer software used The document preparation package T_EX (specifically L^AT_EX) together with the departmental style-file `aums.sty`.

TABLE OF CONTENTS

LIST OF FIGURES	xi
1 INTRODUCTION	1
1.1 Vehicle Rollover	1
1.2 Motivation	1
1.2.1 Rollover Crash Statistics	2
1.2.2 Rollover Crash Costs	3
1.2.3 Electronic Stability Controllers	3
1.3 Current Efforts for Rollover Safety	4
1.3.1 Static Testing	4
1.4 Unmanned Ground Vehicles and Rollover	6
1.5 Thesis Purpose and Contributions	7
1.6 Thesis Organization	9
2 VEHICLE MODELING	10
2.1 Introduction	10
2.2 Vehicle Coordinates	10
2.3 Angular Dynamics	11
2.4 Bicycle Model	12
2.5 Simple Roll Model	15
2.6 Independent Wheel Model	19
2.7 Tire Properties	21
2.7.1 Tire Forces and Slip Angles	21
2.7.2 Tire Models	24
2.8 Simulation Vehicle	29
2.9 Test Maneuvers	29
2.9.1 Quasi-Static Maneuvers	30
2.9.2 Dynamic Maneuvers	34
2.10 Simulations in MATLAB and CarSim	37
2.11 Conclusions on Vehicle Modeling	39
3 VEHICLE ROLLOVER FACTORS	41
3.1 Introduction	41
3.2 Vehicle Rollover Prediction Formulas	41
3.2.1 Static Stability Factor	41
3.2.2 Static Vehicle Rollover Formula	43
3.2.3 Inclusion of Suspension Effects	47
3.3 Properties That Most Influence Vehicle Rollover Propensity	48

3.3.1	CG Height	49
3.3.2	Track Width	53
3.3.3	Understeer Gradient	57
3.3.4	Suspension Stiffness	67
3.3.5	Friction Coefficients	69
3.4	The Inclusion of Understeer Gradient Into the Prediction of Rollover . . .	71
3.4.1	Simulation Results	71
3.4.2	Empirical Trends	72
3.5	Conclusion	74
4	ELECTRONIC STABILITY CONTROLLER DEVELOPMENT	76
4.1	Introduction	76
4.2	ESC Basics	76
4.3	ESC Types	77
4.4	Stability Threshold	78
4.5	Power Reduction	78
4.6	All-Wheel Braking	80
4.7	Independent Wheel Braking	82
4.7.1	Controller Development	82
4.7.2	Controller Behavior	84
4.8	Active Torque Distribution	87
4.9	Steering Control	88
4.9.1	Steering Control with All-Wheel Braking	89
4.9.2	Independent Wheel Braking with Steering Control	92
4.10	ESC with State Estimation	94
4.11	Conclusion	95
5	SIMULATION RESULTS FOR ESC	96
5.1	Introduction	96
5.2	Simulation Results for Varying Vehicle Properties	97
5.2.1	Varying CG Height	98
5.2.2	Varying Weight Split	101
5.3	Simulation Results for Optimized ESC Limits and Inputs	103
5.3.1	Varying CG Height With Optimized ESC Controllers	104
5.3.2	Varying Weight Split With Optimized ESC Controllers	106
5.4	Conclusions	108
6	CONCLUSIONS	109
6.1	Overall Contributions	109
6.1.1	Parameters That Most Influence Rollover	109
6.1.2	Vehicle Rollover Prediction	109
6.1.3	ESC Development	110
6.1.4	Effect of Varying Vehicle Properties on ESC	110

6.2	Difficulties	111
6.3	Recommendations for Future Work	112
	BIBLIOGRAPHY	114
	APPENDICES	120
A	VEHICLE NOMENCLATURE	121
B	VEHICLE PROPERTIES	122
C	ESC CONTROLLER DESCRIPTION	123
C.1	Stability Threshold Stages	123
C.2	ESC Types and Inputs	124
C.3	Power Reduction	125
C.4	All-Wheel Braking	126
C.5	Independent Wheel Braking	128
C.6	Active Torque Distribution	129
C.7	Steering Modification	130
C.8	Steering Modification with All-Wheel Braking	131
C.9	Independent Wheel Braking with Steering Control	132

LIST OF FIGURES

1.1	Static Stability Factor	4
1.2	Static Stability Factor Curve [52]	5
1.3	The rollover of a UGV at the 2004 DARPA Grand Challenge	8
2.1	Vehicle coordinates defined by the SAE [38]	10
2.2	Diagram used for the derivation of the lateral velocity and lateral acceleration of the bike model	11
2.3	The free body diagram for the Bicycle Model	12
2.4	Roll diagram - static	15
2.5	Roll diagram - with roll	15
2.6	The free body diagram of an unsprung mass for roll equation derivation	16
2.7	The free body diagram of a sprung mass for roll equation derivation	17
2.8	The free body diagram of a tire	20
2.9	Tire curve diagram for maximum lateral forces	22
2.10	Front tire slip angle diagram	22
2.11	The tire friction circle used for defining maximum forces allowed [60]	23
2.12	Tire curve for a typical truck tire - Source: CarSim	25
2.13	Pacejka tire curve diagram for maximum lateral forces	29
2.14	The Constant Radius maneuver of a rigid vehicle performed in MATLAB	31
2.15	The vehicle behavior with a constant steer angle and gradually increasing velocity on an understeer vehicle	32
2.16	The SIS maneuver of a rigid vehicle performed in MATLAB	33

2.17	The J-turn maneuver performed in MATLAB	35
2.18	The steer angle inputs for the Fishhook maneuver, defined by NHTSA . .	36
2.19	The Fishhook maneuver performed in MATLAB	37
2.20	Comparison of the SIS maneuver performed in MATLAB and CarSim . .	39
2.21	Comparison of the fishhook maneuver performed in MATLAB and CarSim	40
3.1	SSF Diagram - without roll	42
3.2	SSF Diagram - with roll	42
3.3	Diagram used for the derivation of the roll formula	44
3.4	Lateral Acceleration during Constant Radius maneuver with changing CG heights	49
3.5	Rollover Velocities during Constant Radius maneuver with changing CG heights	50
3.6	Rollover Velocities during Constant Radius maneuver with changing CG heights and weight transfer	52
3.7	Rollover Velocities during Fishhook maneuver with varying CG heights and suspension effects (MATLAB simulation)	53
3.8	Lateral Acceleration during Constant Radius maneuver with a changing track width	54
3.9	Rollover Velocities during Constant Radius maneuver with a changing track width	55
3.10	Rollover Velocities during Fishhook maneuver with changing TW and suspension effects	57
3.11	High-speed cornering with steer and slip angles	58
3.12	Steer angle variations with lateral acceleration	61
3.13	Example curve of the understeer test using the constant radius method .	62
3.14	Example curve of the understeer test using the constant speed method . .	63

3.15	Lateral Acceleration during Constant Radius with a changing weight split	65
3.16	Rollover Velocities during Constant Radius with a changing weight split in CarSim	66
3.17	Position	67
3.18	Lateral acceleration	67
3.19	The lateral acceleration of a vehicle in the SIS maneuver with changing suspension stiffnesses	68
3.20	Paths of vehicles with varying suspension stiffnesses	69
3.21	Lateral accelerations of vehicles with varying suspension stiffnesses	69
3.22	The positions of a vehicle in the fishhook maneuver with changing friction coefficients	70
3.23	Rollover velocities with varying Weight Splits	72
3.24	Rollover velocities with varying $C\alpha$ Values	72
4.1	ESC sensors diagram. Source: IIHS [53]	77
4.2	The vehicle's performance with the power reduction controller	79
4.3	The vehicle's performance with the all-wheel braking controller	80
4.4	The vehicle's braking forces with the all-wheel braking controller	81
4.5	The FBD used for the derivation of brake steer moments	83
4.6	ESC with independent wheel braking. Source: IIHS [53]	84
4.7	The vehicle's behavior with the independent wheel braking controller	85
4.8	The vehicle's longitudinal forces with independent wheel braking	86
4.9	The vehicle's behavior with the added torque controller	87
4.10	The vehicle's longitudinal forces with the added torque controller	88
4.11	The vehicle's behavior with the steering modification controller	89

4.12	The vehicle's behavior with steering modification and constant braking . .	90
4.13	The vehicle's velocity with steering modification and constant braking . .	91
4.14	The vehicle's behavior with independent braking and steering control . . .	92
4.15	The vehicle's velocity with independent braking and steering control . . .	93
4.16	The vehicle's longitudinal forces with independent braking and steering control	94
5.1	The fishhook maneuver with changing CG height and no ESC present . .	98
5.2	The fishhook maneuver with changing CG height and all-wheel braking and steering modification	99
5.3	The fishhook maneuver with changing CG height and independent wheel braking	100
5.4	The fishhook maneuver with changing WS and no ESC present	101
5.5	The fishhook maneuver with changing WS and all-wheel braking and steering modification	102
5.6	The fishhook maneuver with changing WS and independent braking . . .	103
5.7	CG height changes with an optimized all-wheel braking and steering ESC	104
5.8	CG height changes with an optimized independent braking ESC	105
5.9	WS changes with an optimized all-wheel braking and steering ESC	106
5.10	WS changes with an optimized independent braking ESC	107
C.1	The single stage controller	123
C.2	The two stage controller	124
C.3	The braking torques applied to simulate a power reduction	126
C.4	The braking torques applied to simulate a multi-step braking controller . .	127
C.5	The braking torques applied to simulate a variable braking controller . . .	128
C.6	The fishhook maneuver with braking times with independent wheel braking	129

C.7 Position	130
C.8 δ & Lateral Accel.	130
C.9 Position	131
C.10 δ & Lateral Accel.	131

CHAPTER 1
INTRODUCTION

1.1 Vehicle Rollover

Rollover of a vehicle occurs when the lateral acceleration reaches a point where two wheels of the vehicle are lifted off of the ground and the vehicle is rotated toward one side. Vehicle rollover occurs in two ways, either tripped or untripped. Tripped rollover accounts for around 95% of the rollover accidents on today's highways and occurs when a vehicle leaves the roadway and begins to slide sideways, causing the tires to dig into soft ground or strike an object such as a curb. Untripped rollovers normally occur when a top-heavy vehicle attempts to perform an evasive maneuver that it physically cannot handle.

Although most rollovers are tripped, the likelihood of being able to prevent rollover once the tires have become stationary is minimal to none. Also, by examining ways to prevent untripped rollover, stability and traction can be improved, leading to fewer chances for untripped rollover to occur.

1.2 Motivation

With an ever increasing number of passenger vehicles on highways today, fatalities due to vehicle rollover are becoming a larger concern. Increased driver distraction, Sport Utility Vehicle (SUV) and pick-up truck popularity, along with increased highway speeds all lead to more accidents. Automobile manufacturers have been developing and implementing better safety features, improving safety standards, and creating more

rigorous maneuvers for the testing of new vehicles. While these have aided in crash avoidance and severity reduction, more can be done to further save lives and money.

1.2.1 Rollover Crash Statistics

In 2005, noncollision vehicle rollovers accounted for 2.3% of all vehicle accidents on US highways; however, this small percentage accounted for 10.9% of roadway fatalities. Also in 2005, 4,266 lives were lost due to noncollision rollover, an increase of 5% over 2004's 4,045 noncollision rollover fatalities [39, 40, 16].

Table 1.1 - Vehicles in Single-Vehicle Crashes: 1994, 2003, 2004

Vehicle Type - Rollover Occurrence		1994	2003	2004
Passenger Car	Rolled Over	114,116	97,962	94,836
	Total	1,174,709	1,036,538	980,463
	Percentage	9.7 %	9.4 %	9.7 %
Van	Rolled Over	9,942	11,408	11,116
	Total	100,986	129,757	118,678
	Percentage	9.8 %	8.8 %	9.4 %
Pickup	Rolled Over	52,123	49,078	48,933
	Total	276,363	291,675	292,625
	Percentage	18.9 %	16.8 %	16.7 %
Sport Utility	Rolled Over	18,154	57,686	56,962
	Total	73,469	227,770	246,221
	Percentage	24.7 %	25.3 %	23.1 %
Source: NHTSA, NCSA, GES, 1994, 2003, 2004				

Table 1.1 shows the number of vehicle rollover occurrences and the total number of accidents per year [56]. Although the percentage of vehicles that rolled in single-vehicle accidents is generally decreasing, the number of rollovers involving vans and SUVs is on the rise, as is the fatality rate. The National Highway Traffic Safety Administration (NHTSA) has been monitoring rollover incidents closely in the past decade; nevertheless, demonstrating that more needs to be done to prevent this deadly occurrence.

1.2.2 Rollover Crash Costs

Currently, vehicle crashes cost drivers and taxpayers billions of dollars a year. Motor vehicle accidents not only account for vehicle repair costs, but are also responsible for medical costs, productivity losses, rehabilitation costs, travel delays, court and legal costs, emergency services, insurance costs, and the costs to employers. In 2000, the cost of motor vehicle crashes totaled \$230.6 billion dollars in the United States alone [1]. Despite the fact that vehicle rollovers account for a small percentage of roadway accidents, it's costs are high due to the severity of rollover and the fact that most rolled vehicles are considered by insurance companies to be a total loss.

1.2.3 Electronic Stability Controllers

Electronic stability controllers present in new vehicles have shown that rollovers can be avoided and costs can be reduced. For over thirty years, the Insurance Institute of Highway Safety (IIHS) has been conducting analysis of rollover data and crash statistics. With their results, they estimate that over 10,000 fatalities could be avoided each year if ESC was installed in all vehicles on the road [53]. ESC has been proven to reduce fatal multi-vehicle rollover crashes by 32%, fatal single-vehicle crashes by 56%, and total single-vehicle rollover crashes by over 40%. Susan Ferguson, Institute senior vice president for research, states, "The findings indicate that ESC should be standard on all vehicles." She continues, "Very few safety technologies show this kind of large effect in reducing crash deaths" [53]. With the results of early ESC system, NHTSA has required ESC to be installed in all new vehicles by the 2012 model year.

1.3 Current Efforts for Rollover Safety

In addition to the IIHS's study of vehicle accidents, the National Highway Traffic Safety Administration (NHTSA) has been studying the causes and effects of vehicle rollover [21, 19, 20, 22]. Test procedures have been created by NHTSA to examine a vehicle's rollover propensity and compare it to similar vehicles. The testing methods include static and dynamic maneuvers created specifically by NHTSA researchers to effectively reproduce real-life situations. Using these testing procedures, NHTSA has collected data and produced rollover ratings for hundreds of vehicles over the last few years.

1.3.1 Static Testing

For comparison between vehicles, NHTSA has created a method of comparing rollover propensity by calculating a vehicle's Static Stability Factor (SSF). This index is calculated from a vehicle's center of gravity (CG) height (H_{CG}) and the lateral distance between the wheels, or the track width (TW). Figure 1.1 shows how the two properties are measured.

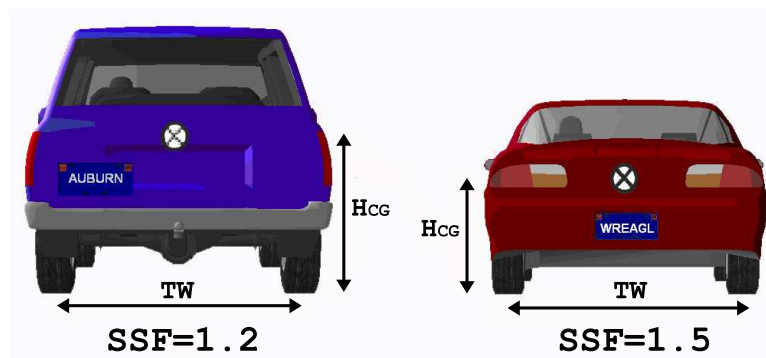


Figure 1.1: Static Stability Factor

Once the two vehicle properties are measured or estimated, the SSF is calculated by dividing the track width by twice the CG height.

$$SSF = \frac{TW}{2 * H_{CG}} \quad (1.1)$$

With the vehicle's SSF known, its value can be compared to other vehicles and a rollover percentage can be estimated. Vehicles with a higher CG and narrower track width have a smaller SSF value (Ex: SUVs, Vans) and have a greater chance for rollover than those with higher SSF values (Ex: Sports Cars), according to the SSF analysis. The SSF can also be plotted on a graph similar to Figure 1.2 and a trend can be observed. Vehicles with a lower SSF value have a higher chance of rollover, and receive a lower star rating from NHTSA.

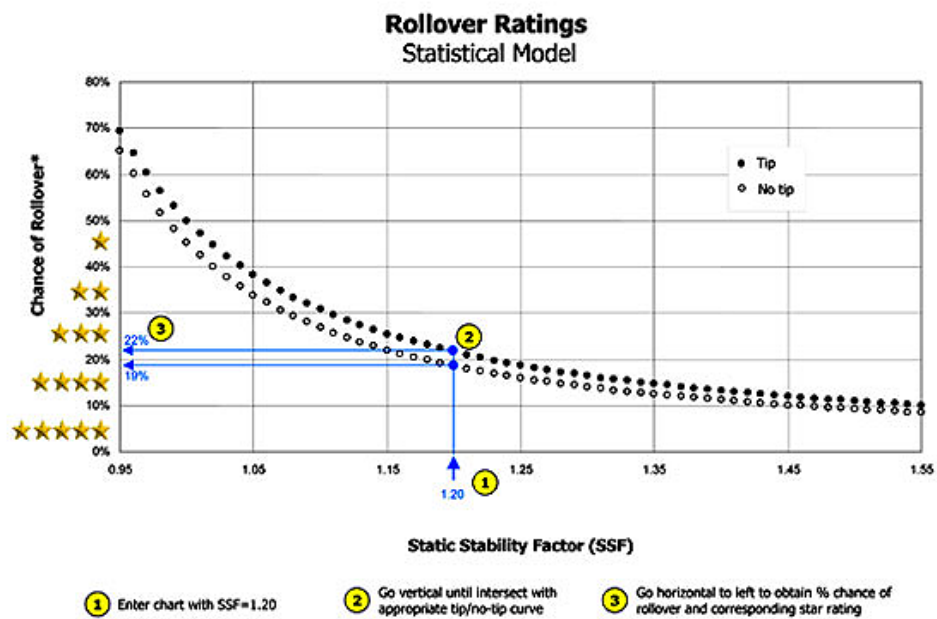


Figure 1.2: Static Stability Factor Curve [52]

The difference in rollover likelihood can be easily shown using the SSF of a vehicle. The derivation and background of this rollover propensity index is discussed further in Chapter 3.

1.4 Unmanned Ground Vehicles and Rollover

Unmanned ground vehicles are beginning to alter the way military operations are accomplished. Within the last two years, defense contractors have been awarded millions of dollars to research and develop UGVs, including a two-year, 1 million dollar contract to Metal Storm [50]. David Smith, Metal Storm CEO, believes that with such an emphasis on the safety of today's ground soldiers, it's no wonder that UGVs are getting some well deserved attention. Smith says, "[UGVs] could be the first line of defense in protecting high-value assets" [31]. John McHale, writer for Military & Aerospace Electronics, says that "... autonomous ground vehicles promise to be a major paradigm shift in ground warfare" [37].

In addition to military UGV's, the Defense Advanced Research Projects Agency (DARPA) has had two UGV races that pushed the limits of UGV technology. In the 2004 Grand Challenge, fifteen teams attempted to navigate the 145 mile course that no team finished. In 2005, the second Grand Challenge had four teams complete the 132 mile course in less than 10 hours. The 2007 Urban Challenge, to be held in November, will once again push the limits of unmanned navigation of ground vehicles. The latest race will put UGVs in a mock city environment and require numerous new technologies to be implemented.

With such a large prize value going to the winners, mission completion is key. Past teams have suffered from vehicle rollover, which immediately eliminates the chance for

2007 DARPA Urban Challenge Top Prizes:

1st Place - \$2 Million

2nd Place - \$1 Million

3rd Place - \$500,000

a win. Figure 1.3 shows the vehicle from team ENSCO rolling during the 2004 Grand Challenge.

Some UGVs also have the ability to be teleoperated. This is where an operator remotely drives the vehicle with sight, normally from vehicle mounted cameras. This method has its limitations due to the fact that the operator has no feedback of the vehicle's roll or lateral acceleration, so it becomes easier to roll. Therefore, there is a need for an ESC to be implemented.

In order for these UGVs to remain stable at the required higher speeds with increased and varying payloads, an adaptive roll controller needs to be developed to allow for variances in loading, vehicle, and road properties. New UGVs are also being required to travel further and at higher speeds, exponentially raising the risk of rollover during operation, which can be detrimental to a mission for larger-scale vehicles. ESC systems, similar to those in today's passenger vehicles, will be a vital component to the control systems of UGVs to maintain their stability as speeds increase to reduce mission times.

1.5 Thesis Purpose and Contributions

Since vehicle rollover is dangerous, costly, and detrimental, its aspects need to be studied to find how it can be prevented. The research presented in this thesis includes an investigation into the properties that most influence rollover, in order to analyze how changes in these properties alter vehicle dynamics. Additionally, this thesis investigates various ESC algorithms to see how they are affected by these changes.



Figure 1.3: The rollover of a UGV at the 2004 DARPA Grand Challenge

The largest contribution of this thesis is the identification of factors that are the greatest threats to a vehicle's stability. After identifying the key factors, the Static Stability Factor equation is examined and a formula is created to predict when a vehicle will be pushing the limits of stability based upon a few key parameters. The formulas are then tested in simulation and proven to be a good estimate of vehicle rollover. This analysis can then be used to predict roll limits and stability thresholds for varying vehicle configurations.

Several types of stability controllers are derived and created in simulation, and two of the controllers are compared and contrasted for effectiveness and adjustability to changing vehicle properties. Although individual methods of stability control have been analyzed, this thesis is one of the first to analyze the adaptability of the ESC systems.

1.6 Thesis Organization

Chapter 2 Vehicle Model Development - Chapter 2 derives the vehicle model used for stability investigation, defines test procedures, and introduces simulations created in MATLAB and CarSim.

Chapter 3 Vehicle Rollover Factors - Chapter 3 examines the factors that influence vehicle rollover, discusses formulas used for predicting vehicle rollover, and investigates the appropriateness of the formulas.

Chapter 4 Electronic Stability Controller Development - Chapter 4 describes the various types of stability controllers developed in simulation.

Chapter 5 Simulation Results of ESC - Chapter 5 investigates the adaptability of two types of ESC systems to varying vehicle parameters. It then looks at the methods and results of ESC optimization.

Finally chapter 6 completes the comparison of ESC systems and the effectiveness of the rollover prediction formulas.

CHAPTER 2
VEHICLE MODELING

2.1 Introduction

To begin studying the aspects of vehicle rollover, an advanced model is required. The model is based off of the basic “Bicycle Model” that accounts for basic vehicle properties [23, 49, 38]. The model is then modified to include vehicle roll and suspension characteristics [60, 3, 14, 48, 47, 26, 30]. Finally, the model is extended further to include individual wheel dynamics, braking, and acceleration forces.

2.2 Vehicle Coordinates

The coordinates used for the vehicle model are defined by the Society of Automotive Engineers (SAE), and are described by Gillespie and Milliken [23, 38] and shown in figure 2.1.

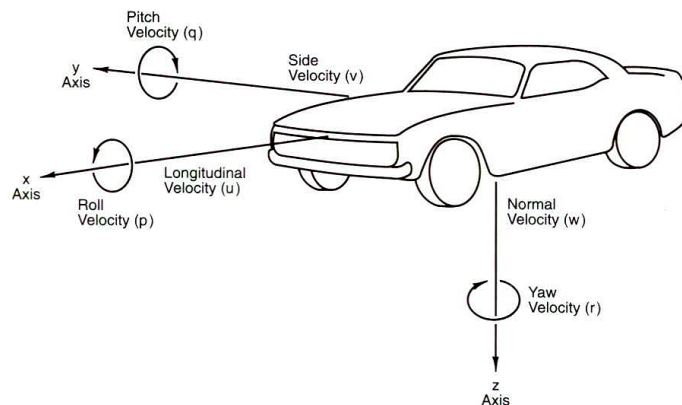


Figure 2.1: Vehicle coordinates defined by the SAE [38]

The SAE convention defines the longitudinal axis of the vehicle to be x , the lateral axis to be y , and the vertical axis to be z toward the ground. Roll is defined as rotation about the x axis, Pitch is rotation about the y axis, and Yaw is rotation about the z axis.

2.3 Angular Dynamics

To begin the analysis, lateral acceleration a_y and velocity are calculated for a steady state turn. figure 2.2 shows how the lateral velocity and lateral acceleration are derived.

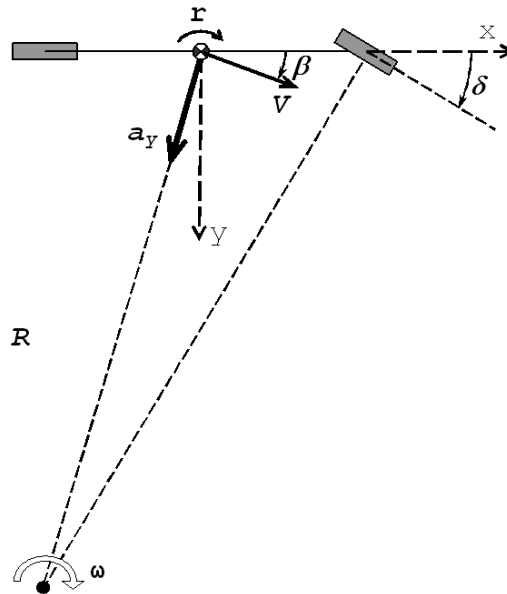


Figure 2.2: Diagram used for the derivation of the lateral velocity and lateral acceleration of the bike model

Since the turning is steady state, the radius of the turn (R) is constant, and $\dot{V}_y = 0$, so there is no lateral sliding. Also, the yaw rate of the vehicle (r) is equal to the angular

velocity of the vehicle (ω), in reference to the point of rotation. The steady state angular acceleration a_y consists of only the centripetal acceleration, and can be written in terms of velocity and yaw rate or turning radius as shown below.

$$V_x = R * \omega = R * r \quad (2.1)$$

$$a_y = \dot{V}_y = R * \omega^2 = R * r^2 = \frac{V_x^2}{R} = V * r \quad (2.2)$$

2.4 Bicycle Model

The ‘‘Bicycle Model’’ is simply a two wheeled vehicle model that is used to study basic vehicle dynamics. In this research, the Bicycle Model is used to describe the lateral vehicle dynamics only. Roll, pitch, weight transfer, and longitudinal wheel slip are assumed to be negligible and are not taken into account in the Bicycle Model. Also, steer angles and tire slip angles (α) for the left and right tires are combined into averages of the two. The following figure shows the free body diagram (FBD) for the bicycle model.

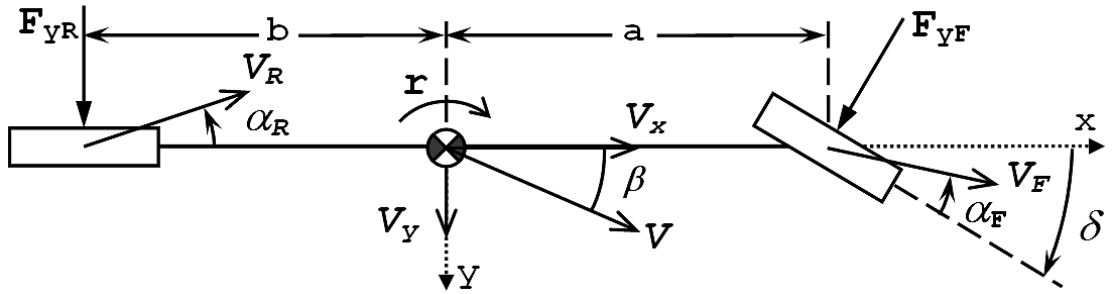


Figure 2.3: The free body diagram for the Bicycle Model

In order to find the lateral dynamic properties for the Bicycle Model, summations of the forces are taken in the lateral (y) and longitudinal (x) directions from Figure 2.3

as shown below.

$$\sum F_x = MT * a_x = F_{yF} * \sin(\delta) \quad (2.3)$$

$$\sum F_y = MT * a_y = F_{yR} + F_{yF} * \cos(\delta) \quad (2.4)$$

Forces due to braking, acceleration, rolling resistance, and air drag are ignored for now, but will be added later. MT is the total mass of the vehicle (sprung and unsprung). In order to solve for the yaw rate (r), the moment is taken at the center of gravity.

$$\sum M_{CG} = I_z * \dot{r} = -b * F_{yR} + a * F_{yF} * \cos(\delta) \quad (2.5)$$

By simply rearranging Equation (2.5), the vehicle yaw acceleration can be found.

$$\dot{r} = \frac{1}{I_z} * [F_{yf} * a * \cos(\delta) - F_{yr} * b] \quad (2.6)$$

Vehicle sideslip (β) is the angle between the vehicle's heading and course and is calculated by taking the arcsine of the lateral and total velocities of the vehicle.

$$\beta = \sin^{-1} \frac{V_y}{V} \quad (2.7)$$

From Figure 2.3, the relationships for the longitudinal and lateral velocities can be derived. At higher speeds, the vehicle slip angle (β) will play a role in the vehicle

dynamics. Without the effects of yaw rate, the equations are:

$$V_y = V * \sin(\beta) \quad \dot{V}_y = \dot{V} * \sin(\beta) + V * \dot{\beta} * \cos(\beta) \quad (2.8)$$

$$V_x = V * \cos(\beta) \quad \dot{V}_x = \dot{V} * \cos(\beta) + V * \dot{\beta} * \sin(\beta) \quad (2.9)$$

With effects of yaw rate added, the equations are:

$$\dot{V}_y = \dot{V} * \sin(\beta) + V * \dot{\beta} * \cos(\beta) + V * r * \sin(\beta) \quad (2.10)$$

$$\dot{V}_x = \dot{V} * \cos(\beta) + V * \dot{\beta} * \sin(\beta) - V * r * \cos(\beta) \quad (2.11)$$

These equations will be used later in the derivation of the roll angle. In a steady-state turn, the centripetal acceleration can be found to be:

$$a_{cen} = V_x * r = V * r * \cos(\beta) \quad (2.12)$$

By rearranging Equation (2.4) and substituting in Equation (2.12), the lateral acceleration can be found.

$$a_y = \dot{V}_y + a_{cen} = \frac{F_{yR} + F_{yF} * \cos(\delta)}{MT} \quad (2.13)$$

$$\dot{V}_y = \frac{F_{yR} + F_{yF} * \cos(\delta)}{MT} - V * r * \cos(\beta) \quad (2.14)$$

Note that the above equations include the effects of centripetal acceleration and sideslip. The lateral tire forces used in Equations (2.13) and (2.14) are derived using various tire models. This will be discussed further in Section 2.7.

2.5 Simple Roll Model

The next step in increasing the complexity of the vehicle model is adding the roll dynamics. By doing this, the vehicle model includes vertical and lateral forces for the left and right sides of the vehicle, and lateral weight transfer is included.

The simple vehicle roll model is made by creating a two-dimensional diagram of the sprung and unsprung masses. The sprung mass is held up by a fictitious pivot arm (d_1), from the vehicle's roll center, the effective pivot point at which the sprung mass pivots. Spring forces are initialized as zero after the static deflection. figures 2.4 and 2.5 show how the roll model is derived.

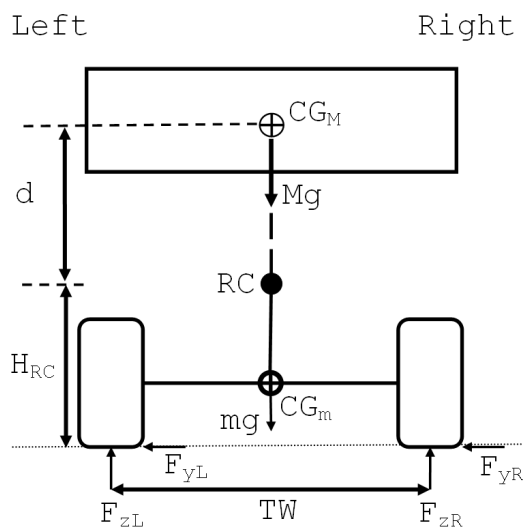


Figure 2.4: Roll diagram - static

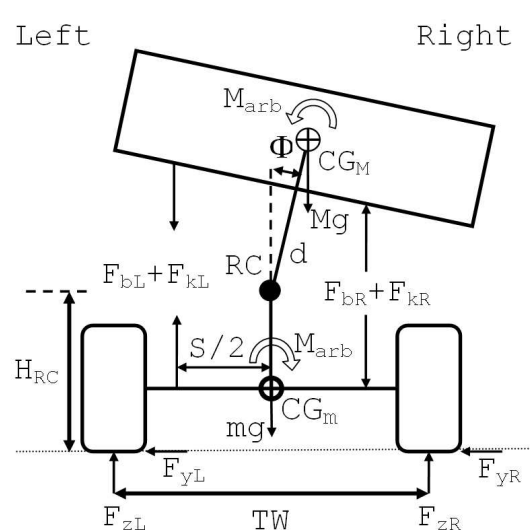


Figure 2.5: Roll diagram - with roll

In order to derive the roll dynamics, the roll model is split up into Unsprung and Sprung halves. figures 2.6 and 2.7 show the FBDs used for the derivation of the equations of motion for the vehicle roll.

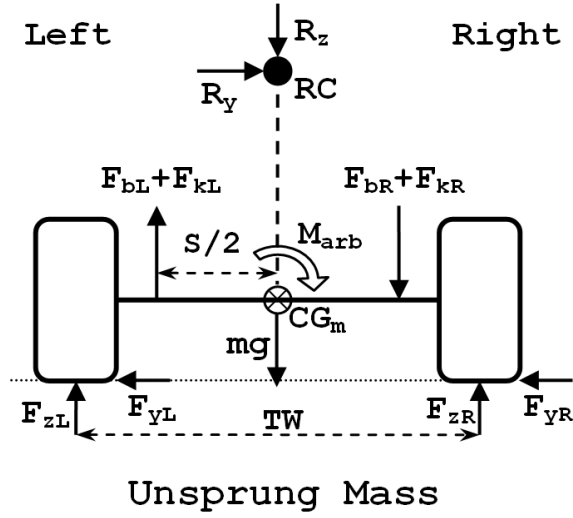


Figure 2.6: The free body diagram of an unsprung mass for roll equation derivation

The weight of the vehicle is accounted for with resultant forces R_z and R_y . In order to solve for the equations of motion, forces are added and the moment is taken at the roll center for the unsprung mass in Figure 2.6.

$$\sum F_y = m * \ddot{y} = 0 = R_y - F_{yL} - F_{yR} \quad (2.15)$$

$$\sum F_z = m * \ddot{z} = 0 = F_{zL} + F_{zR} + F_{sL} - F_{sR} - R_z - m * g \quad (2.16)$$

$$\begin{aligned} \sum M_{RC} = I_x * \ddot{\phi}_{Unsprung} = 0 = h_{RC} * (F_{yL} + F_{yR}) + \frac{TW}{2} * (F_{zL} - F_{zR}) \\ + B * \dot{\phi} + K_{\phi} * \phi + M_{ARB} \end{aligned} \quad (2.17)$$

Here, B is the roll damping of the vehicle, K_{ϕ} is the roll stiffness, and M_{ARB} is the moment applied by the anti-roll, or torsion bar. The equations are solved with the assumption of steady-state axle dynamics. Rearranging Equations (2.15) and (2.17)

yields:

$$m * \ddot{y} = R_y - F_{yL} - F_{yR} = 0 \quad (2.18)$$

$$\frac{TW}{2} * (F_{zR} - F_{zL}) = B * \dot{\phi} + K_{\phi} * \phi + M_{ARB} + h_{RC} * (F_{yL} + F_{yR}) \quad (2.19)$$

By combining the previous equations with ones taken from the sprung mass, seen in Figure 2.7, the vehicle model can be further expanded to include roll angles and weight transfer.

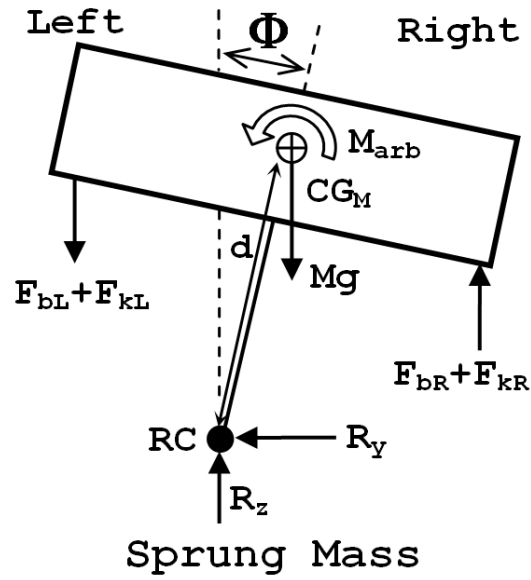


Figure 2.7: The free body diagram of a sprung mass for roll equation derivation

The forces for the sprung mass are also added together and the moment is taken again at the roll center.

$$\sum F_y = M * a_y = R_y \quad (2.20)$$

$$\sum F_z = M * a_z = R_z + F_{sR} - F_{sL} - M * g = 0 \quad (2.21)$$

$$\begin{aligned} \sum M_{RC} &= I_x * \ddot{\phi} = M * g * d * \sin(\phi) + M * \ddot{y} * d * \cos(\phi) \\ &- M_{ARB} - B * \dot{\phi} - K_\phi * \phi = 0 \end{aligned} \quad (2.22)$$

Solving for the roll acceleration ($\ddot{\phi}$), the following equation can be derived.

$$\ddot{\phi} = \frac{1}{I_x} * [M * g * d * \sin(\phi) + M * \ddot{y} * d * \cos(\phi) - M_{ARB} - B * \dot{\phi} - K_\phi * \phi] \quad (2.23)$$

Substituting in Equation (2.10), the roll acceleration is found.

$$\begin{aligned} \ddot{\phi} &= \frac{1}{I_x} * [M * g * d * \sin(\phi) - B * \dot{\phi} - K_\phi * \phi - M_{ARB} \\ &+ M * (\dot{V} * \sin(\beta) + V * \dot{\beta} * \cos(\beta) + V * r * \sin(\beta)) * d * \cos(\phi)] \end{aligned} \quad (2.24)$$

The weight transfer equations can also be formed from these equations. Rearranging Equations (2.15) and (2.20) and substituting for R_y yields:

$$MT * \ddot{y} = R_y = F_{yL} + F_{yR} \quad (2.25)$$

Substituting this into the unsprung moment, the following equation is derived:

$$\frac{TW}{2} * (\Delta F_z) = \frac{TW}{2} * (F_{zR} - F_{zL}) = B * \dot{\phi} + K_\phi * \phi + M_{ARB} + h_{RC} * MT * \ddot{y} \quad (2.26)$$

In order to account for different weight splits, the weight transfer equation is split into front and rear components. Also, \ddot{y} is altered to include yaw rate, resulting in the following equation for the front and rear weight transfer.

$$\begin{aligned}\Delta F_{zf} &= \frac{2}{TW_f} * [B_f * \dot{\phi}_f + K_{\phi f} * \phi + M_{ARBF} \\ &+ h_{RCf} * MT_f * (\dot{V} * \sin(\beta) + V * \dot{\beta} * \cos(\beta) + V * r * \sin(\beta))] \quad (2.27)\end{aligned}$$

$$\begin{aligned}\Delta F_{zr} &= \frac{2}{TW_r} * [B_r * \dot{\phi}_r + K_{\phi r} * \phi + M_{ARBr} \\ &+ h_{RCr} * MT_r * (\dot{V} * \sin(\beta) + V * \dot{\beta} * \cos(\beta) + V * r * \sin(\beta))] \quad (2.28)\end{aligned}$$

Vertical tire forces can then be calculated by taking the static load and subtracting or adding the weight transferred during the maneuver.

$$\begin{aligned}F_{z f L} &= \frac{F_{zf}}{2} - \Delta F_{zf} & F_{z f R} &= \frac{F_{zf}}{2} + \Delta F_{zf} \\ F_{z r L} &= \frac{F_{zr}}{2} - \Delta F_{zr} & F_{z r R} &= \frac{F_{zr}}{2} + \Delta F_{zr}\end{aligned} \quad (2.29)$$

Because the tire lateral forces are a function of vertical load, these vertical forces for the individual tires can now be used for solving the lateral tire forces. In order to find these lateral forces, a model of the tire is required as shown in Section 2.7.

2.6 Independent Wheel Model

In order to implement independent wheel braking, the vehicle model needs to include the dynamics of the independent wheels and tires [15]. To do this, a free body diagram is derived for an individual wheel. Figure 2.8 shows the side view of a tire, including braking and engine torques.

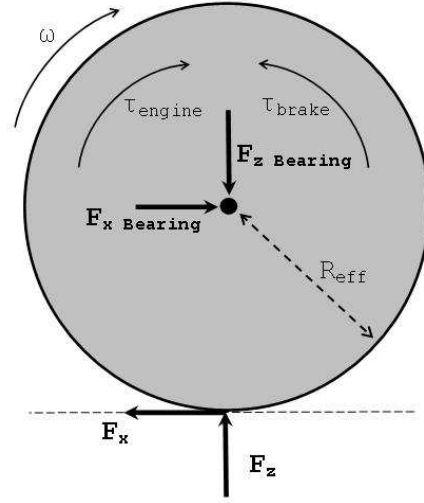


Figure 2.8: The free body diagram of a tire

After analysis of the tire FBD, the results in the following set of equations are derived and used to describe the tire dynamics:

$$\sum F_x = M * a_x = F_{xBearing} - F_x \quad (2.30)$$

$$\sum F_z = M * a_z = F_{zBearing} - F_z = 0 \quad (2.31)$$

$$\sum M_{Bearing} = I_w * \dot{\omega} = R_{eff} * F_x + \tau_{engine} - \tau_{brake} \quad (2.32)$$

Then solving for the longitudinal force, the solution becomes:

$$F_x = \frac{1}{R_{eff}} [I_w * \dot{\omega} + \tau_{brake} - \tau_{engine}] \quad (2.33)$$

The force in Equation (2.33) is the longitudinal force applied by the vehicle to the tire. Although this force includes the effects of engine and braking torque, tire models

will still limit the lateral and longitudinal forces allowed by the tires. To correctly account for these effects, tire models must be investigated and applied to the vehicle model.

2.7 Tire Properties

In order to properly model a vehicle with pneumatic tires, a model must be implemented to describe the lateral and longitudinal forces that are limited by physical properties of a tire.

2.7.1 Tire Forces and Slip Angles

The forces that are allowed by a tire depends on several factors, however there is a maximum friction force allowed when a non-linear model is used. This peak tire force is dependent upon the vertical force and slip angle of the tire, and other factors such as air pressure, surface characteristics, and temperature. Figure 2.9 depicts a typical tire curve in which the peak force can be seen.

The tires slip angle (α) and cornering stiffness (C_α) will be discussed in greater detail later in this section.

The total horizontal tire force is divided up into lateral and longitudinal directions. Figure 2.10 shows how the tire's velocity components are defined.

The magnitudes of these forces are limited by physical properties that can be explained the tire friction circle [10]. Figure 2.11 demonstrates how the tire forces are limited using the concept of the friction circle. As seen in the figure, if the vehicle is accelerating or braking, the peak lateral force allowed by the tires is decreased.

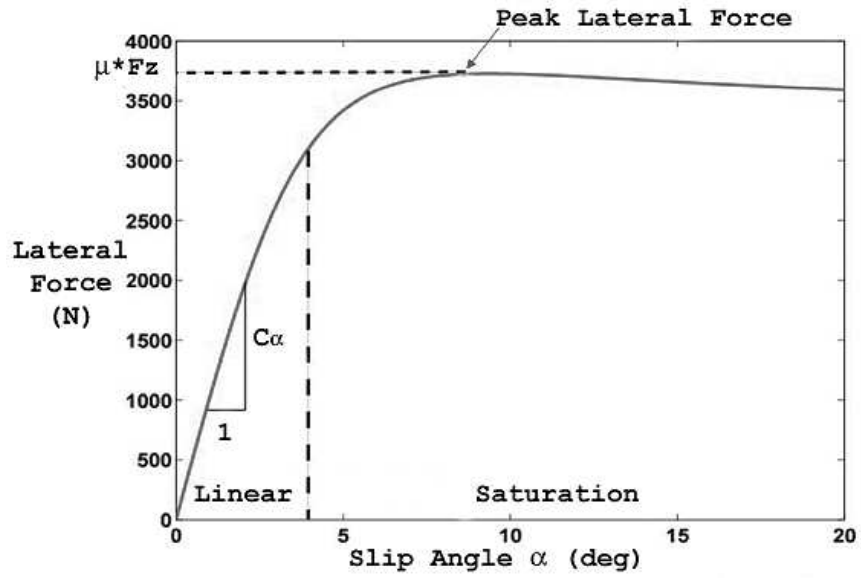


Figure 2.9: Tire curve diagram for maximum lateral forces

Equation (2.34) defines how the maximum lateral and longitudinal forces allowed by the tire are limited by the peak tire force.

$$F_z * \mu \geq F_{tire} = \sqrt{F_x^2 + F_y^2} \quad (2.34)$$

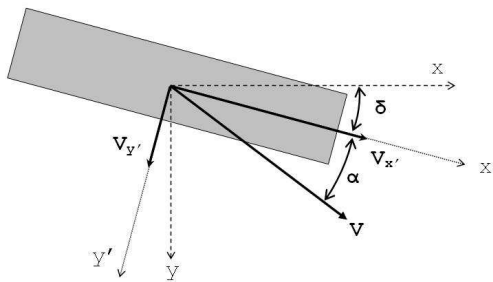


Figure 2.10: Front tire slip angle diagram

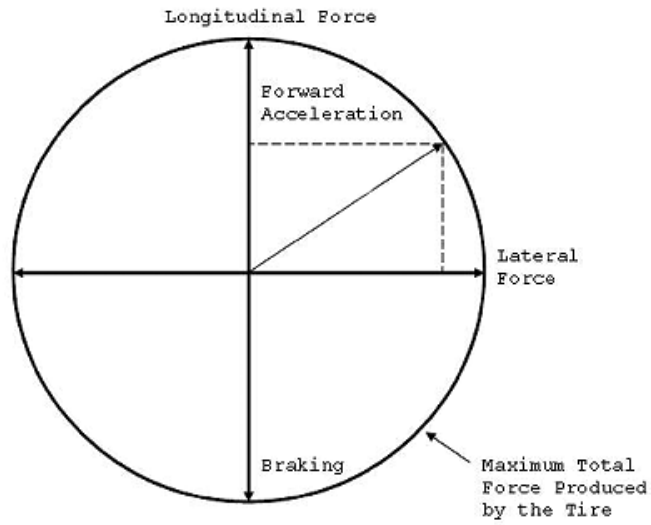


Figure 2.11: The tire friction circle used for defining maximum forces allowed [60]

The peak tire force is a function of the vertical tire force, and the tire-ground friction coefficient (μ). The tire-ground friction coefficient is considered to be constant in simulation for simplicity; however, in actuality, it changes due to variations in load, tire, and surface conditions. With the tire's velocities broken up into lateral and longitudinal components and the steer angle averaged from left and right tires, the tire's slip angle (α) can be solved. From Figure 2.10, the slip angles of the tires can be found. Equations (2.35), (2.36), (2.37), and (2.38) show the slip angles calculated from the tire's velocity components.

$$\alpha_{fL} = \tan^{-1} \left[\frac{V * \sin(\beta) + r * a}{V * \cos(\beta) + r * \frac{tw_f}{2}} \right] - \delta \quad (2.35)$$

$$\alpha_{fR} = \tan^{-1} \left[\frac{V * \sin(\beta) + r * a}{V * \cos(\beta) - r * \frac{tw_f}{2}} \right] - \delta \quad (2.36)$$

$$\alpha_{rL} = \tan^{-1} \left[\frac{V * \sin(\beta) - r * b}{V * \cos(\beta) + r * \frac{tw_r}{2}} \right] \quad (2.37)$$

$$\alpha_{rR} = \tan^{-1} \left[\frac{V * \sin(\beta) - r * b}{V * \cos(\beta) - r * \frac{tw_r}{2}} \right] \quad (2.38)$$

One could add a rear steer component by simply adding in δ_{rear} to account for the addition of a rear steer angle to the bicycle model. Equations (2.35), (2.36), (2.37), and (2.38) also include effects of the vehicle's yaw rate, which is sometimes removed. These effects could have been ignored; however, with the large yaw rates induced during some rollover maneuvers, the model is more accurate when these terms are included.

2.7.2 Tire Models

Several tire models are available to capture the tire characteristics shown previously in Figure 2.9. The most popular tire models include the linear, Dugoff, and Pacejka tire models, and a look-up table [10]. The linear tire model is acceptable for slow speed maneuvers; however, since vehicle roll is being studied, higher speeds are used and the model will not accurately capture the dynamics of the tires in these ranges. The Dugoff and Pacejka tire models have previously been proven accurate and are widely accepted, and simulations described in this thesis use both models.

Simulations in CarSim were done using a look-up table model. Here, a vertical force and slip angle are given, and the simulator looks up the correct lateral and longitudinal

forces in a table. Although this method can be very accurate, it requires data taken from tire tests and cannot be easily modified. Figure 2.12 shows the lateral force curve for a typical truck tire in the CarSim tire library.

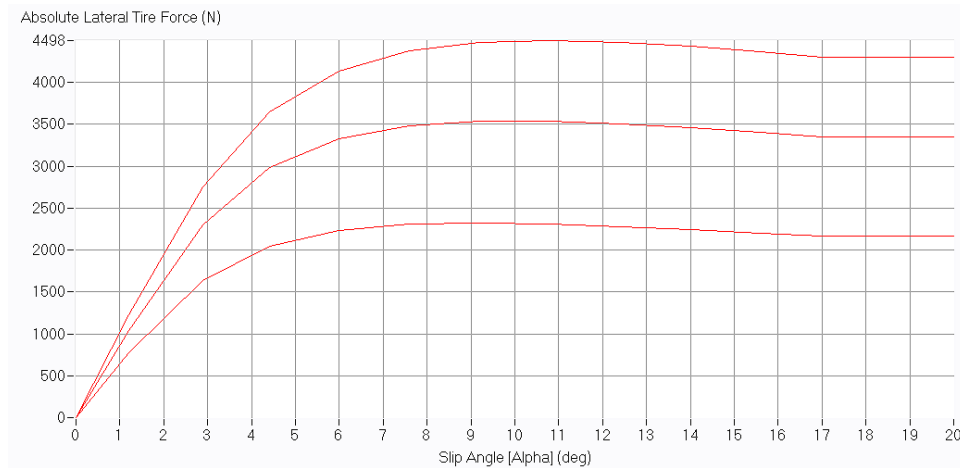


Figure 2.12: Tire curve for a typical truck tire - Source: CarSim

Dugoff's Model

The Dugoff Tire model was first published in 1969 as a method for finding the lateral force allowed by a tire [11, 12]. Instead of the actual parabolic shape of the tire forces, the Dugoff model assumes that a uniform pressure is distributed on the tire's contact patch. This simplification of the tire's forces allows easier calculations, and requires fewer parameters to be known. Another advantage of this model is that tire stiffness values for the lateral and longitudinal directions can be independently defined.

The equations for the tire forces using the Dugoff tire model are as follows:

$$F_y = -C_\alpha * \tan(\alpha) * f(\lambda) \quad (2.39)$$

$$F_x = -C_\sigma * \frac{\sigma_x}{1 + \sigma_x} * f(\lambda) \quad (2.40)$$

where C_α is the tire's cornering stiffness, C_σ is the longitudinal stiffness, and σ_x is the longitudinal slip ratio. The parameters F_λ and λ are defined as:

$$f(\lambda) = \begin{cases} (2 - \lambda) * \lambda & \text{if } \lambda < 1 \\ 1 & \text{if } \lambda \geq 1 \end{cases}$$

$$\lambda = \frac{\mu * F_z * (1 + \sigma_x)}{[(C_\sigma * \sigma_x)^2 + (C_\alpha * \tan(\alpha))^2]^{\frac{1}{2}}}$$

where F_z is the tire's normal force, and μ is the friction coefficient for the tire and road. The lateral force allowed is directly proportional to the tire cornering stiffness, and the longitudinal force allowed is proportional to the longitudinal tire stiffness.

The Pacejka Model

In the 1960s, Hans Pacejka became a lead researcher into the properties of pneumatic passenger vehicle tires. His research led him to publish several papers [43, 42] and a book [44] on this subject. His tire model is considered to be quite accurate and is widely used in modeling of tires today.

The non-linear equations for the Pacejka begins with the general equation [49]:

$$Y(X) = D * \sin(C * \tan^{-1}(B * x - E(B * x - \tan^{-1}(B * x)))) \quad (2.41)$$

where $Y(X) = y(x) + S_v$ and $x = X - S_h$. S_v is the vertical shift and S_h is the horizontal shift that can be included in the model. Due to the fact that this thesis is not an investigation into tires and the shift parameters are not well known, these properties were set to zero. Y is the output variable (F_x , F_y , or M_z) and X is the input variable

(slip angle α or slip ratio σ_x). Equation (2.41) is then simplified to solve for the lateral and longitudinal forces allowed by the tires.

$$F_y = D * \sin(C * \tan^{-1}(B_y * \alpha - E(B_y * \alpha - \tan^{-1}(B_y * \alpha)))) \quad (2.42)$$

$$F_x = D * \sin(C * \tan^{-1}(B_x \alpha - E(B_x * \alpha - \tan^{-1}(B_x * \alpha)))) \quad (2.43)$$

The input variable is set to be the slip angle α , and B is adjusted when solving for lateral or longitudinal forces. To fill in the force equations, several tire properties must be known. The first, C in Equation (2.44), is the shape factor.

$$C = \frac{2}{\pi} * \sin^{-1} \left(\frac{y_s}{D} \right) \quad (2.44)$$

This property is independent of the normal force distributed on the tire. The second Pacejka tire property, D in equation 2.45, is the key factor in determining the maximum lateral force on the tire curve.

$$D = a_1 * F_z^2 + a_2 * F_z \quad (2.45)$$

This property is dependent on only the normal force distributed on the tire and the Pacejka parameters. The third Pacejka tire property, E in equation 2.46, is the curve factor of the tire curve.

$$E = a_6 * F_z^2 + a_7 * F_z + a_8 \quad (2.46)$$

This property is also dependent on only the normal force distributed on the tire and the Pacejka parameters, but affects the curvature of the maximum tire force curve. The

fourth Pacejka tire property, B , is derived from Equations (2.47) and (2.48). For the lateral tire forces, BCD is defined as:

$$B_yCD = a_3 * \sin(a_4 * \tan^{-1}(a_5 * F_z)) \quad (2.47)$$

And for the longitudinal case:

$$B_xCD = \frac{a_3 * F_z^2 + a_4 * F_z}{e^{a_5 * F_z}} \quad (2.48)$$

BCD is effectively the cornering stiffness, C_α , and defines the slope of the tire curve at small slip angles α .

Parameters a_0, a_1, \dots, a_8 are constant terms defined for each tire. These values are found from test data and are dependent on the tire. Table 2.1 shows parameters taken from a paper written by Pacejka in 1989 [42].

Table 2.1 - Pacejka Tire Parameters

$a_0=0$	$a_5=0.208$
$a_1=-22.1$	$a_6=0$
$a_2=1011$	$a_7=-0.354$
$a_3=1078$	$a_8=0.707$
$a_4=1.82$	

The resulting lateral and longitudinal forces are dependent upon the slip angles of the tire, vertical force, and tire properties. Figure 2.13 shows the results for a tire modeled using the Pacejka tire model. The tire's cornering stiffness C_α and peak force are altered with changing normal forces; however a point is reached where increasing the normal tire force allows little change in lateral force produced.

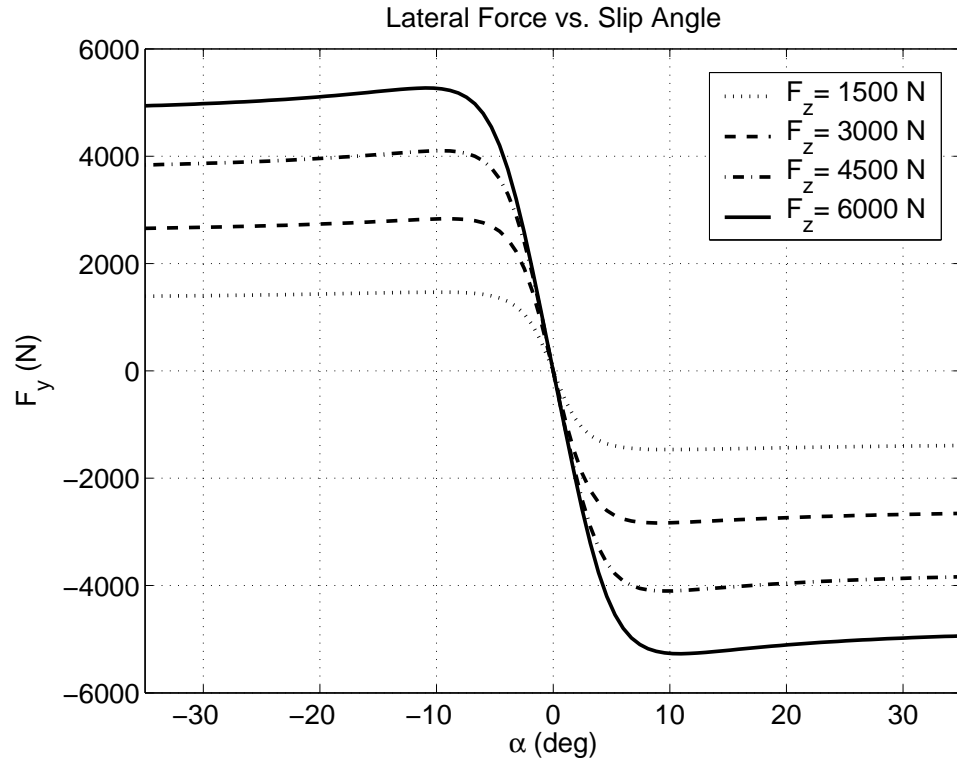


Figure 2.13: Pacejka tire curve diagram for maximum lateral forces

2.8 Simulation Vehicle

The vehicle modeled in this thesis is a typical SUV with properties taken from a 2000 Chevrolet Blazer. The vehicle was chosen due to previous knowledge of the parameters, and experimental testing has previously been done to confirm their accuracy. Actual properties used in this thesis can be found in Appendix B.

2.9 Test Maneuvers

In order to correctly compare the derived vehicle model to that in CarSim, testing maneuvers must be created to perform validation. NHTSA has created several types of

maneuvers for vehicle rollover testing [22, 8]. The maneuvers are designed to test certain aspects of the vehicle's behavior. Quasi-static maneuvers test the vehicles likelihood to rollover in steady-state turning, while dynamic maneuvers provoke transient vehicle properties that are brought about by dynamic weight transfer and suspension effects. For simulations, the friction coefficient (μ) can be altered, depending on the simulated surface.

2.9.1 Quasi-Static Maneuvers

Quasi-static rollover testing is composed of maneuvers that test a vehicle's propensity for rollover with a model that removes the effects of transients. Maneuvers that fall under the quasi-static realm include the constant radius and the steadily increasing steer. These maneuvers gradually increase the vehicle's steer angle or velocity, causing a semi-static rollover. The quasi-static testing done in this thesis begins with a rigid vehicle, and then the suspension is added in order to investigate its effect during the quasi-static maneuvers. Although, the quasi-static maneuvers incorporate the main factors that affect vehicle rollover, they do not include effects of vehicle roll due to suspension configurations and other transient properties.

2.9.1.1 Constant Radius

The constant radius maneuver consists of a vehicle going around a circular track with a constant turning radius (R). The vehicle simulation is begun at a stop or slow speed, and then a low constant longitudinal acceleration is applied to the vehicle. Figure 2.14 shows the vehicle's performance during a standard constant radius simulation. The maneuver is considered to be quasi-static due to the fact that it does not excite

the dynamic behavior of the vehicle until wheel lift occurs. Suspension transients are minimal, since the roll rate is small, and the lateral acceleration is limited by the friction coefficient of the roadway.

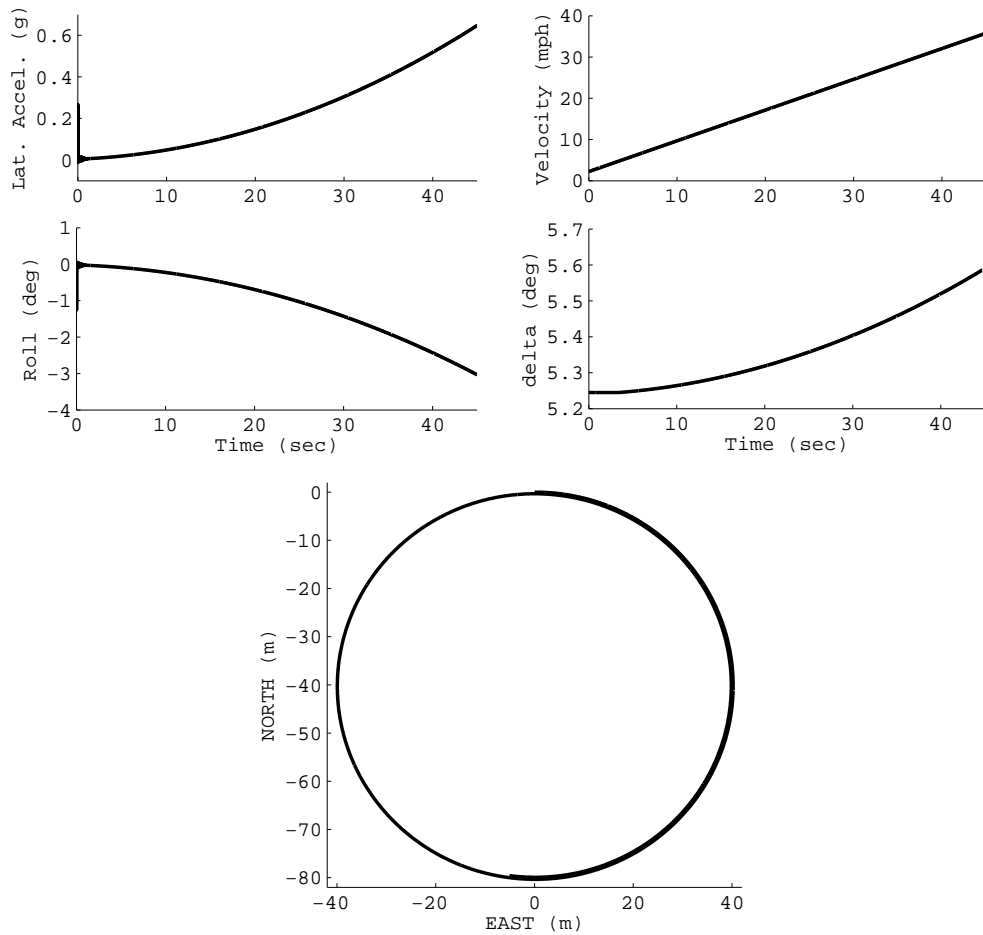


Figure 2.14: The Constant Radius maneuver of a rigid vehicle performed in MATLAB

Obstacles to overcome in this simulation include the fact that steer angle will not be constant to hold the constant radius. Due to the increasing velocity, the vehicle will become more understeer, caused by the increasing slip angles. Figure 2.15 shows what would occur if the steer angle were held constant while steadily increasing in velocity.

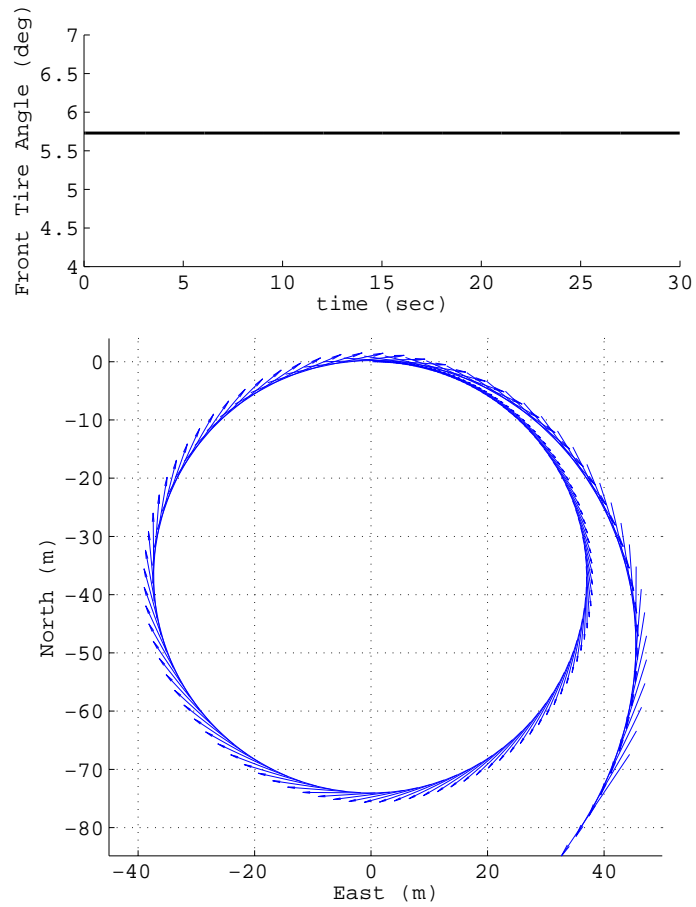


Figure 2.15: The vehicle behavior with a constant steer angle and gradually increasing velocity on an understeer vehicle

As the vehicle increases in velocity, the vehicle's path is widened, and the radius is not constant. Since the vehicle modeled is slightly understeer, the steer angle must increase to hold a constant radius during the acceleration. The understeer gradient of a vehicle is discussed in detail in Chapter 3.

2.9.1.2 Steadily Increasing Steer

The Steadily Increasing Steer (SIS) maneuver consists of a vehicle traveling at a constant velocity, and uniformly increasing the steer angle. The maneuver is considered to be quasi-static due to the fact that it does not excite the suspension dynamics, similar to the CR test. Figure 2.16 shows how a rigid vehicle performs in the SIS Maneuver.

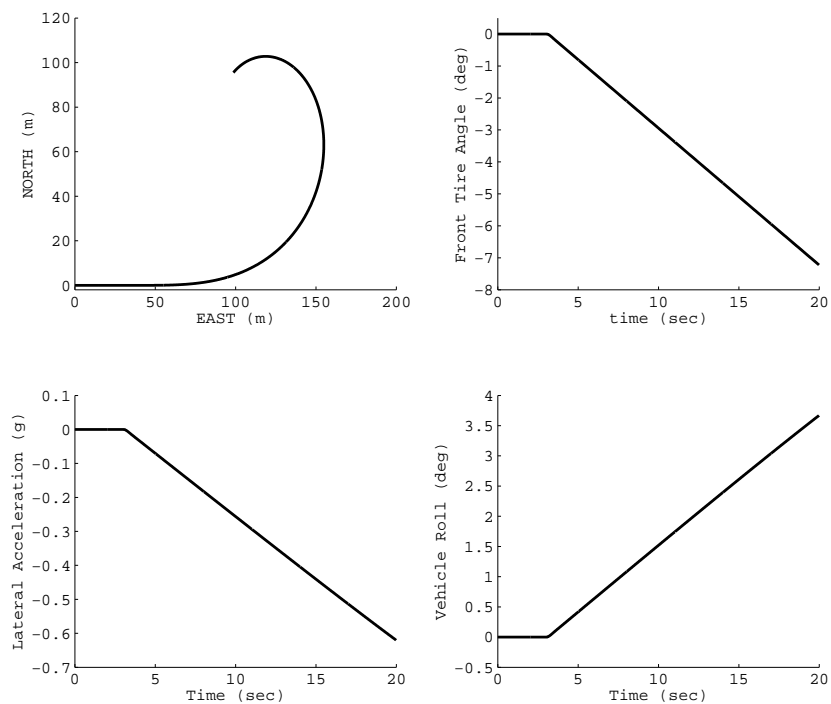


Figure 2.16: The SIS maneuver of a rigid vehicle performed in MATLAB

Although the maneuver can be used to analyze a vehicle's behavior during a quasi-static maneuver, NHTSA uses it to define maximum steer angles in other maneuvers. For example, when the lateral acceleration reaches 0.3 g during this maneuver, the steer

angle is taken, multiplied by 6.5, and used for the maximum steer angle in the fishhook maneuver.

2.9.2 Dynamic Maneuvers

Since real life vehicle rollovers are caused by dynamic maneuvers, testing that incorporates the effects created by vehicle transients should be conducted. In 2004, NHTSA began to test a vehicle's rollover propensity with dynamic maneuvers, in order to more accurately assess a vehicle's rollover propensity [22]. The maneuvers defined by NHTSA are created to excite certain vehicle dynamics that are not taken into account in the static and quasi-static testing procedures. The maneuvers included in NHTSA's testing are the J-turn, the fishhook, and the double lane change. The J-turn maneuver is a result of a step steer angle applied during a constant velocity run. The fishhook maneuver simulates a road edge recovery maneuver that emulates a sinusoidal steering input that greatly increases the vehicle's chances for rollover. The double lane change maneuver is quite similar to the fishhook maneuver, in that it requires two steer angles, but it does not excite the vehicle dynamics as much as the fishhook, and will not be discussed further in this thesis.

2.9.2.1 J-Turn

The J-turn maneuver is one of the simplest dynamic test that can be performed. It consists of a vehicle driving at a constant velocity with the application of a sudden and large steer angle. The vehicle's behavior during the maneuver is shown in Figure 2.17. The J-turn maneuver is a good test of how weight transfer affects a vehicle when a step steer input is applied. It is also a highly-repeatable maneuver, although its profile is not

one usually seen on actual roadways. For this reason, the fishhook maneuver is a better choice for testing real-life situations.

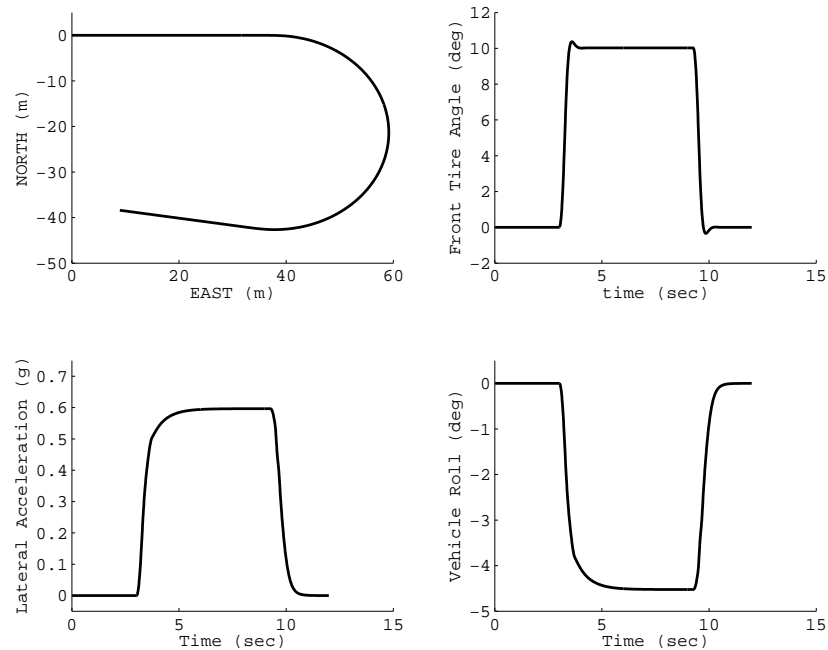


Figure 2.17: The J-turn maneuver performed in MATLAB

2.9.2.2 Fishhook

The fishhook maneuver developed by NHTSA is a good example of a real-world road edge recovery maneuver. The fishhook is also an excellent maneuver due to its repeatability and its ability to excite the dynamics of a vehicle that influence rollover [62].

The inputs of NHTSA's fishhook maneuver are defined by a vehicle's performance during other maneuvers. The maximum steer angle, A , is defined from the vehicle's performance during the SIS maneuver at 50 mph using a continuously growing steer

angle input of 13.5 deg/sec at the handwheel. When the vehicle reaches 0.3 g of lateral acceleration, the steer angle is measured, and multiplied by 6.5 to get A , the fishhook maximum steer angle. Figure 2.18 shows the steer input for the NHTSA fishhook maneuver. It is usually performed at 50 mph , although other speeds are acceptable as long as they are compared to other vehicles tested at the same speed.

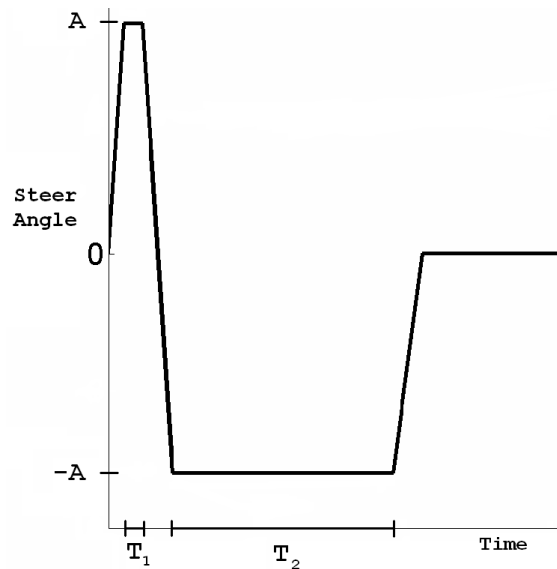


Figure 2.18: The steer angle inputs for the Fishhook maneuver, defined by NHTSA

The time constants T_1 and T_2 were set by NHTSA to be 0.25 and 3.0 seconds respectively. The times are chosen for their ability to excite the vehicle's roll rate into a semi-sinusoidal reaction. Figure 2.19 shows the behavior of the modeled SUV in the fishhook maneuver performed in MATLAB.

For simulations in this thesis, the fishhook maneuver is the dynamic test used due to the fact that it is easily repeatable, simulates real-world rollover threats, and is able to excite the vehicle's dynamic properties.

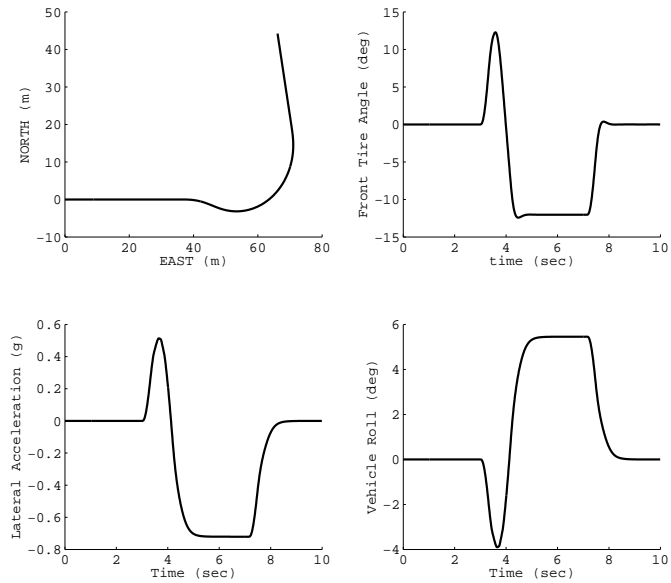


Figure 2.19: The Fishhook maneuver performed in MATLAB

2.10 Simulations in MATLAB and CarSim

The simulations in this thesis were created using MATLAB and CarSim. MATLAB, an interactive programming environment, has a great ability to allow the user to define exactly what is desired, since the model dynamics are user defined. CarSim, a commercially available simulation package for multibody vehicle dynamics, has several advantages in that it provides a more complex vehicle model, and already has tested vehicle models built in. It allows the user to create or modify preexisting steering inputs, velocity profiles, vehicles, and roads among other things.

Of course, simulations in both programs have their limitations. The simulation of vehicle dynamics has been researched and published by several authors [28, 55] and the limitations of 3-dimensional vehicle simulations have been discussed by Day and Garvey

[9]. MATLAB's limitations are small, although they include the requirement that the all of the vehicle properties must be found and inserted by the user, all equations of the vehicle must be fully developed and the programmer must be certain that all units are consistent. This is not the case with CarSim, since all of the vehicle dynamic equations are built in to the software package. The limitations of CarSim include the fact that some properties are hard to set, user inputs are limited, and equations used in the vehicle model are not known.

In order to verify the suitability of the simulations, maneuvers were performed in both programs and then compared with each other. The first maneuver, the SIS, is shown in Figure 2.20. The results from the simulations are fairly uniform. A slight difference can be seen in the yaw rate and lateral acceleration, likely due to a difference in one of the many tire properties incorporated in the CarSim model. The difference can be shown in the position plot, although the results were deemed close enough for testing purposes in this thesis.

The second maneuver used for comparison is the fishhook. Figure 2.21 shows the vehicle's behavior during the dynamic maneuver. The results of the fishhook maneuver comparison are similar to the SIS maneuver, although there is a slight difference in steer angle between the maneuvers. Despite the small variation in steer angle (due to a smoothing function in MATLAB simulation), the results for the lateral acceleration, yaw rate, and position are actually closer to each other than in the SIS maneuver. The only other discrepancy between the two simulations is a small oscillation in the lateral acceleration during the CarSim simulation. This is due to minimal differences in the spring rate and damping in the suspension or tires. Once again, for the requirements in this thesis, the resulting discrepancy in the two simulations is acceptable.

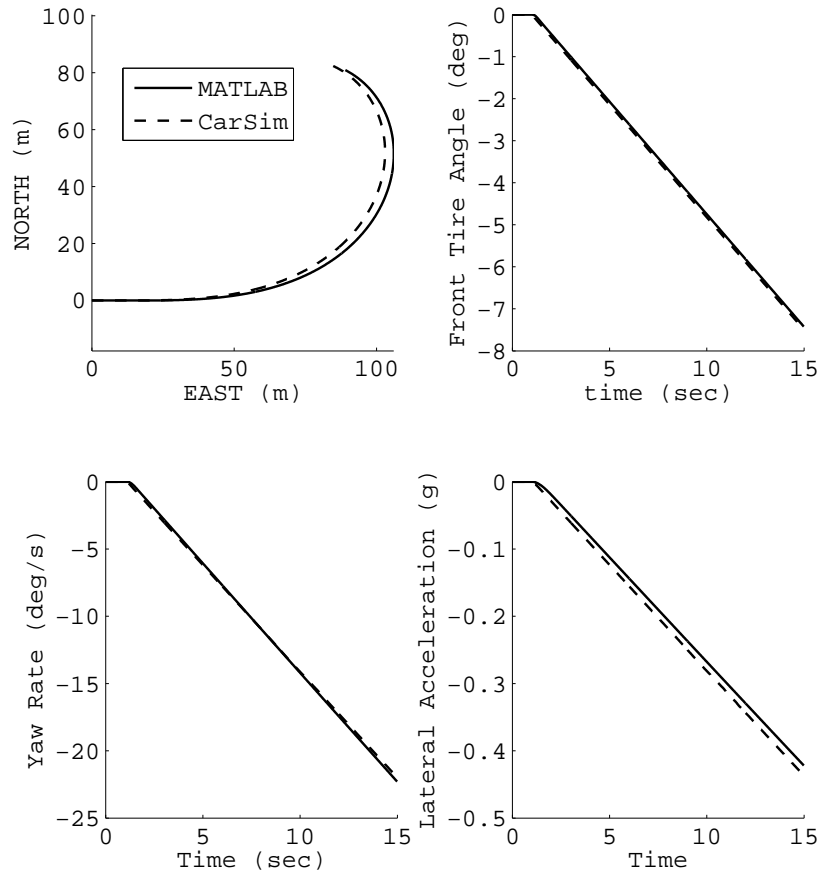


Figure 2.20: Comparison of the SIS maneuver performed in MATLAB and CarSim

2.11 Conclusions on Vehicle Modeling

The vehicle model developed in this chapter has been implemented in a MATLAB simulation and has been tested for accuracy. With prior testing by others and a comparison to the commercially developed vehicle-modeling software CarSim, the vehicle model exhibits true-to-life vehicle behavior. With this vehicle model, testing with the developed quasi-static and dynamic maneuvers can now be performed in order to investigate

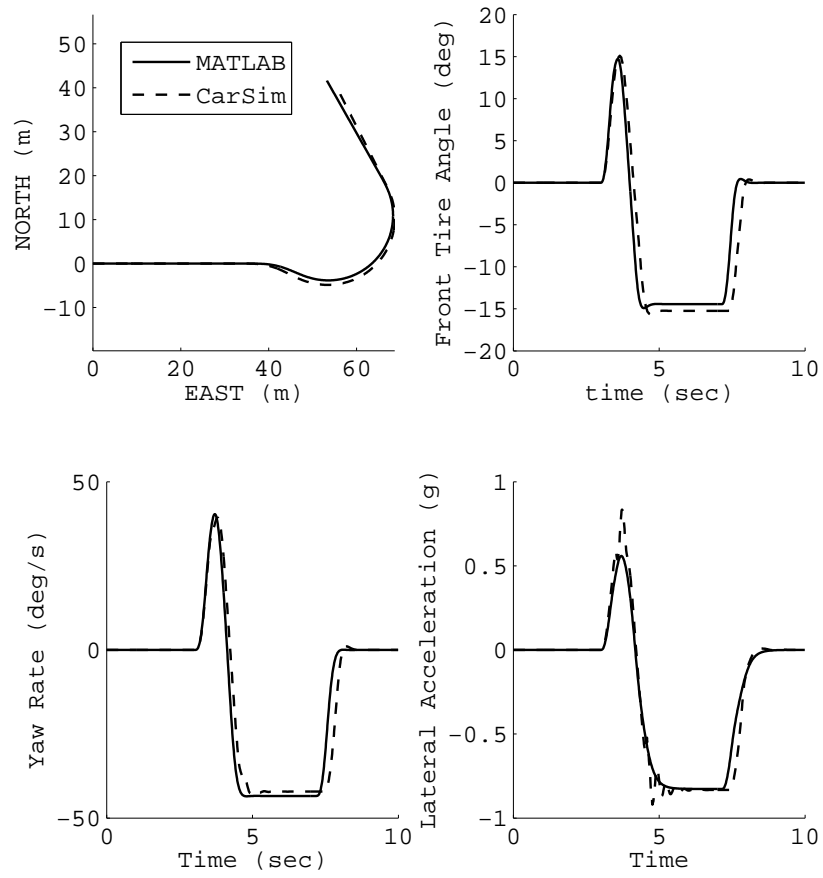


Figure 2.21: Comparison of the fishhook maneuver performed in MATLAB and CarSim

the properties that affect vehicle rollover and ESC systems can be inserted to the vehicle model to test how the rollover properties can be accounted for in the roll controllers.

CHAPTER 3
VEHICLE ROLLOVER FACTORS

3.1 Introduction

Several properties affect how a vehicle will perform during evasive maneuvers. With a good knowledge of these properties, rollover formulas can be derived and tested for accuracy. Testing can then be done with the rollover formulas to see if the maximum lateral acceleration and velocity before rollover are accurately predicted when vehicle properties such as CG height, track width, and understeer gradient are altered.

3.2 Vehicle Rollover Prediction Formulas

One important aspect of studying vehicle rollover is the knowledge of when a vehicle will rollover. In this chapter, two types of vehicle rollover formulas are to be discussed: the Static Stability Factor and another that is derived to predict when a vehicle will rollover, given some key vehicle properties.

3.2.1 Static Stability Factor

NHTSA's basic measurement of vehicle rollover propensity is the Static Stability Factor (SSF). This static test ignores all vehicle properties other than the center of gravity height and track width (the width between the left and right tires).

The SSF equation is derived by finding what lateral force would be required to push the vehicle over, when the outer wheel is tripped. Figures 3.1 and 3.2 show the diagrams

used during derivation. In Figure 3.2, there are no forces on the inner wheel since the FBD is made at the point where the vertical force on that wheel is zero.

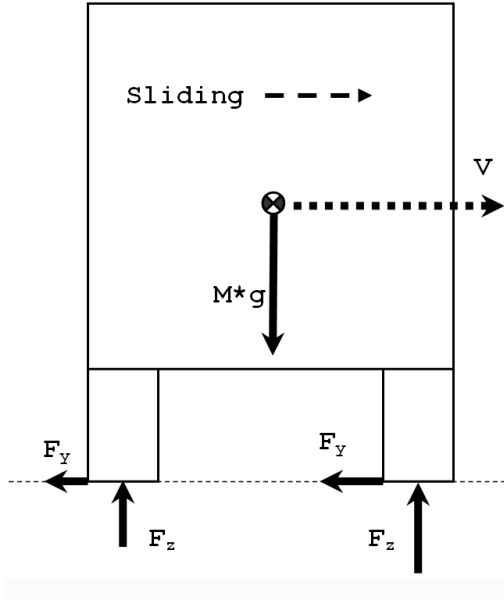


Figure 3.1: SSF Diagram - without roll

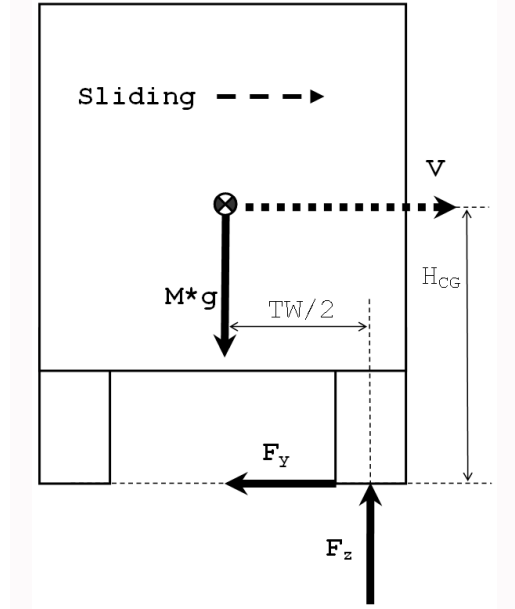


Figure 3.2: SSF Diagram - with roll

To begin developing the SSF equation, the forces in the horizontal and lateral directions are added and the moment is taken about the CG. Both are set to zero, since the system is considered to not be accelerating (i.e. in steady state).

$$\sum F_y = M * a_y = F_y \quad (3.1)$$

$$\sum F_z = M * a_z = M * g - F_z = 0 \quad (3.2)$$

Rearranging Equations (3.1) and (3.2), one can solve for F_y and F_z .

$$M * a_y = F_y \quad (3.3)$$

$$M * g = F_z \quad (3.4)$$

The moment is also taken at the center of gravity to complete analysis.

$$\sum M_{CG} = \frac{TW}{2} * F_z - H_{CG} * F_y = 0 \quad (3.5)$$

Rearranging Equation (3.5) and replacing values for F_y and F_z to get the SSF, the basic equation can be found.

$$H_{CG} * M * a_y = \frac{TW}{2} * M * g \quad (3.6)$$

The above equation can be further rearranged to solve for a_y to obtain the SSF equation. When a_y is divided by g , a unitless value is created with the value that is used as the Static Stability Factor. Equation (3.7) shows the formula for the SSF.

$$SSF = \frac{a_y}{g} = \frac{TW}{2 * H_{CG}} \quad (3.7)$$

This equation is essentially the value of lateral acceleration (in units of “g”s) needed to roll a vehicle when the friction coefficient is high enough to allow for tripping.

3.2.2 Static Vehicle Rollover Formula

In order to define a rollover threshold, an equation predicting the point of rollover would be greatly beneficial. Previous research has been done on the creation of a rollover prediction formula, however, little has been published with simulations or experimental data validating the formula [24, 23, 45, 32].

In order to do this without too much complexity, some assumptions must be made as well as some vehicle properties ignored. The first step is to define what is going to be considered when a vehicle rollover is eminent. Several ways to define vehicle rollover

detection have been previously published [25, 60], but for the purpose of creating a formula, rollover is to be considered eminent when a vehicle's normal force is distributed on only the outer tires of the vehicle (i.e. vertical forces on the inner tire become zero).

Another simplification that must be made is to eliminate the effects of suspension characteristics. By stiffening the suspension to a point of rigidity, the whole vehicle can be considered to be a solid mass and suspension transients is ignored. This not only removes suspension effects, it also throws out changes in CG height and lateral distance from the CG to the tires. Figure 3.3 shows how the forces are distributed over the simplified vehicle model.

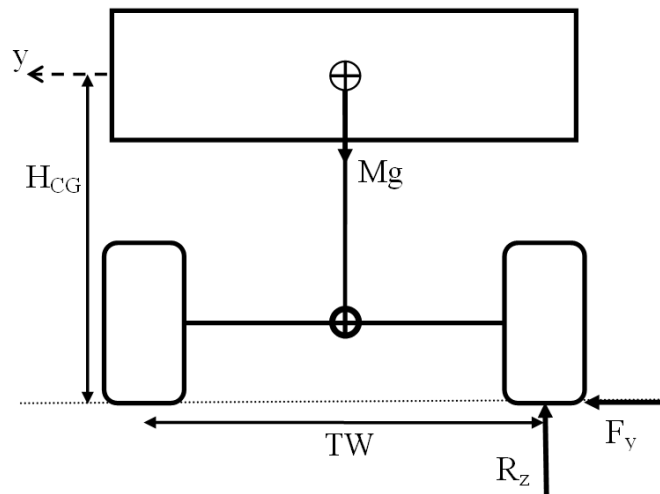


Figure 3.3: Diagram used for the derivation of the roll formula

With the simplified vehicle model, one can now take a summation of the forces in the vertical and lateral directions.

$$\sum F_y = M * a_y = F_y \quad (3.8)$$

$$\sum F_z = M * a_z = M * g - R_z \quad (3.9)$$

Rearranging equations 3.8 and 3.9, one can solve for R_y and F_z .

$$F_y = M * a_y = M * \frac{V^2}{R} = M * V * r \quad (3.10)$$

$$M * g = R_z \quad (3.11)$$

The moment can also be taken at the center of gravity to further the analysis.

$$\sum M_{CG} = \frac{TW}{2} * R_z - H_{CG} * F_y = 0 \quad (3.12)$$

By plugging in Equations (3.10) and (3.11) into equation (3.12), one can get an equation relating the track width, gravitational force, CG height, velocity, and yaw rate.

$$\frac{TW}{2} * M * g - H_{CG} * M * V * r = 0 \quad (3.13)$$

By simplifying and rearranging Equation (3.13), the following result is given:

$$\frac{TW}{2 * H_{CG}} = SSF = \frac{V * r}{g} = \frac{V^2}{R * g} \quad (3.14)$$

In Equation (3.14), the static stability factor of a vehicle can be compared to various vehicle properties. The equation can be rearranged further to estimate critical vehicle properties. If the CG height, track width, and yaw rate / radius of curvature are known, one can solve for the critical velocity that rollover will occur.

$$V_{Rollover} = \frac{TW * g}{2 * r * H_{CG}} = \sqrt{\frac{TW * R * g}{2 * H_{CG}}} \quad (3.15)$$

If the velocity, track width, and yaw rate / radius of curvature are known, one can solve for the critical CG height that rollover will occur.

$$H_{CG_{Rollover}} = \frac{TW * g}{2 * r * V} = \frac{TW * R * g}{2 * V^2} \quad (3.16)$$

If the velocity, CG height, and yaw rate / radius of curvature are known, one can solve for the critical track width that rollover will occur.

$$TW_{Rollover} = \frac{2 * H_{CG} * r * V}{g} = \frac{2 * H_{CG} * V^2}{R * g} \quad (3.17)$$

And finally if the velocity, CG height, and track width are known, one can solve for the critical yaw rate ($r_{Rollover}$) or radius of curvature ($R_{Rollover}$) that rollover will occur.

$$r_{Rollover} = \frac{TW * g}{2 * V * H_{CG}} \quad (3.18)$$

$$R_{Rollover} = \frac{2 * H_{CG} * V^2}{TW * g} \quad (3.19)$$

For the above equations to hold, the SSF value must be less or equal than the friction coefficient ($SSF \leq \mu$). This is a requirement since the vehicle will most likely slide out if μ is too low. When μ is too low, the frictional forces can become less than the lateral tire forces. Once this occurs, the tire slip angles become large and the tires and the vehicle will experience sideslip.

3.2.3 Inclusion of Suspension Effects

To include suspension effects, a look at the transients involved with weight transfer and suspension effects must be taken. When a vehicle is going around a turn, the center of gravity is shifted laterally outward, leading to a roll angle, and a change in the distance from CG to the contact patches on the wheels. Work has been previously done by Carlson and Gerdes [5], as well as Gillespie [23] to show the effects of dynamics of suspension and weight transfer in dynamic maneuvers.

To take the lateral shift of the CG into account, Gillespie uses a scalar to reduce the value of the SSF equation [23]. The equation that used in his work for the prediction of rollover turns into:

$$\frac{a_y}{g} = \frac{TW}{2 * H_{CG}} * \left[\frac{1}{1 + R_\phi * \left(1 - \frac{H_{RC}}{H_{CG}}\right)} \right] \quad (3.20)$$

The scalar that he added in [23], $\left[\frac{1}{1 + R_\phi * \left(1 - \frac{H_{RC}}{H_{CG}}\right)} \right]$, can be statically reduced using some known vehicle parameters. Gillespie states that for passenger cars, $\frac{H_{RC}}{H_{CG}}$ equals about 0.5 and the roll rate (R_ϕ) is generally around 6 degrees/g, or 0.1 radians/g. Substituting in these values into the above equation, the scale factor becomes around 0.95. In other words, the rollover threshold is reduced by about 5% due to transients involved with suspension dynamics.

Although the roll center and CG heights are vehicle specific, the reduction value will be assumed to be generally universal for passenger cars. For vehicles with a larger CG height and different suspension setups such as SUVs and trucks, a larger scale factor may be needed.

Gillespie continues saying that the rollover formula could be also altered from the addition of lateral tire deflection experienced in a turn. This effect could contribute to

another 5% reduction in possible lateral acceleration that a vehicle can handle before rollover. Testing in this thesis incorporates stiffer than normal tires, so that tire effects are minimal.

To include the suspension effects into the the SSF and rollover prediction formulas, a scale factor (κ) has been added. Effectively, the weight transfer and suspension geometry effects reduce the maximum rollover velocity.

$$SSF = \kappa * \frac{TW}{2 * H_{CG}} \quad (3.21)$$

$$V_{Rollover} = \kappa * \frac{TW * g}{2 * r * H_{CG}} = \kappa * \sqrt{\frac{TW * R * g}{2 * H_{CG}}} \quad (3.22)$$

With the knowledge acquired from Gillespie, the range of the scale factor would be from 0.9 to 0.95 since the vehicle is a typical SUV, where weight transfer is greater than a typical passenger car. The actual value of $\kappa = 0.92$ was chosen from an analysis of earlier simulation data taken from the vehicle.

3.3 Properties That Most Influence Vehicle Rollover Propensity

Several properties that are vehicle and road dependent play a role in the likelihood a vehicle will rollover during evasive maneuvers. Table 3.1 identifies the vehicle properties thought to have the greatest influence on vehicle rollover.

Table 3.1 - Properties Studied for Influence on Rollover Propensity:

CG Height
Track Width
Understeer Gradient
- Weight Split
- Tire Cornering Stiffness ratios (front/rear)
Suspension Stiffness
Friction Coefficients

Simulations were created in CarSim to test the vehicle roll formula derived above. In order to find the critical rollover velocity, a constant radius test was chosen, with a steady longitudinal acceleration of 0.833 m/s^2 . This maneuver not only allows for the precise control of the vehicle, it also removes any dynamic behaviors from vehicle transients that could further complicate the initial analysis performed in this section.

3.3.1 CG Height

The first property that is tested is the effect of CG height of the vehicle on rollover propensity. As shown in Figure 3.4, with all other properties held constant, the CG height is varied from 0.5 to 0.9 meters, in increments of 0.1 meters. For this simulation, the track width is 1.5 m, and the turn radius is 40 m. The simulation is run for each vehicle setup, and the lateral accelerations and longitudinal velocities of the vehicle are recorded and compared.

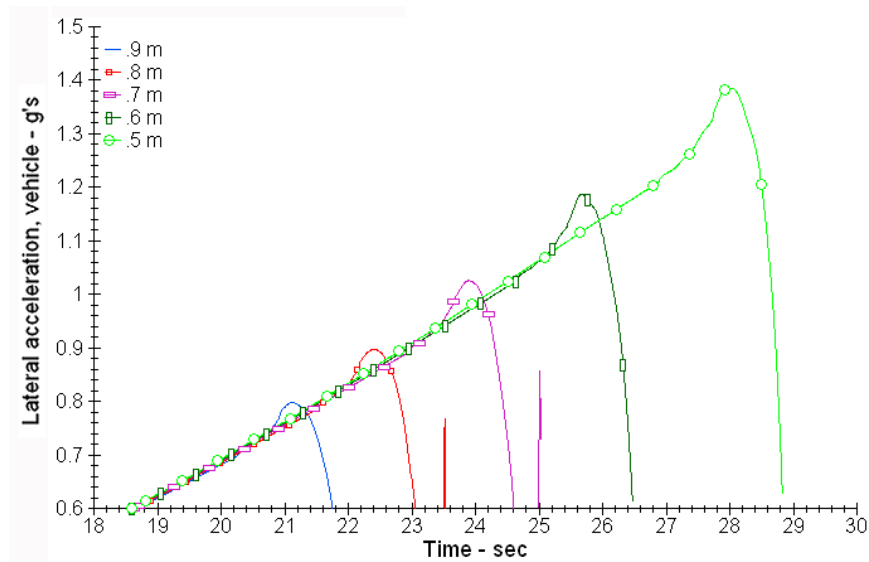


Figure 3.4: Lateral Acceleration during Constant Radius maneuver with changing CG heights

Table 3.2 - Lateral Accelerations with Changing H_{CG}

H_{CG} (m)	SSF	Rollover a_y	% Diff.
0.9	0.83	0.80	3.75 %
0.8	0.94	0.91	3.30 %
0.7	1.07	1.03	3.88 %
0.6	1.25	1.20	4.17 %
0.5	1.50	1.39	7.91 %

Values of the peak lateral acceleration from the simulation are compared to the SSF values in Table 3.2. The SSF of the vehicle provides an adequate measure of the maximum lateral acceleration achieved before rollover when CG height is varied on the rigid vehicle.

Figure 3.5 shows the results of the peak velocities during the maneuver.

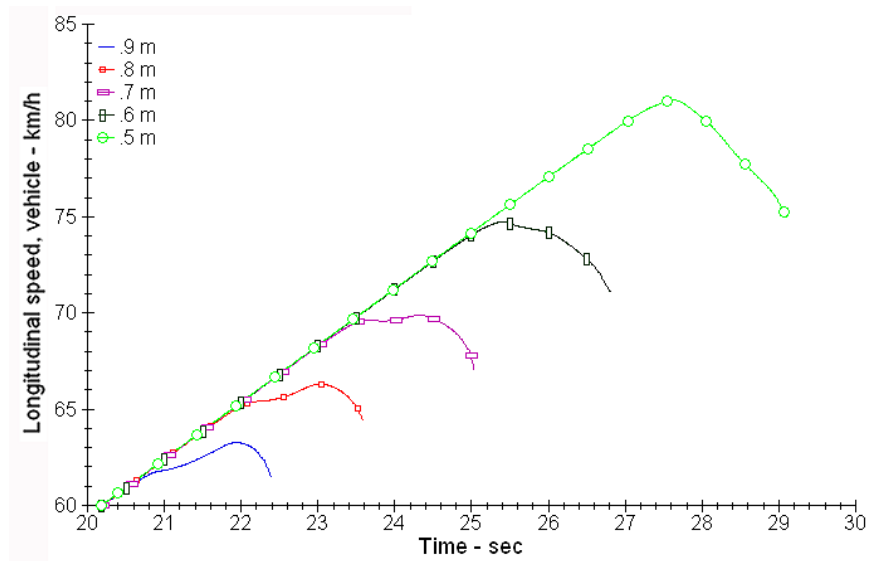


Figure 3.5: Rollover Velocities during Constant Radius maneuver with changing CG heights

With the values taken from the rollover testing, the peak velocities can be compared to the rollover Equation (3.15). Table 3.3 shows the values taken from simulation, as well as the solutions from Equation (3.15) and the percent difference of the two.

Table 3.3 - Critical Velocity Comparisons with Changing CG Height

H_{CG} (m)	$V_{Rollover}$ from Sim. (km/hr)	$V_{Rollover}$ from Eq. (km/hr)	% Diff.
0.9	63.4	65.1	2.6 %
0.8	66.4	69.1	4.1 %
0.7	69.8	73.8	5.7 %
0.6	74.8	79.7	6.5 %
0.5	81.2	87.3	7.5 %

One source for the discrepancy between the simulation and analytical prediction is the fact that the peak velocity for the vehicle in simulation is somewhere between two-wheel-lift, and a roll angle of 90° . This can be seen in Figures 3.5 and 3.6 where the peak velocities are not always well defined. It would be difficult to correctly extract the point of time when the vehicle's inner wheels were both off of the ground. Also, other sources of error could include tire deformation, slipping, and slight suspension deflection (which is not captured in Equation (3.22)).

To test the rollover equation with the effect of suspension transients, Figure 3.6 shows that there is a reduction in the maximum rollover velocity allowed by the vehicle in the constant radius simulation in CarSim. This trend is predicted using Equation (3.15) with $\kappa = 0.92$ and is shown in Table 3.4. The errors are reduced with the scale factor, and the rollover velocity predictions are adequate and acceptable.

In order to investigate the effect of CG height variations on a vehicle with transients caused by weight transfer and suspension characteristics, simulations were created and

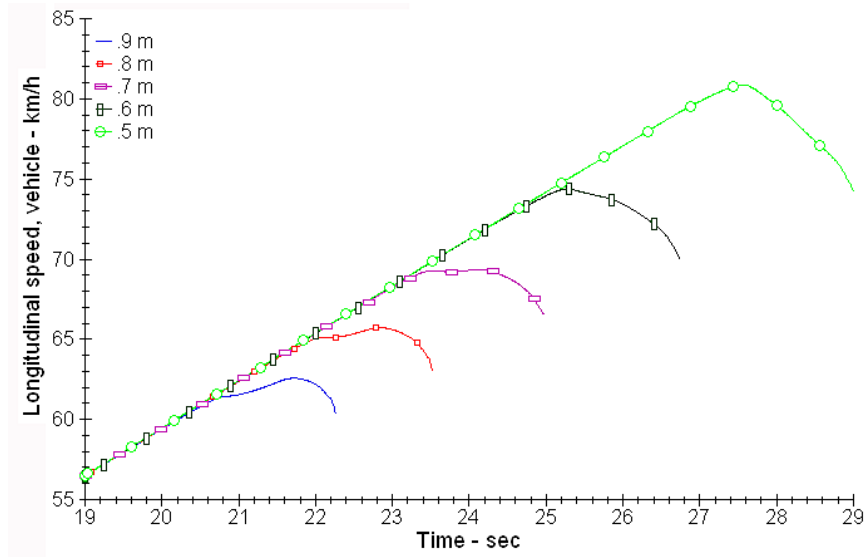


Figure 3.6: Rollover Velocities during Constant Radius maneuver with changing CG heights and weight transfer

Table 3.4 Critical Velocity Comparisons with Changing CG Height & Transients

H_{CG} (m)	$V_{Rollover}$ from Sim. (km/hr)	$V_{Rollover}$ from Eq. (km/hr)	% Diff.
0.9	62.7	59.9	4.7 %
0.8	65.6	63.5	3.3 %
0.7	69.1	67.9	1.8 %
0.6	73.7	73.3	0.5 %
0.5	80.2	80.3	0.1 %

run in MATLAB. Figure 3.7 shows the maximum velocities allowed before rollover in the fishhook maneuver.

The trend of lower rollover velocities for higher CG heights is the same for the dynamic testing in MATLAB, however the percent differences between the rollover velocities is larger. This is likely due to differences in suspension and tire characteristics in MATLAB and CarSim setups. One interesting trend that can be noticed is the slightly parabolic shape of the rollover velocities. Although the equation for SSF and rollover

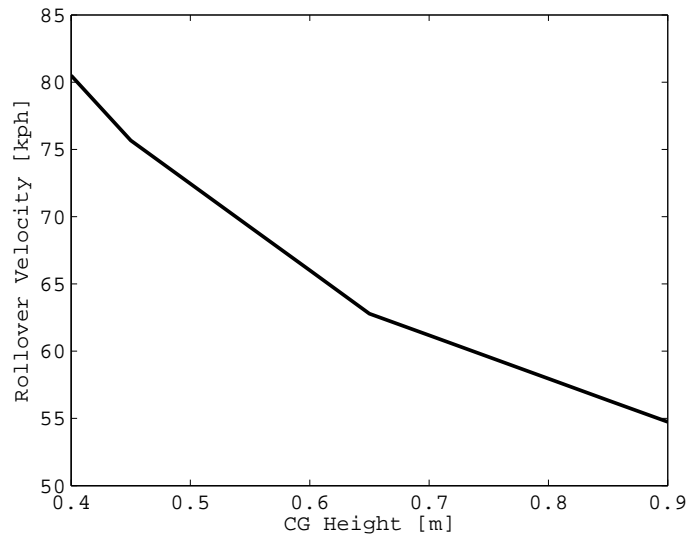


Figure 3.7: Rollover Velocities during Fishhook maneuver with varying CG heights and suspension effects (MATLAB simulation)

velocity is linearly dependent on the CG height, the simulation results show that the relationship is not exactly linear. This effect is likely due to the transients and suspension / tire deflection.

3.3.2 Track Width

The second property to affect rollover propensity that is tested is the track width of the vehicle. With all other properties held constant, the track width of the vehicle is varied from 1.2 to 1.7 meters, in increments of 0.1 meters. The simulation is again run for each setup, and the lateral accelerations and rollover velocities of the vehicle are recorded and compared to the other configurations. The rollover lateral accelerations are compared to the ones calculated from the SSF formula. The predicted values perfectly

Table 3.5 - Lateral Accelerations with Changing TW

H_{CG} (m)	SSF	Rollover a_y	% Diff.
1.2	1.00	1.0	0 %
1.3	1.08	1.08	0 %
1.4	1.17	1.16	0.8 %
1.5	1.25	1.26	0.8 %
1.6	1.33	1.34	0.7 %
1.7	1.42	1.42	0 %

fit to the simulated results. Figure 3.9 shows the results of the peak velocities during the maneuver.

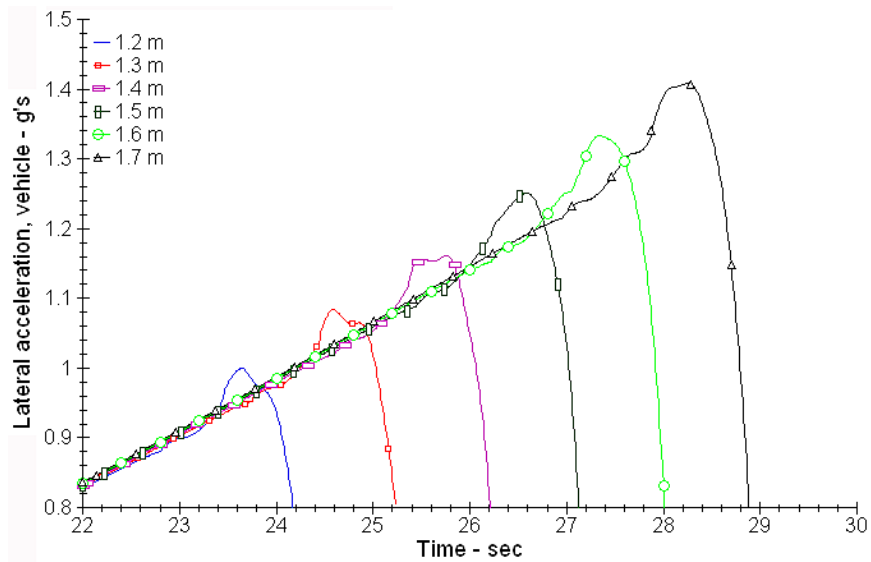


Figure 3.8: Lateral Acceleration during Constant Radius maneuver with a changing track width

This time, the differences in SSF and rollover lateral acceleration are lower than with the previous tests. Simulations are once again run to test the suitability of Equation (3.15) to track width variations. Figure 3.9 also contains better defined peaks of velocity

during the test maneuvers than the CG height variations. Again, other sources of error could include tire deformation, slipping, and slight suspension deflection.

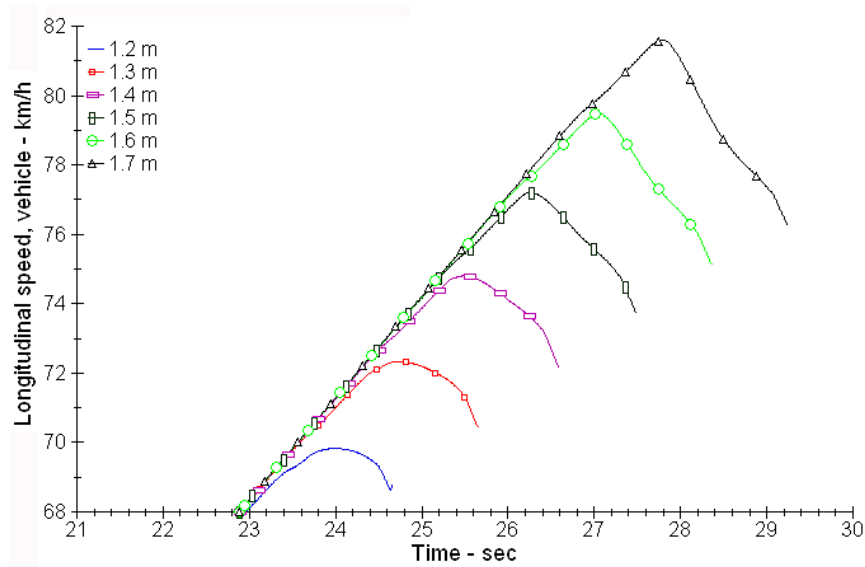


Figure 3.9: Rollover Velocities during Constant Radius maneuver with a changing track width

Again, the peak velocities can be compared to the rollover Equation (3.15). Table 3.6 shows the values taken from CarSim simulation, as well as the solutions from Equation (3.15) and the percent difference of the two analysis.

Table 3.6 - Critical Velocity Comparisons with Changing TW

TW (m)	$V_{Rollover}$ from Sim. (km/hr)	$V_{Rollover}$ from Eq. (km/hr)	% Diff.
1.2	69.8	71.3	2.1 %
1.3	72.4	74.2	2.5 %
1.4	74.8	77.0	2.9 %
1.5	77.2	79.7	3.2 %
1.6	79.6	82.4	3.4 %
1.7	81.6	84.9	4.0 %

Table 3.1: The rollover formula solutions versus the simulated rollover velocity

Testing is also done to see how suspension transients affect simulations with changes in track width. Here, the errors in the simulated rollover velocity and the velocity calculated from the modified rollover formula (in Table 3.7) are larger than without the weight transfer (in Table 3.6). This discrepancy could be fixed by altering the scale factor κ ; however, the scale factor is still a good fit for the overall results of the vehicle. Figure 3.3.2 shows the results when vehicle's suspension is added and is no longer considered rigid.

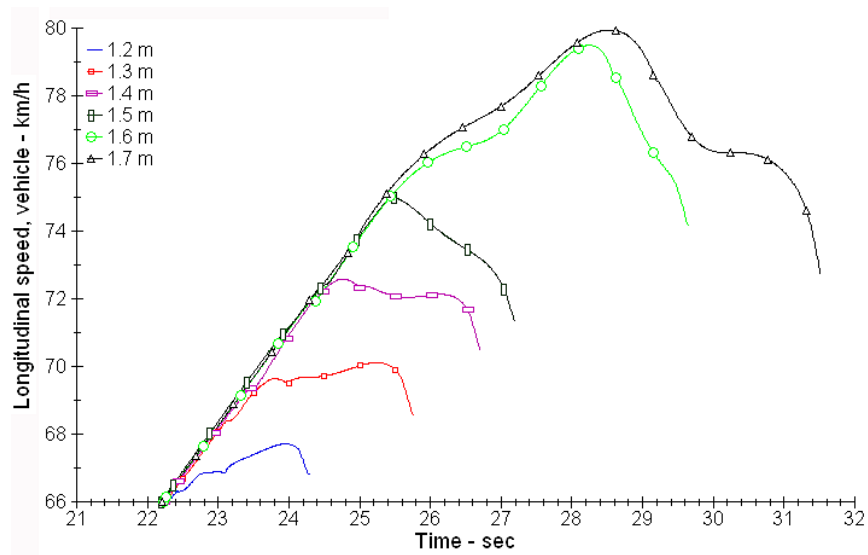


Table 3.7 - Critical Velocity Comparisons with Changing TW

TW (m)	$V_{Rollover}$ from Sim. (km/hr)	$V_{Rollover}$ from Eq. (km/hr)	% Diff.
1.2	67.6	65.6	3.0 %
1.3	70.1	68.3	2.6 %
1.4	72.4	70.9	2.1 %
1.5	75.0	73.4	2.2 %
1.6	79.2	75.8	4.5 %
1.7	79.8	78.1	2.2 %

Simulations were again done in MATLAB to verify the results from CarSim. In the fishhook maneuver, the change in track width once again created a linear relationship to rollover velocity. This is to be expected, since the predicted rollover velocity is directly proportional to the track width. The rollover velocities that occurred during the fishhook maneuver are more linear than with the changing CG height simulations. Another interesting occurrence shown in later simulations is the fact that all of the vehicle properties (a_y , ϕ , V_y , etc...) are similar, right up until the point of rollover.

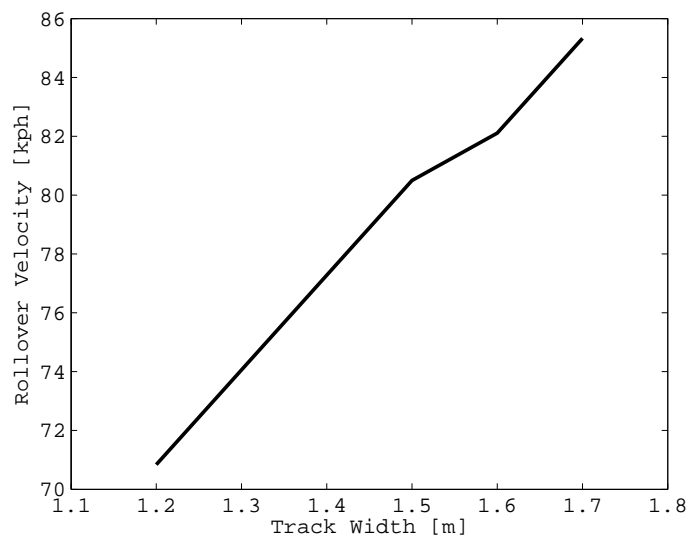


Figure 3.10: Rollover Velocities during Fishhook maneuver with changing TW and suspension effects

3.3.3 Understeer Gradient

The understeer gradient of a vehicle can greatly influence how a vehicle handles in a turn. The value is dependent upon vehicle and tire properties and suspension characteristics. This derivation of the understeer gradient follows the discussions published by

Rajamani and Gillespie [49, 23]. Figure 3.11 shows a diagram of a vehicle going around a turn at high speeds.

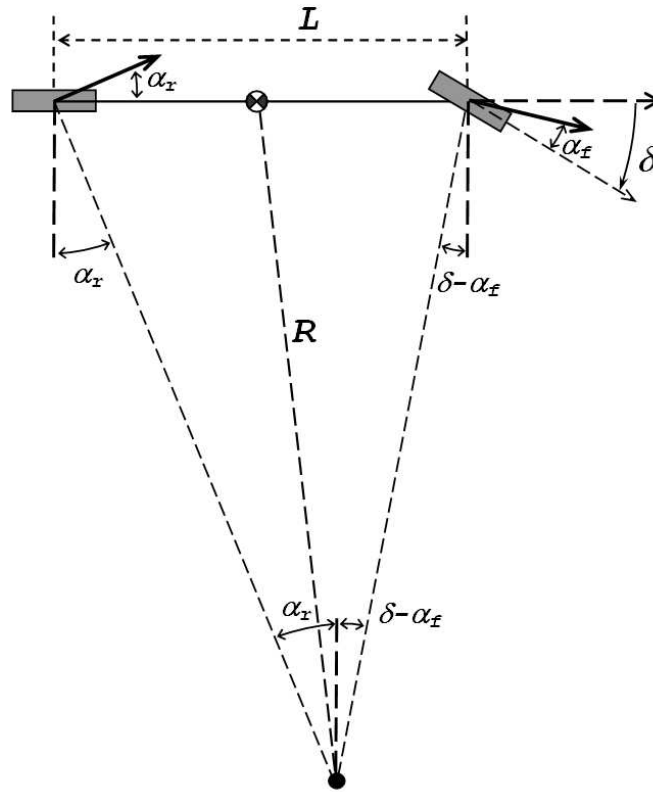


Figure 3.11: High-speed cornering with steer and slip angles

With the assumption that the turning radius is much larger than the wheel base of the vehicle ($R \gg L$), the following equation can be derived:

$$\delta - \alpha_F + \alpha_R = \frac{L}{R} \quad (3.23)$$

The equation can be rearranged to find the steer angle to hold the turn (similar to the Ackerman Steering Angle):

$$\delta = \frac{L}{R} + \alpha_F - \alpha_R \quad (3.24)$$

Note that δ is in terms of radians. If δ and α are in degrees, the equation becomes $\delta = 57.3 * \frac{L}{R} + \alpha_F - \alpha_R$. The slip angles α_F and α_R can be related to properties such as the turning radius (R) using the similar procedures as before. Using the small angle approximations, the following equations can be derived by summing forces in the lateral direction and taking the moment at the CG:

$$\sum F_y = MT * a_y = MT * \frac{V_x^2}{R} = F_{yF} + F_{yR} \quad (3.25)$$

$$\sum M_{CG} = F_{yF} * a + F_{yR} * b = 0 \quad (3.26)$$

Equation (3.26) can be rearranged and simplified to form the relationship between the front and rear tire forces.

$$F_{yF} = \frac{F_{yR} * b}{a} \quad (3.27)$$

After substituting the new lateral tire force relationship equation into Equation (3.25), the lateral force for the front tires can be put into terms of mass, velocity, and turning radius.

$$F_{yR} = MT * \frac{a}{L} * \frac{V_x^2}{R} = M_R * \frac{V_x^2}{R} = W_R * \frac{V_x^2}{g * R} \quad (3.28)$$

where M_R is the weight on the rear axle of the vehicle, calculated using the wheelbase and the distance from the CG to the front axle, i.e. $M_R = MT * \frac{a}{L}$. An equation for the front lateral tire forces can be made using the same relationships as above.

$$F_{yF} = MT * \frac{b}{L} * \frac{V_x^2}{R} = M_F * \frac{V_x^2}{R} = W_F * \frac{V_x^2}{g * R} \quad (3.29)$$

where M_F is the weight on the rear axle of the vehicle, calculated similarly to the method above, i.e. $M_F = MT * \frac{b}{L}$.

Next, it is assumed that slip angles are small, and a linear tire curve can be used so that the lateral tire forces are proportional to the slip angles, such that $F_y = C_\alpha * \alpha$. The slip angles can now be solved for, in terms of mass, cornering stiffness (C_α), velocity, and turning radius as shown below.

$$\alpha_F = \frac{F_{yF}}{2 * C_{\alpha F}} = \frac{W_F}{2 * C_{\alpha F}} * \frac{V_x^2}{g * R} \quad \alpha_R = \frac{F_{yR}}{2 * C_{\alpha R}} = \frac{W_R}{2 * C_{\alpha R}} * \frac{V_x^2}{g * R} \quad (3.30)$$

The slip angles can now be substituted back into the Equation (3.24) to produce the following relationship:

$$\delta = \frac{L}{R} + \alpha_F - \alpha_R = \frac{L}{R} + \left[\frac{W_F}{2 * C_{\alpha F}} - \frac{W_R}{2 * C_{\alpha R}} \right] * \frac{V_x^2}{g * R} \quad (3.31)$$

$$\delta = \frac{L}{R} + K_{us} * a_y \quad (3.32)$$

where:

$$K_{us} = \frac{W_F}{2 * C_{\alpha F}} - \frac{W_R}{2 * C_{\alpha R}} \quad (3.33)$$

The parameter K_{us} in the above equation is called the understeer gradient. The sign of the understeer gradient defines whether a vehicle is considered to be ‘‘Understeer’’ ($K_{US} > 0$), ‘‘Oversteer’’ ($K_{US} < 0$), or ‘‘Neutral Steer’’ ($K_{US} = 0$). Figure 3.12 shows how the steering angle is dependent upon the lateral acceleration of the vehicle for the three cases.

The properties that establish the understeer gradient are the weight split (the amount of weight on the front/rear) and the tire cornering stiffness ratio (front/rear)

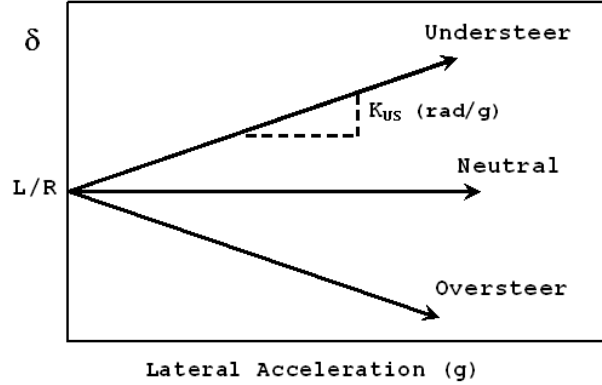


Figure 3.12: Steer angle variations with lateral acceleration

using the above relationship. In reality, K_{US} is a function of several vehicle properties since the cornering stiffness is a function of suspension, load, and other vehicle parameters. Gillespie defines two tests that adequately estimate the understeer gradient of a vehicle, while mirroring normal driving situations [23].

Using a constant radius test and multiple runs at varying velocities, one can derive the understeer gradient. By taking the derivative of Equation (3.32), one gets:

$$\frac{\partial \delta}{\partial a_y} = \frac{\partial(L/R)}{\partial a_y} + K_{US} * \frac{\partial a_y}{\partial a_y} \quad (3.34)$$

and since the radius of turn is constant, the first term cancels out.

$$K_{US} = \frac{\partial \delta}{\partial a_y} \quad (3.35)$$

With the above equation, the understeer gradient is in terms of the change in steer angle over the change in lateral acceleration. This can be easily seen in Figure 3.13, where

the vehicle is either understeer at all speeds (limit understeer), or is understeer at low lateral accelerations and becomes oversteer at higher values (limit oversteer).

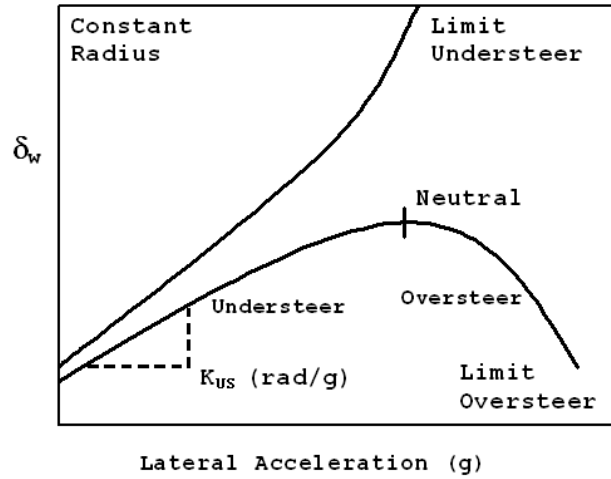


Figure 3.13: Example curve of the understeer test using the constant radius method

Using the constant speed method, one can derive the understeer gradient using maneuvers that mimic normal driving. By using Equation (3.32) again and substituting in the relationship $R = \frac{V^2}{a_y} - \frac{V}{r}$, one gets:

$$\delta = \frac{L}{R} + K_{US} * a_y = \frac{L * a_y}{V^2} + K_{US} * a_y \quad (3.36)$$

and the derivatives can be once again taken to get:

$$K_{US} = \frac{\partial \delta}{\partial a_y} - \frac{\partial(L/V^2)}{\partial a_y} \quad (3.37)$$

With the above equation, the understeer gradient is in terms of the change in steer angle and the change in lateral acceleration, since speed and wheelbase are constant. Figure 3.14 shows how it is determined if a vehicle is understeer or oversteer with this method.

The Ackerman steer angle gradient (the last term in the previous equation) is plotted on the figure with at a constant slope. Vehicles with δ values higher than the Ackerman steer angle are considered understeer, while lower values portray oversteer vehicles. See Gillespie [23] for a more detailed description of testing methods of K_{US} .

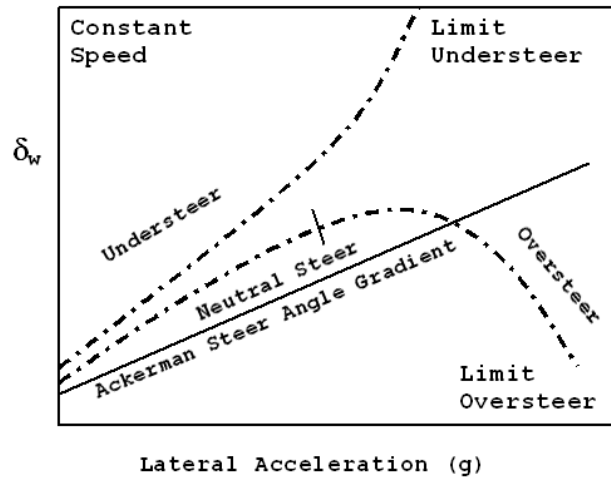


Figure 3.14: Example curve of the understeer test using the constant speed method

Understeer

Vehicles can be described as understeer when the understeer gradient, K_{us} , is greater than zero. The understeer gradient is defined as follows:

$$\frac{W_F}{C_{\alpha F}} > \frac{W_R}{C_{\alpha R}} \implies \alpha_F > \alpha_R \implies K_{us} > 0 \quad (3.38)$$

In a constant radius turn, an understeer vehicle requires an increasing steer angle with an increase in speed to maintain the constant radius turn. Most passenger cars are designed to be understeer, in order to allow the everyday driver to be able to handle the vehicle in evasive maneuvers.

Oversteer

Vehicles can be described as oversteer when the understeer gradient, K_{us} , is less than zero.

$$\frac{W_F}{C_{\alpha F}} < \frac{W_R}{C_{\alpha R}} \implies \alpha_F < \alpha_R \implies K_{us} < 0 \quad (3.39)$$

An oversteer vehicle will want to turn more when the vehicle's velocity is increasing (the back end wants to slide out). Vehicles are not usually designed to be oversteer due to driving difficulties associated with the setup. In the constant radius test, the steer angle in an oversteer vehicle would have to be decreased as the longitudinal velocity increases to maintain the CR turn.

Neutral Steer

Vehicles can be described as neutral steer when the understeer gradient, K_{us} , is equal to zero.

$$\frac{W_F}{C_{\alpha F}} = \frac{W_R}{C_{\alpha R}} \implies \alpha_F = \alpha_R \implies K_{us} = 0 \quad (3.40)$$

A neutral steer vehicle would optimize the handling characteristics during turning; however, a slightly understeer configuration is actually desired in production vehicles due to handling requirements.

Weight Split

Previous research has been done on the effects of the longitudinal location of the CG [59, 60, 61]. This property, known as weight split (WS), has been proven to play

a role in the rollover propensity (even though it is not captured in the SSF equation), especially in 15-passenger vans, trucks, and SUVs that have been overloaded toward the rear. The weight split of a vehicle is usually shown as a ratio of the weight on the front axle to the weight on the rear axle. For example, a vehicle with 60% of the weight on the front axle is referred to as a 60/40 WS vehicle.

Simulations in CarSim are performed with changing weight split. With the CG height set to 0.6 m and track width set to 1.5 m, the SSF is equal to 1.25. The maximum lateral accelerations, shown in Figure 3.15, show that the weight split and understeer gradient of a vehicle can influence rollover propensity.

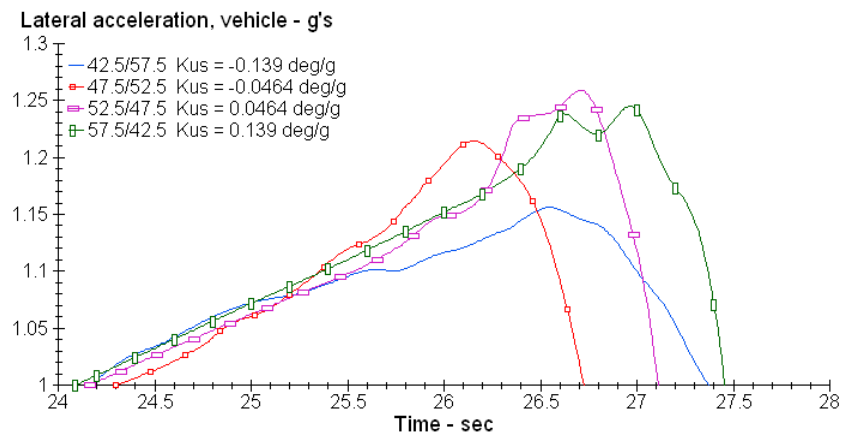


Figure 3.15: Lateral Acceleration during Constant Radius with a changing weight split

The oversteer vehicles roll earlier than the understeer vehicles; however, while the lateral accelerations for the understeer vehicles are close to the SSF predicted values, the oversteer vehicles have more error between the simulated and predicted values. The 42.5/57.5 WS vehicle has over a 13% error lateral acceleration when compared to the SSF value.

Longitudinal velocity can also be examined during the constant radius turn as well. Figure 3.16 shows the peak velocities attained before rollover occurs when the weight split is altered.

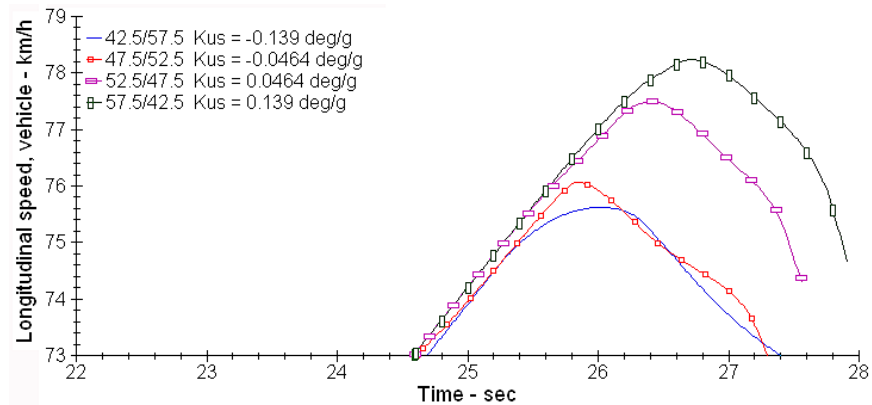


Figure 3.16: Rollover Velocities during Constant Radius with a changing weight split in CarSim

Since weight split is not taken into account in the rollover velocity formula, it is constant for all configurations of the vehicle. The results from simulation differ by only 2.6 km/hr, or 3.5 %. The inclusion of the understeer gradient into the rollover prediction formulas is discussed in greater detail in Section 3.4.

Tire Cornering Stiffness Ratios (front/rear)

The other property that affects the understeer gradient is the tire cornering stiffness ratio from front to rear. The cornering stiffnesses is not usually the same for vehicles since it is a factor of tire properties and forces. Additionally, one of the principal factors in tire cornering stiffness is inflation pressure. Due to the fact that drivers may not correctly monitor tire pressure, the cornering stiffness can be changed when the weight split remains neutral causing a noticeable difference in how a vehicle handles.

Figures 3.17 and 3.18 show how the vehicle is affected when the cornering stiffness ratio (front/rear) is altered and the friction coefficient is 1.25.

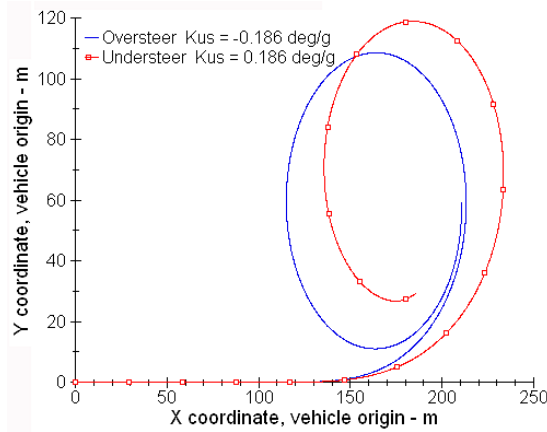


Figure 3.17: Position

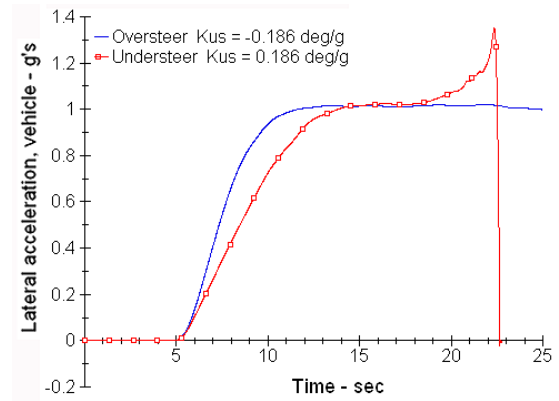


Figure 3.18: Lateral acceleration

When the front cornering stiffness is much greater than the rear (oversteer), the rear of the vehicle begins to slide out. This can be seen in Figure 3.17, where the turn radius for the oversteer vehicle is smaller than the understeer vehicle. Also the understeer vehicle with higher rear cornering stiffness eventually rolls, while the oversteer vehicle does not roll. Although large changes in the ratio of cornering stiffness does not happen often, it has been proven that it does affect vehicle rollover and handling.

3.3.4 Suspension Stiffness

Another factor that is investigated to test its influence on rollover is the suspension stiffnesses. Although this is not directly accounted for in the SSF or rollover velocity equations, it does affect how the weight transfer scale factor is decided. Variances in the suspension stiffness can affect how much or how little the CG of a vehicle will move in the lateral direction around a turn. This will in turn affect the cornering stiffnesses of

the vehicle, further changing the understeer gradient. With a soft suspension, the weight transfer will increase and the vehicle will likely roll over earlier.

Figure 3.19 shows the results of the lateral accelerations of a vehicle performing the steadily increasing steer maneuver with a varying suspension stiffness. As predicted, the vehicle with the soft suspension rolls when the lateral acceleration reaches 1.05 g. The vehicle with a medium suspension stiffness rolls around 1.2 g, and the vehicle with a stiff suspension rolls around 1.27 g.

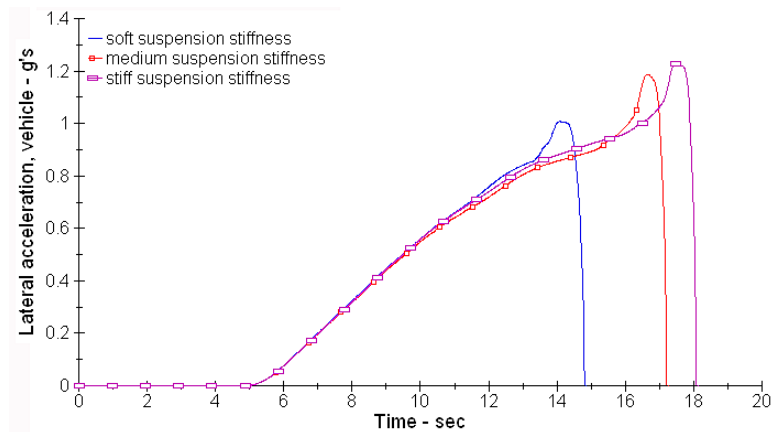


Figure 3.19: The lateral acceleration of a vehicle in the SIS maneuver with changing suspension stiffnesses

The maximum lateral accelerations could be predicted with the original and modified SSF formulas. For the rigid suspension, the SSF is equal to 1.25, an error of less than 2% from the simulated results. For the vehicle with the medium suspension stiffness, the modified SSF formula should be used with $\kappa = 0.92$. The SSF would become 1.15, giving a 4% error. With the loose suspension, the scale factor should be altered to account for the increased weight transfer. With $\kappa = 0.88$, the SSF is then 1.1 g, an error of around 5% when compared to the results from figure 3.19.

Simulations in CarSim were then performed to test the effects of suspension stiffness during dynamic maneuvers. As expected, the vehicle with the soft suspension rolled earlier than the other two configurations. Figures 3.20 and 3.21 show the vehicles' performances during the fishhook maneuver.

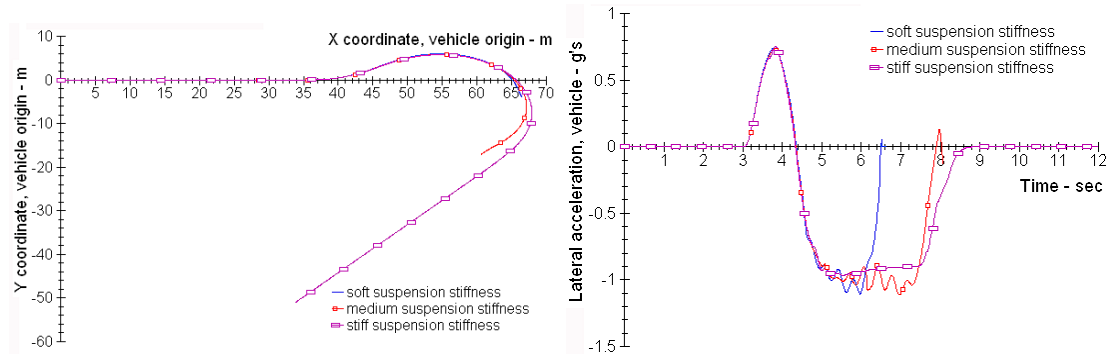


Figure 3.20: Paths of vehicles with varying suspension stiffnesses

Figure 3.21: Lateral accelerations of vehicles with varying suspension stiffnesses

Both the vehicles with soft and medium suspension stiffnesses rolled during the simulations. The soft suspension caused the vehicle to rollover soon after the second steer input, while the medium suspension allowed for the vehicle to hold the turn longer. Both vehicles that rolled had some oscillatory behavior before rollover. This could likely be avoided by increasing the damping of the vehicles' suspensions. On the other hand, the vehicle with the rigid suspension was able to complete the fishhook maneuver without rolling.

3.3.5 Friction Coefficients

The last property to be analyzed for vehicle rollover tendencies is the friction coefficient between the tire and ground. It is widely known that with a slick surface, a vehicle will slide out before rollover has a chance to take place. This behavior is due to the fact

that a slick surface has a low friction coefficient (μ). On a wet or icy road, μ can be as low as 0.3 (limiting the maximum lateral acceleration to 0.3 g), while a dry surface has a coefficient of around 1. For some of the testing done in this thesis, the coefficient was increased to 1.3 or greater in order to ensure the incidence of rollover.

Figure 3.22 shows simulations of the fishhook maneuver created in CarSim. When the friction coefficient is 0.3 and 1.0, the vehicle tends to slide and rollover does not occur; but when the coefficient is 1.3, the vehicle rolls right after the second steer input is applied. This is due to the fact that the overall tire force applied is greater than the lateral acceleration applied.

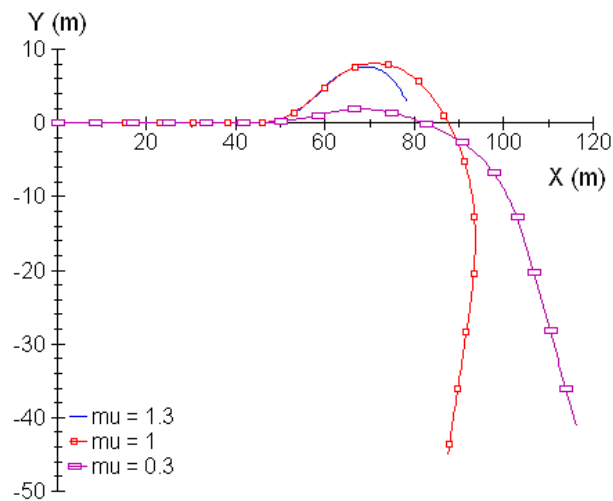


Figure 3.22: The positions of a vehicle in the fishhook maneuver with changing friction coefficients

Using Equation (2.34) can be used to help predict the occurrence of sliding and of rollover likelihood. Since $F_{tire} \leq F_z * \mu$, if the $SSF \leq \mu$, there is a large chance that rollover could occur. However, if the $SSF > \mu$, chances of rollover are reduced due to the fact that the vehicle will most likely slide before an untripped rollover will occur.

3.4 The Inclusion of Understeer Gradient Into the Prediction of Rollover

It was shown in Section 3.3.3 that the understeer gradient plays a role in vehicle rollover propensity. To further improve the rollover prediction formulas, the effects of the understeer gradient should be taken into account. Although it sounds simple, modifying the rollover velocity equations into a form that includes the understeer gradient greatly increases their complexity. In addition to seeking a simpler form of these equations, an investigation into empirical data taken from simulation was done to look for trends in the data that could be simply inserted into the rollover prediction equations.

3.4.1 Simulation Results

In order to further investigate the effects that understeer gradient has upon vehicle rollover, more simulations were created using CarSim. The Constant Radius and Fishhook maneuvers were chosen for their ability to analyze the vehicle quasi-static and dynamic behaviors in rollover cases. The friction value used in the simulations was set to 1.5, a high value chosen to ensure enough lateral force to allow the vehicle to rollover.

For the first case, four vehicle setups were chosen, with alterations only in weight split. Figure 3.23 displays the rollover velocities for the different vehicle configurations. For both maneuvers, the rollover velocity increased as the weight was shifted forward. This trend will be discussed further in Subsection 3.4.2.

For the changing tire cornering stiffness case, three vehicle setups were chosen. Figure 3.24 displays the rollover velocities for the understeer, neutral steer, and oversteer conditions. For the constant radius maneuver, the rollover velocity remains almost constant as the vehicle setup changes. As before, the fishhook maneuver results in a linear

increase in rollover velocity as the vehicle becomes understeer. This trend will also be discussed further in Subsection 3.4.2. The discrepancy in the CR and Fishhook maneuver trends shows why it is difficult to derive an equation that predicts rollover with changing values of understeer gradient.

3.4.2 Empirical Trends

In Figures 3.23 and 3.24, it is shown that trends in the rollover velocity as a function of K_{US} show up in the data. Although the trends are not completely uniform for all of the simulation results, their linearity shows that a scale factor based upon the understeer gradient could improve the estimated rollover velocities. By adding the scale factor $(1 + K_{US})$ into Equation (3.15), the velocities predicted fit the empirical data better than the prior method.

$$V_{Rollover} = \kappa * \frac{TW * g}{2 * r * H_{CG}} * (1 + K_{US}) = \kappa * \sqrt{\frac{TW * R * g}{2 * H_{CG}}} * (1 + K_{US}) \quad (3.41)$$

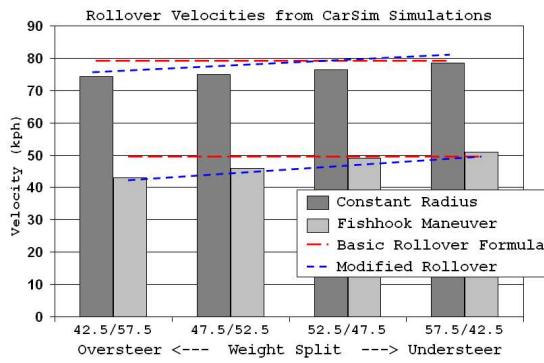


Figure 3.23: Rollover velocities with varying Weight Splits

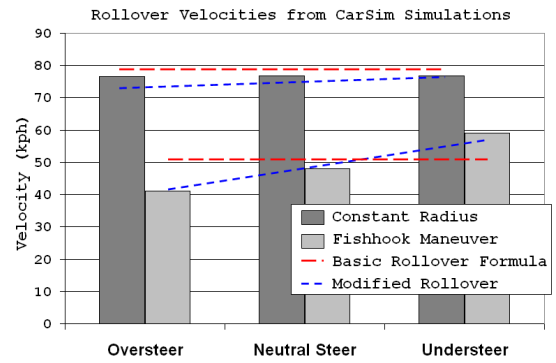


Figure 3.24: Rollover velocities with varying C_{α} Values

Table 3.8 compares the critical rollover velocities from CarSim simulations to the predicted values found using Equation (3.41). Using the derived rollover equation, the estimated rollover velocity for all of the vehicle configurations with changing WS would be 79.7 kph for the CR maneuver, and 49.6 kph for the Fishhook maneuver. However, with the modified equation, the value is scaled for each setup. Although the total error is about the same, the predicted values follow the trend shown from the CarSim results.

Table 3.8 - Critical Rollover Velocity for Changing Weight Splits (kph)

<i>Constant Radius</i>						
WS (F/R)	$K_{US}(deg/g)$	CarSim	Eq. (3.15)	% err.	Eq. (3.41)	% err.
42.5 / 57.5	-0.139	74.2	79.7	7.4 %	71.6	3.6 %
47.5 / 52.5	-0.0464	74.7	79.7	6.7 %	72.8	2.5 %
52.5 / 47.5	0.0464	76.2	79.7	4.6 %	74.0	2.9 %
57.5 / 42.5	0.139	78.2	79.7	1.9 %	75.0	4.3 %
<i>Fishhook</i>						
42.5 / 57.5	-0.139	43	49.6	15.3 %	42.9	0.2 %
47.5 / 52.5	-0.0464	46	49.6	7.8 %	44.4	3.6 %
52.5 / 47.5	0.0464	49	49.6	1.2 %	46.9	4.5 %
57.5 / 42.5	0.139	51	49.6	2.8 %	49.6	2.8 %

Somewhat similar results were found when changing values of tire cornering stiffness. Using the basic derived equation, the critical rollover velocity for the all of the vehicle setups is 79.7 kph for the CR maneuver, and 51.6 kph for the fishhook maneuver. Table 3.9 shows the results of the critical velocities when the changes in understeer gradient are included. The results for Equation (3.41) are not as consistent for this case as the previous, partially due to the data taken from the CarSim simulations. Although the critical velocities change a good deal in the fishhook maneuver, they are almost constant in the constant radius maneuver. The errors are however greatly reduced when the understeer gradient is taken into account for the Fishhook maneuver.

Table 3.9 - Critical Rollover Velocity for Changing $C\alpha$ Values (kph)

<i>Constant Radius</i>						
Config.	$K_{US}(deg/g)$	CarSim	Eq. (3.15)	% err.	Eq. (3.41)	% err.
Oversteer	-1.82	76.6	79.7	4.1 %	71.0	7.9 %
Neutral Steer	0.0	76.8	79.7	3.8 %	73.3	4.8 %
Understeer	1.82	76.7	79.7	4.0 %	75.7	1.3 %
<i>Fishhook</i>						
Oversteer	-1.82	41	51.6	25.9 %	41.4	1.0 %
Neutral Steer	0.0	48	51.6	7.5 %	47.5	1.0 %
Understeer	1.82	59	51.6	14.3 %	56.0	5.3 %

It could be argued that the high friction coefficient could be the reason that the trends are not completely universal for the changing understeer gradient values. In order to examine this, the same simulations were run with different friction coefficients (1.3, 1.25, 1.2, 1.0). In these cases, some or all of the vehicles ended up sliding excessively and not completing the desired maneuver. Since the research presented in this thesis is focused on vehicle rollover, an in-depth analysis into the sliding of the vehicle will not be further discussed.

Despite the trends only being shown with empirical results, the rollover prediction formula is improved with the understeer gradient scale factor included. Work is continuing on the investigation of an improvement to Equation (3.41).

3.5 Conclusion

In this chapter, the Static Stability Factor was derived, and modified to include the effects of transients due to weight transfer and suspension configurations. Formulas were derived for the rollover threshold as a function of critical rollover properties, such as velocity, track width, CG height, and radius of turn/yaw rate. Although simulations

were created to test the validity of the rollover velocity equation, testing could have as well been done to examine Equations (3.16)-(3.19). The simulations created in CarSim and MATLAB verified the formula's accuracy for predicting the velocity before rollover. With the knowledge of the effects of key vehicle properties on rollover, research can now be done to see how electronic stability controllers are affected by variances these properties.

CHAPTER 4

ELECTRONIC STABILITY CONTROLLER DEVELOPMENT

4.1 Introduction

It is well known that Electronic Stability Controllers (ESC) have been saving lives throughout the last decade [27]. In a recent mandate by NHTSA, ESC will be required to be in all new vehicles by the 2012 model year (2011 calendar year) [41]. Despite the new requirements, some companies have decided to make it a standard feature earlier than the required date. For example, Ford Motor Company is making ESC standard in all passenger vehicles by the end of 2009 [18].

Previous research into the effectiveness of ESC systems shows that the technology saves lives [1, 34, 33, 58]. Over the last century, the IIHS has also looked into crash data and found that ESC has saved lives on US highways. This chapter discusses the basics of ESC systems, types of ESC systems, and the derivation of various types that have been explored in simulation in this thesis. The simulations in this chapter were created in MATLAB with the vehicle model derived in Chapter 2.

4.2 ESC Basics

ESC is an extension of Anti-Lock Brake systems (ABS), using similar sensors and actuators. In Figure 4.1, the sensors used in a typical ESC system are shown. With the yaw rate, steer angle, lateral acceleration, and wheel speed measurements, the ESC can estimate the vehicle's course, and decide if the error in course (where the vehicle is pointed) and heading (where the vehicle is traveling) is too large (i.e. sideslip or lateral

velocity). If the error is larger than a predefined limit, the ESC system is triggered, and the vehicle reacts to reduce the understeer or oversteer error.

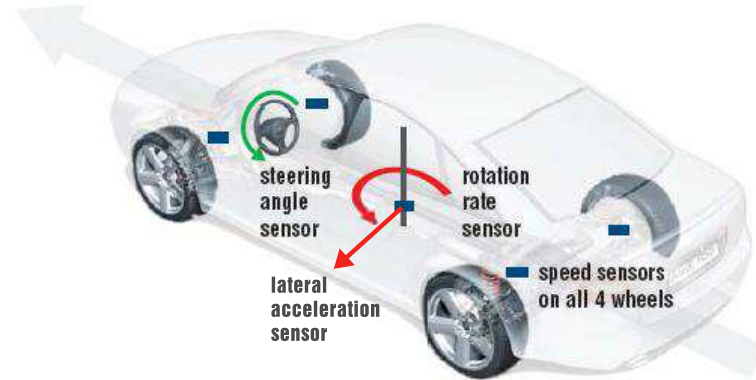


Figure 4.1: ESC sensors diagram. Source: IIHS [53]

4.3 ESC Types

Several types of ESC are currently being implemented in today's vehicles. With the predicted number of lives saved, as well as the proven success rate, there are obvious reasons for ESC systems to be in every ground vehicle. Table 4.1 shows the types of Stability Controllers tested in this thesis using the simulations created in MATLAB. The systems begin with simple power reduction controllers, and then become more complex with variable braking and steering control [4, 57, 63, 35, 17].

Table 4.1 - ESC Types:

Power Reduction
All-Wheel Braking
Independent Wheel Braking
Active Torque Distribution
Steering Modification
Steering Modification with All-Wheel Braking
Independent Wheel Braking with Steering Control

4.4 Stability Threshold

In order to keep the vehicle in a safe region, the limits on handling must be defined. Several vehicle properties that predict rollover can be observed, but not all are easy to measure. For example, the simplest property that would anticipate rollover is the vertical forces on the tires. When rollover occurs, it is always preceded by the vertical force on the inner tires of the vehicle going toward zero. In actuality, the vertical forces on a tire are hard to measure at best. To set a limit on vehicle stability, easily measured properties must be used.

From simulation results, it has been shown that vehicle rollover is also preceded by higher than normal values of lateral acceleration and yaw rate. If an ESC system is to set a limit on the maximum value of lateral acceleration and yaw rate allowed, the controller would have an easily measurable, accurate method of stability enhancement. It would also be possible to measure roll rate for an estimate of roll, which could in turn be used in the ESC system. The sensors used, a lateral accelerometer and a gyroscope, are also being installed into more production vehicles today than ever, due to lowering production and installation costs.

4.5 Power Reduction

The most basic type of controller used for stability maintenance is the power reduction controller. When an unsafe level of lateral acceleration or yaw rate is detected, the torque delivered from the engine is reduced on all drive wheels, slowing the vehicle to a safer level of dynamics to prevent rollover.

Simulations in MATLAB show how effective the controller can be. Figure 4.2 displays how the vehicle reacts when the controller is applied during the fishhook maneuver, causing a reduction in velocity. In this simulation, the engine torque was limited when the vehicle reached a magnitude of 0.4 g of lateral acceleration.

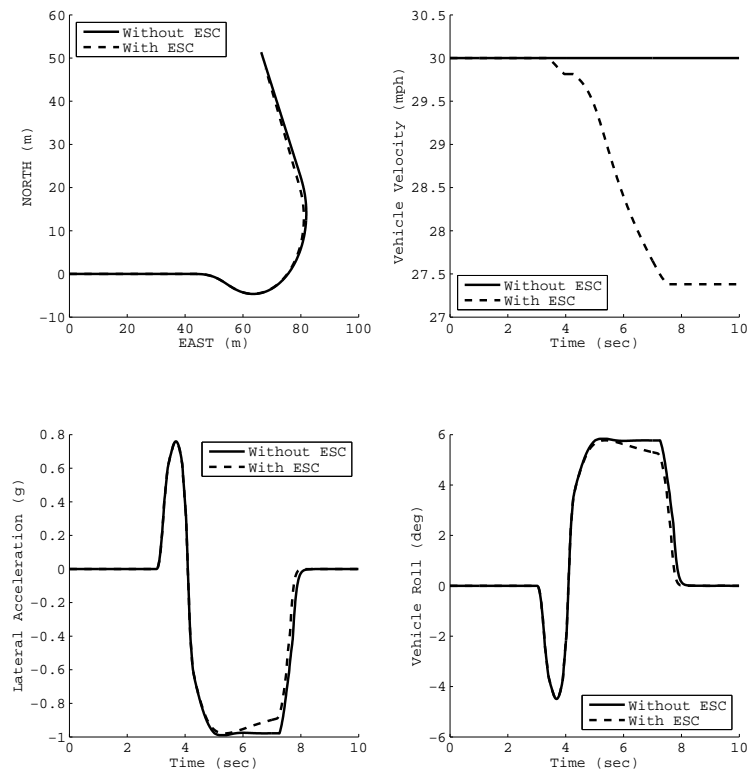


Figure 4.2: The vehicle's performance with the power reduction controller

A negative aspect of the controller is that it is often too weak to keep the vehicle stable during evasive maneuvers. In Figure 4.2, the lateral acceleration and roll angle are only slightly reduced by the controller. By only limiting the power fed to the tires, the

vehicle may not be slowed enough to prevent rollover at higher speeds. Adding braking torques to the engine power reduction can increase the ESC's effectiveness.

4.6 All-Wheel Braking

The all-wheel braking controller is somewhat similar to the power reduction controller; however, instead of only reducing the positive driving torques, a braking force is applied to all four wheels. Figure 4.3 shows how the all-wheel braking controller can keep the vehicle in the stability threshold during the evasive maneuver.

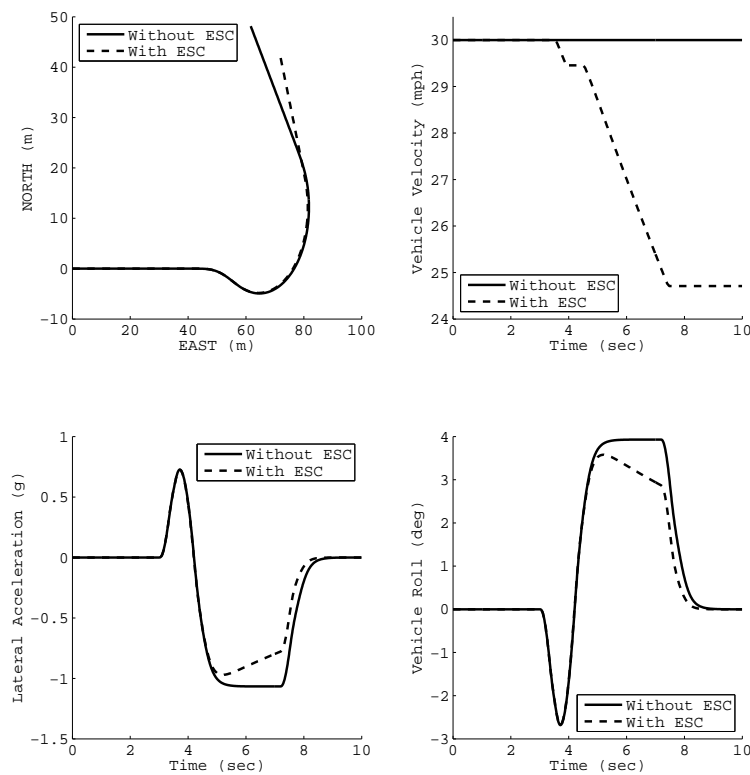


Figure 4.3: The vehicle's performance with the all-wheel braking controller

Figure 4.4 displays the braking forces applied to the vehicle during the maneuver. The ESC implemented in this simulation contained a two stage system, where the first stage limits the lateral acceleration to 0.3 g. Once that value is reached, a braking force of 667 N is applied at the contact patch of every wheels (200 N-m of torque). The second stage is triggered once the lateral acceleration reaches or exceeds 0.45 g. A braking force of 1500 N is then applied at each tire (450 N-m of torque). These braking forces were backed out of previous test data where hard braking occurred, and simulations were created to justify the results.

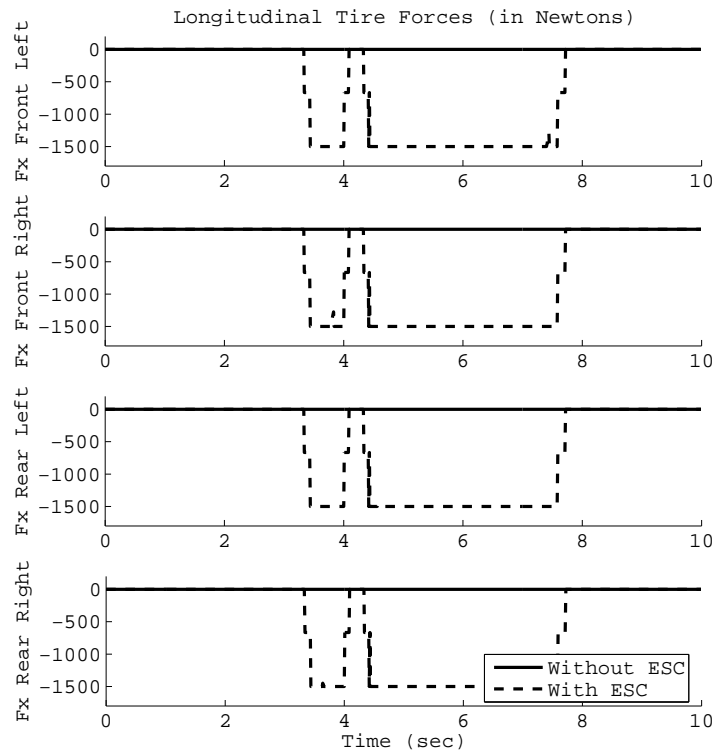


Figure 4.4: The vehicle's braking forces with the all-wheel braking controller

The all-wheel braking controller's simplicity allows it to be added to any vehicle with computer controlled braking. Drawbacks of the controller are similar to the power reduction controller. Although the controller should have enough braking torque to greatly reduce the vehicle's velocity during an evasive maneuver, the vehicle may have too much weight transfer to effectively prevent rollover. The controller also adds increased longitudinal wheel forces, which can cause tire saturation and lock-up or sliding, due to the friction circle limits discussed previously in Chapter 2. The controller can be made much more effective by adding individual wheel braking torques. Independent braking requires separate brake modules for each wheel, but it's popularity is growing.

4.7 Independent Wheel Braking

A proper vehicle ESC system should include the ability to control the speeds of individual wheels. With the added degree of control, torques can be applied to the wheels that would more accurately keep the vehicle in the stability region. By putting a braking torque on specified wheels during a turn, the vehicle's yaw rate error can be controlled more than by applying the braking torque to all wheels. Additionally, the vehicle's longitudinal velocity is reduced, resulting in a reduction in lateral acceleration and yaw rate among other things. The underlying property that is used in this controller is brake steer [46]. By braking the wheels on one side of the vehicle, an added moment is applied, and the vehicle's yaw rate will be reduced or enlarged, depending on the need.

4.7.1 Controller Development

In order to understand how the vehicle will behave when certain wheels are braked, a free body diagram is created, and the moments are taken about the CG. Figure 4.5

shows the FBD used for the brake steer derivation. The steer angle is assumed to be small enough to discount its effects upon the longitudinal braking forces. With the brake steer moment and the difference in desired and actual yaw rate, the controller has enough information to apply braking forces to reduce the yaw error.

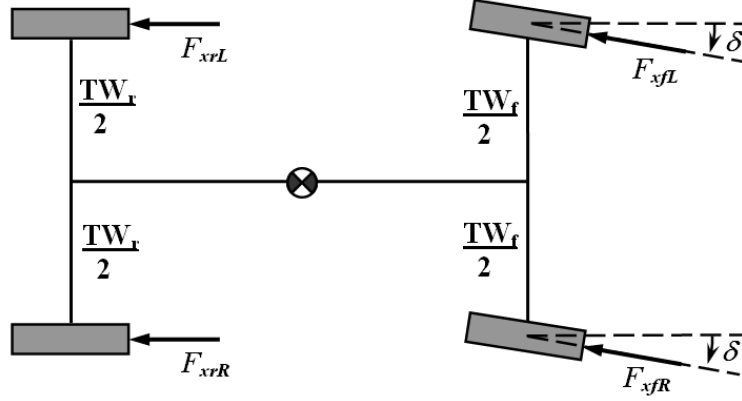


Figure 4.5: The FBD used for the derivation of brake steer moments

Using the FBD in Figure 4.5, and assuming that the steer angle (δ) is small, the following moment can be calculated:

$$M_{BS} = \frac{tw_f}{2} * [F_{x_{fR}} - F_{x_{fL}}] + \frac{tw_r}{2} * [F_{x_{rR}} - F_{x_{rL}}] \quad (4.1)$$

$$M_{BS} = \frac{tw_f}{2} * F_{BS_f} + \frac{tw_r}{2} * F_{BS_r} \quad (4.2)$$

Independent braking has been well studied for the application in ESC systems [7]. If the vehicle is oversteer, the outer wheels will be braked in a turn to decrease the vehicle's yaw rate and reduce the error in the vehicle's course and heading. Alternately, if the vehicle is understeer, the inner wheels will be braked to increase the vehicle's yaw rate and reduce the error in the vehicle's course and heading. Figure 4.6 shows how a typical independent wheel braking controller works. The application of braking torques to

independent wheels can be varied to increase the effectiveness of the stability controller. Depending on the level of lateral acceleration and yaw rate, the brake pressures could be altered in order to achieve maximum performance while turning.

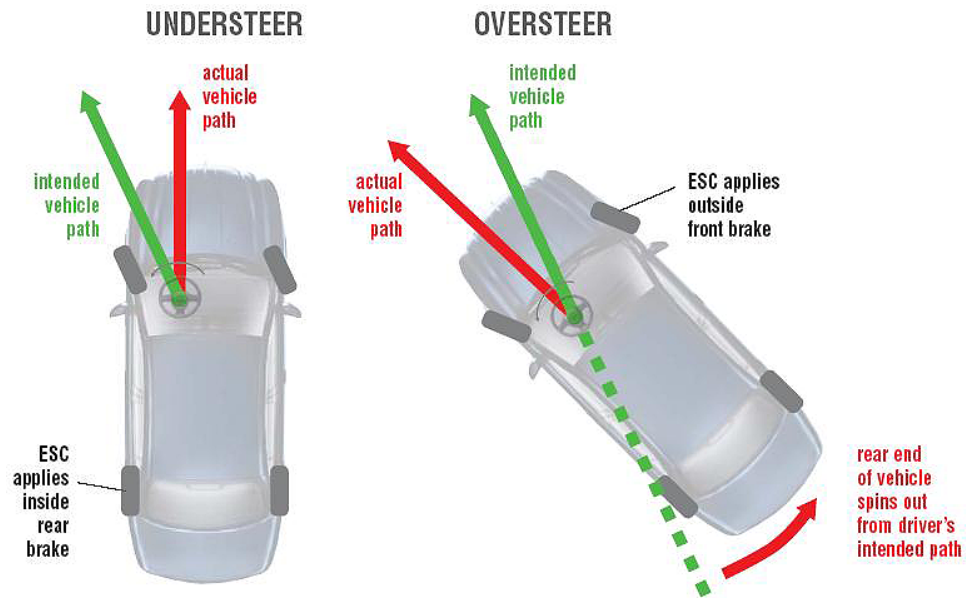


Figure 4.6: ESC with independent wheel braking. Source: IIHS [53]

4.7.2 Controller Behavior

From the derived controller with independent wheel braking, one can see how the vehicle reacts in Figure 4.7. For the understeer vehicle modeled, the controller applies a variable braking torque to the inner wheels of the vehicle when the stability threshold is compromised (once again set to 0.4 g of lateral acceleration). The control gains were not optimized for the research in this thesis and therefore additional improvement could be possible with careful study and implementation.

Although Figure 4.6 shows one wheel being braked, the simulations created in MATLAB used braking on both front and rear wheels on one side of the vehicle, depending

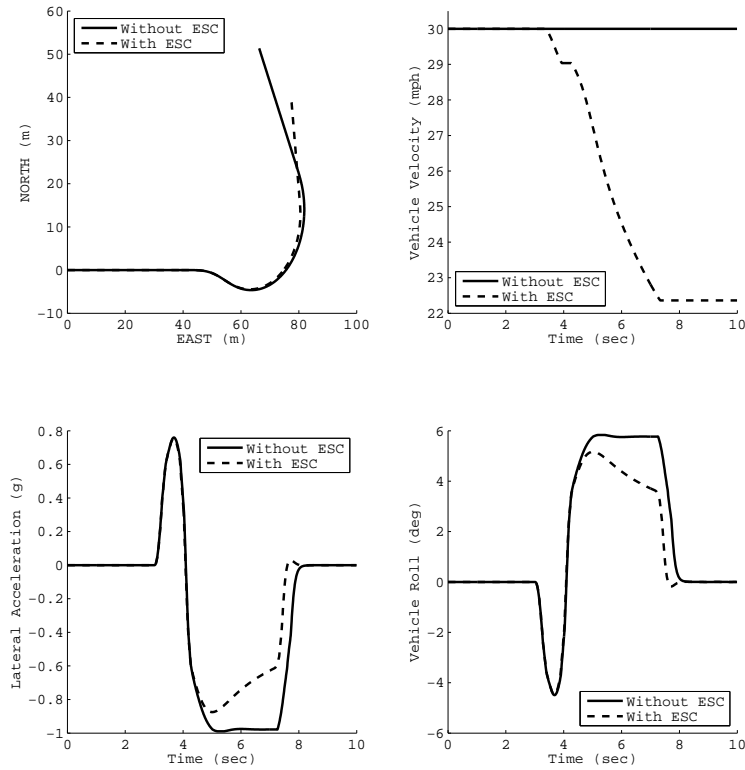


Figure 4.7: The vehicle's behavior with the independent wheel braking controller

upon the understeer / oversteer conditions. Early results showed that the controller is more effective with the added braking forces from two wheels rather than from just one wheel. Figure 4.8 shows the braking forces applied to the wheels from the simulation depicted in Figure 4.7. Once again the braking forces and stability limits could be optimized to increase the stability controllers effectiveness. Since the vehicle modeled is slightly understeer, braking is applied to the vehicle's inner wheels. This induces a brake moment that slows the vehicle down while reducing the yaw rate error.

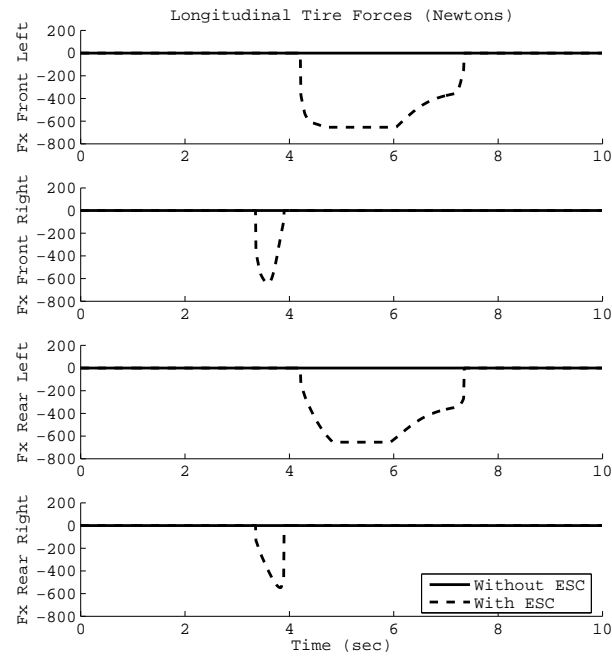


Figure 4.8: The vehicle's longitudinal forces with independent wheel braking

The controller used in this simulation once again has two stages. The first stage sets limits of lateral acceleration to 0.3 g for normal driving. Once that threshold is crossed, independent braking is applied to the desired wheels with a controller that applies somewhere between 667 N and 1500 N of braking force, depending on the value of lateral acceleration. The second stage of the controller applies 1500 N of braking force to the desired wheels once 0.45 g of lateral acceleration is breached.

Since this controller is quite effective in maintaining stability and is going being implemented in most production cars within the next few years, this controller will be further investigated in Chapter 5 to see how effective the controller can be when it is subjected to changing vehicle parameters.

4.8 Active Torque Distribution

Another method for traction and stability control is the active distribution of engine torque to the outer or inner wheels using active differentials. This method has been implemented on Acura's RL, where it adds the engine torque distribution to the independent wheel braking to correct for understeer and oversteer. Figure 4.9 shows the vehicle's behavior during the fishhook maneuver.

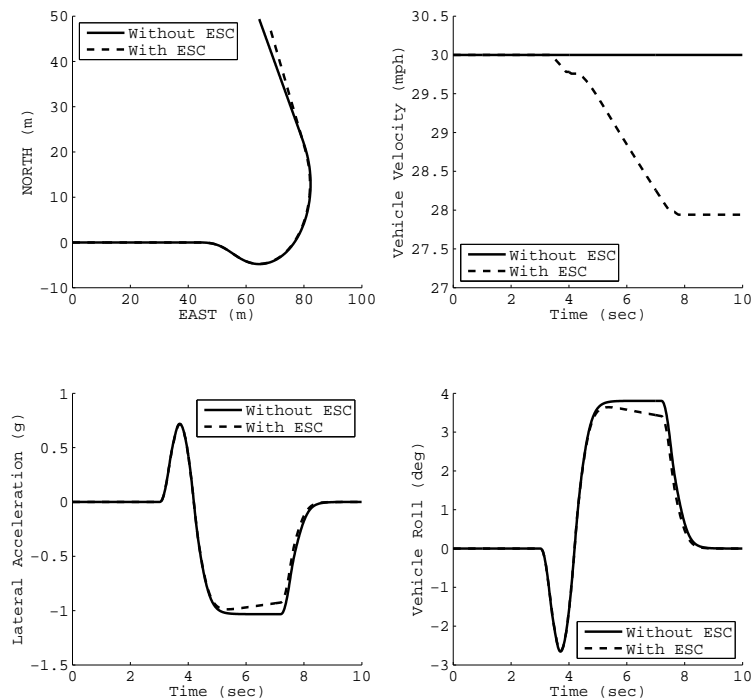


Figure 4.9: The vehicle's behavior with the added torque controller

By adding torques to the outer wheels and braking the inner wheels of the understeer vehicle, the vehicle's yaw rate error is greatly reduced, but the overall lateral acceleration and roll angle are not reduced by much. Figure 4.10 displays the braking and engine

forces applied at the wheels. Although the overall results are good for this method, its application is also going to be limited due to the fact that its installation into production vehicles is quite expensive.

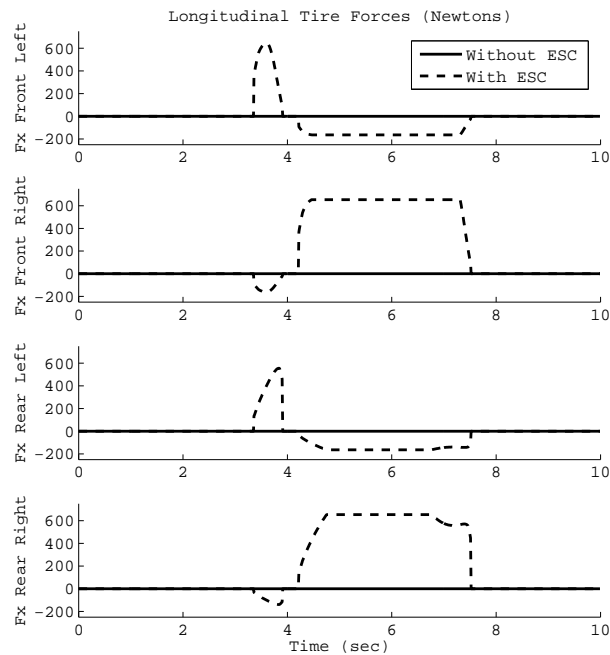


Figure 4.10: The vehicle's longitudinal forces with the added torque controller

4.9 Steering Control

Another method for vehicle stability control uses active steering modification. When a vehicle enters a curve with too much speed, the controller will limit the magnitude of the steer angle input. Figure 4.11 shows an example of this controller. Although the yaw rate and lateral acceleration are limited to a safe limit, the vehicle's path is not what is desired. This type of controller would not be acceptable for today's highways because

obstacle avoidance is often required. In order for a controller with steering modification to work, it must be combined with braking forces.

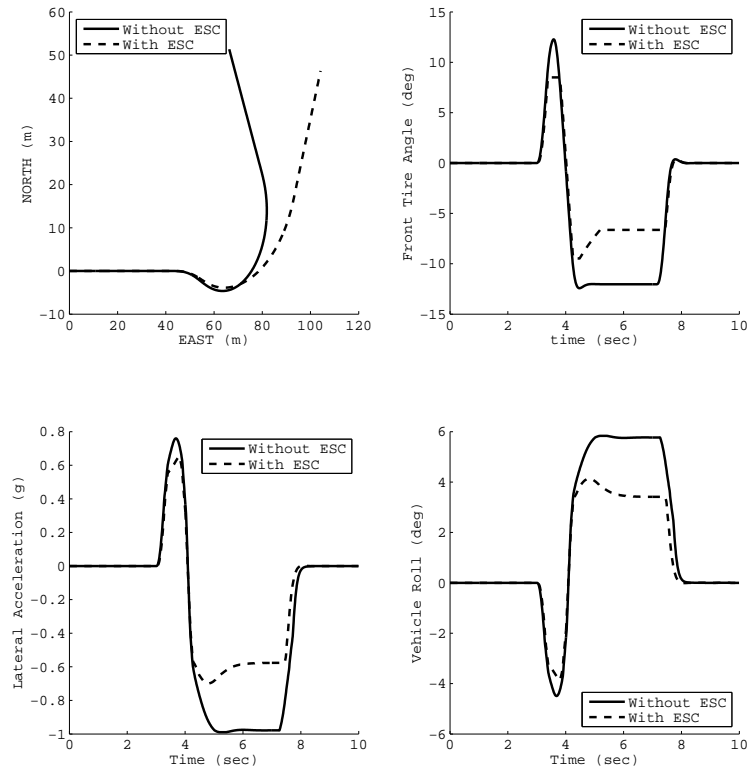


Figure 4.11: The vehicle's behavior with the steering modification controller

4.9.1 Steering Control with All-Wheel Braking

By combining two of the previous controllers, another ESC system can be created. With steering modification and all-wheel braking, the vehicle's stability can be increased while trying to reduce the yaw error. Figure 4.12 shows the vehicle's performance with

this controller. The yaw error is reduced from the steering only controller, and the maximum values of the roll angle and lateral acceleration are reduced.

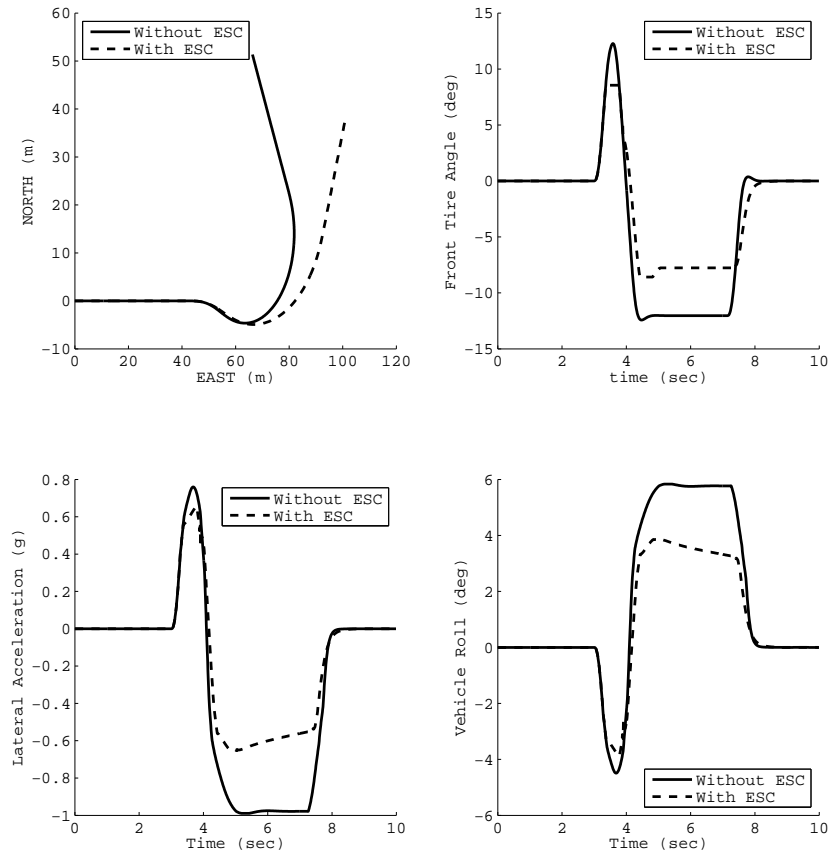


Figure 4.12: The vehicle's behavior with steering modification and constant braking

With this controller, the vehicle's velocity is reduced by over ten percent, due to the simple braking algorithm. The ESC limits the lateral acceleration to 0.4 g, while 1500 N of braking force (450 N-m of torque) is applied to all of the wheels once that threshold is crossed. Figure 4.13 displays the change in velocity of the vehicle during the maneuver.

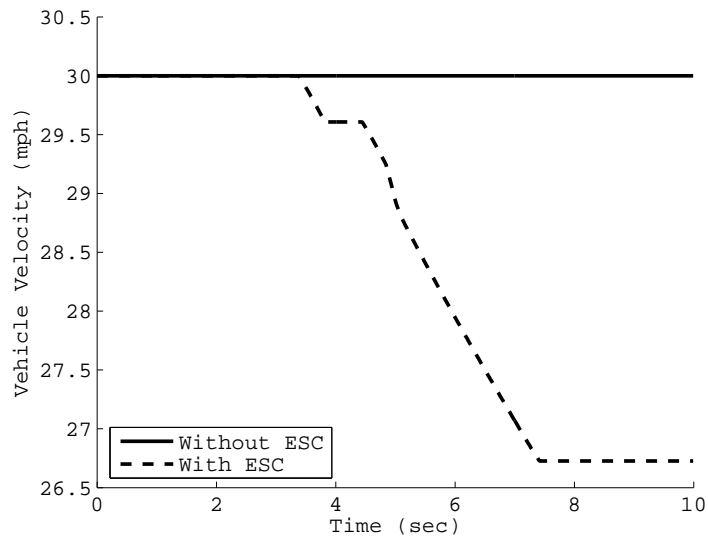


Figure 4.13: The vehicle’s velocity with steering modification and constant braking

This controller is similar to one used by Randal Whitehead in his research on his masters thesis [60]. In that work, the controller was implemented on a scaled vehicle in order to test the suitability of scaled vehicles for rollover testing. This was the most advanced controller possible for the scaled vehicle setup that he used. For this reason, and the fact that the implementation costs of this controller are low, this controller and the independent braking controller will be the focus of Chapter 5 to further investigate the performance of the two controllers to prevent rollover under various vehicle scenarios.

4.9.2 Independent Wheel Braking with Steering Control

By expanding the previous controller to include independent wheel braking, the stability of the vehicle can be further guaranteed [6, 2]. Figure 4.14 shows how a vehicle behaves with the independent wheel braking and steering modification controller. With the initial setup of the controller, the vehicle's stability is slightly enhanced, as the yaw rate and lateral acceleration are reduced. Also, the yaw error is greatly reduced, and the vehicle almost keeps the desired path.

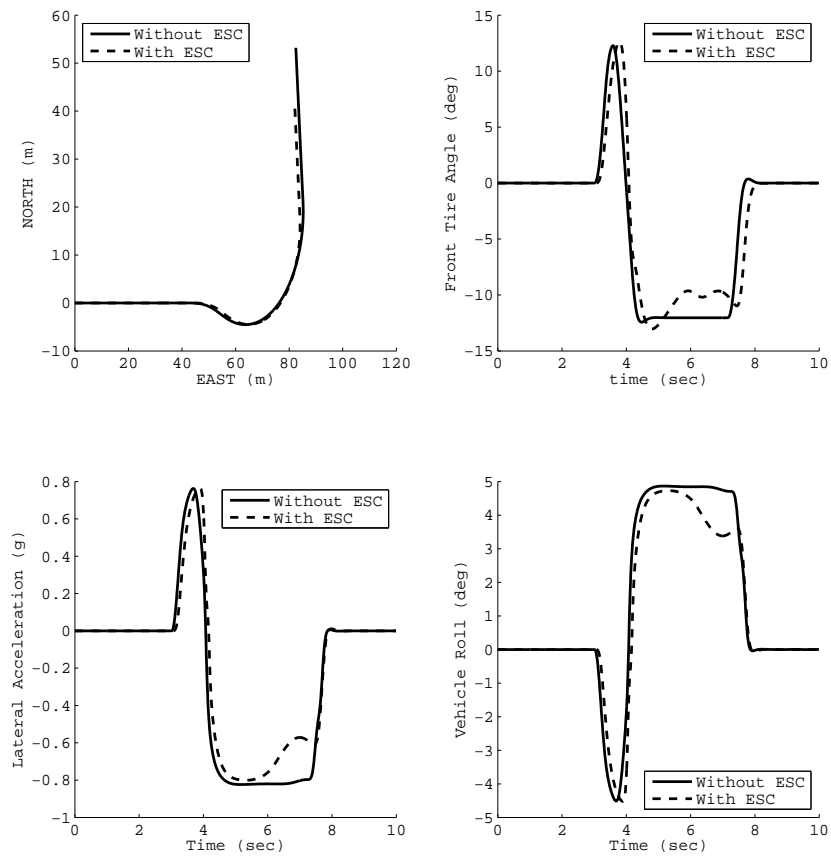


Figure 4.14: The vehicle's behavior with independent braking and steering control

Figure 4.15 shows the velocities of the vehicles. The velocity of the ESC equipped vehicle is reduced by over 5 miles per hour. This reduction in combination with the moment applied by brake steer allows the steering controller to keep the vehicle on the ideal path.

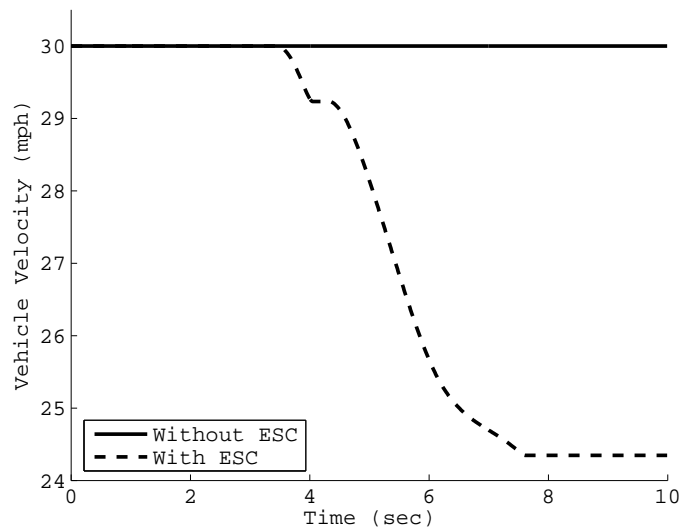


Figure 4.15: The vehicle's velocity with independent braking and steering control

Figure 4.16 displays the longitudinal forces applied by the independent braking controller. Although this controller seems to be somewhat ideal, its implementation is not as simple as others. Priorities must be made in order to establish what aspect of the controller is dominant. Therefore, this controller, along with the active torque distribution, would be a good area of research for future work.

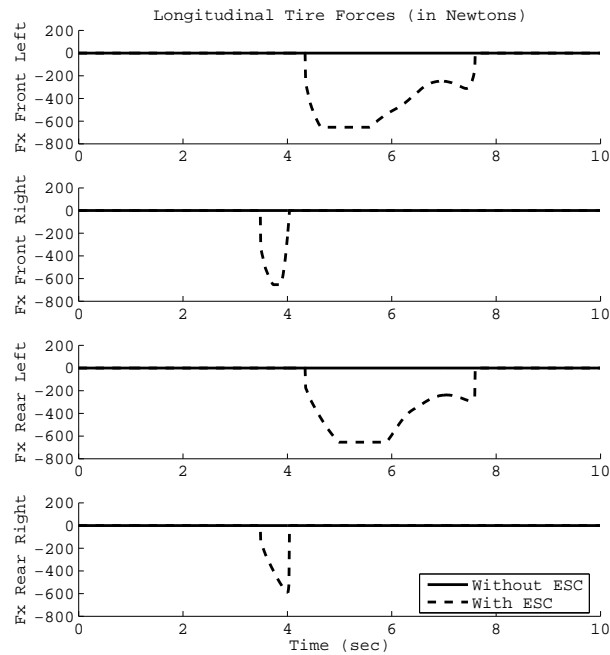


Figure 4.16: The vehicle’s longitudinal forces with independent braking and steering control

4.10 ESC with State Estimation

Research on the estimation of vehicle mass, sideslip, and roll parameters has been done throughout the last decade [29, 36, 51]. Dustin Edwards has been investigating the methods of estimation of vehicle properties (tire split, tire friction, and weight split) that could be used to optimize stability controllers [13]. Solmaz, Akar, and Shorten have also been investigating the estimation of CG height using sliding mode controllers [54]. With a knowledge of the CG location and other vehicle properties, ESC systems can be adjusted to limit the maximum lateral acceleration and yaw rate to different values, depending on the loading conditions. The implementation of state estimation, mainly CG height and longitudinal location (WS), would be another good area for future

research. The benefits of the knowledge of these properties could be rather large, and are discussed briefly in Chapter 5.

4.11 Conclusion

This chapter introduced a variety of electronic stability controllers that could be useful in improving the handling of a vehicle and the prevention of rollover. In Chapter 5, the all-wheel braking with steering modification and the independent braking controllers will be specifically studied for the prevention of rollover using MATLAB simulations with the roll model developed in Chapter 2.

CHAPTER 5
SIMULATION RESULTS FOR ESC

5.1 Introduction

Since it has been shown in Chapter 3 that certain vehicle properties can affect how a vehicle handles during extreme maneuvers, this chapter investigates how some ESC systems are affected by these changing vehicle properties. For two controllers, the independent braking and the all-wheel braking with steering modification introduced in Chapter 4, the robustness of the controller is studied to investigate how they are affected with changing CG height and weight split. The effect that track width has upon stability controllers will not be discussed since track width is a fixed vehicle property. These vehicle properties were chosen because they exhibited the ability to change the maximum lateral acceleration and velocity allowed before rollover.

This chapter is divided into four different sections that include simulations used for comparisons of ESC with the vehicle property variations:

- Varying CG Height

- No ESC
- All-Wheel Braking and Steering Modification
- Independent Braking

- Varying Weight Split

- No ESC
- All-Wheel Braking and Steering Modification
- Independent Braking

- **Varying CG Height With Optimized ESC Controllers**
 - All-Wheel Braking and Steering Modification
 - Independent Braking
- **Varying Weight Split With Optimized ESC Controllers**
 - All-Wheel Braking and Steering Modification
 - Independent Braking

5.2 Simulation Results for Varying Vehicle Properties

To investigate the effect of changing vehicle properties on the two ESC controllers, simulations in MATLAB were created that allowed multiple test runs with varying vehicle parameters set by the user. The maneuver chosen was the NHTSA fishhook due to the fact that it has been shown to most excite the rollover dynamics of the vehicle. The velocity chosen for the testing in this section is 35 miles per hour. This velocity was chosen due to the fact that it induced rollover in about half of the simulations when ESC was not present. With rollover occurring in some of the uncontrolled simulations, it is then known that critical lateral accelerations and yaw rates are achieved, and ESC would become crucial to the vehicle's stability in many of the maneuvers.

5.2.1 Varying CG Height

The first vehicle property to be examined is the CG height. Without any ESC implemented, the vehicle will perform in a manner depicted in Figure 5.1. Without any ESC present, the vehicle with CG heights of 0.8 and 0.9 meters roll after the second steer input is applied. The results for the position and lateral acceleration for the other simulations are almost identical, while the roll angle differs.

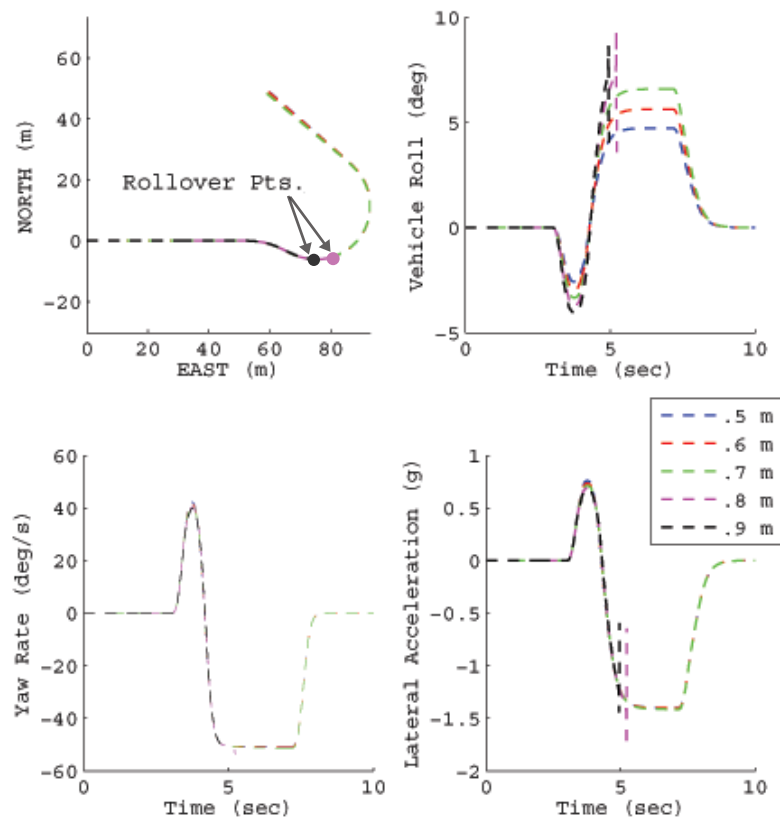


Figure 5.1: The fishhook maneuver with changing CG height and no ESC present

Since it is now known how the vehicle behaves with changing CG height, testing the all-wheel braking and steering modification controller can be done. Figure 5.2 shows how the vehicle behaves during the fishhook maneuver with the ESC. When the all-wheel braking and steering modification controller is applied using the same stability threshold and brake forces, all of the vehicles in simulation remain stable. As the CG height is increased, the ESC system applies a higher brake force due to the increased yaw rates and lateral accelerations created by the vehicle.

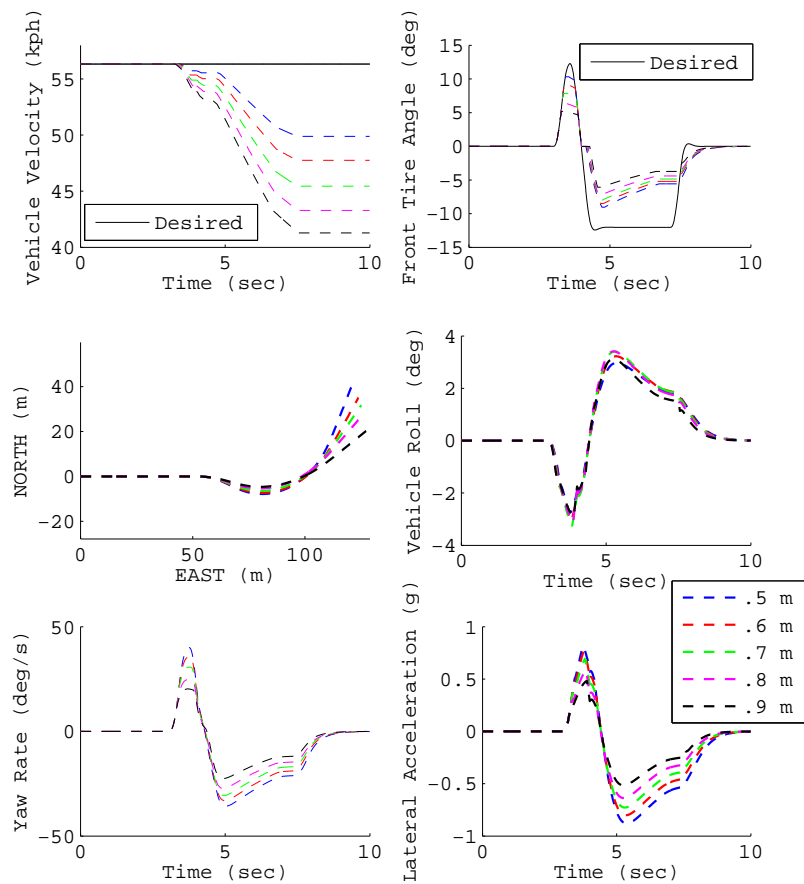


Figure 5.2: The fishhook maneuver with changing CG height and all-wheel braking and steering modification

As seen in Figure 5.3, the independent braking controller prevents the rollover when the CG height is 0.8 m; however, rollover still occurs when it is 0.9 m. It does not reduce the lateral acceleration and yaw rate as much as the previous controller, but it does greatly reduce the yaw error.

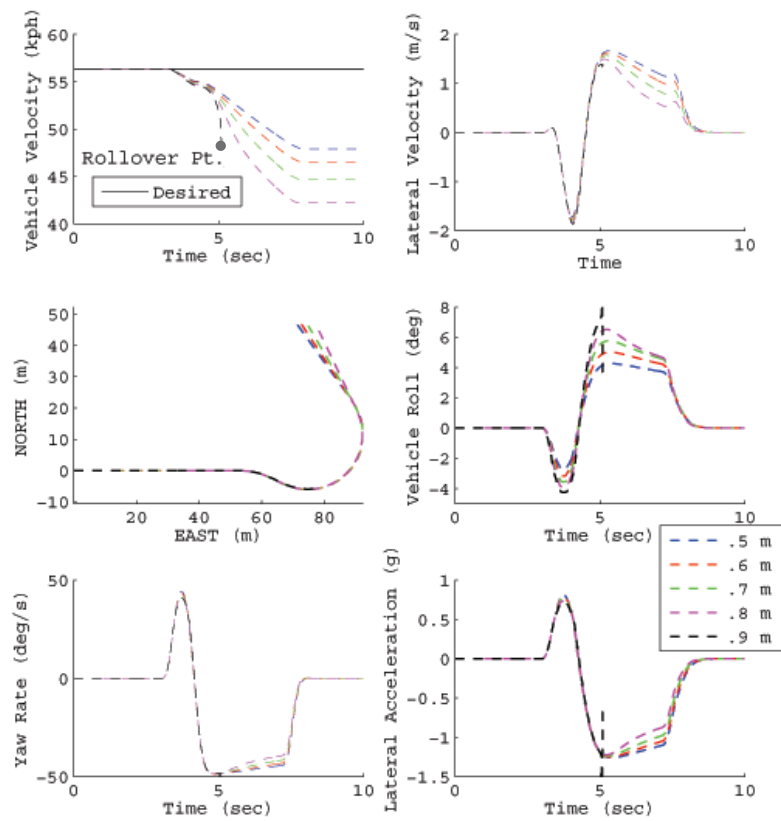


Figure 5.3: The fishhook maneuver with changing CG height and independent wheel braking

5.2.2 Varying Weight Split

The other vehicle property to be examined is the weight split. Without any ESC implemented, the vehicle will perform in a manner depicted in Figure 5.4. In this simulation all of the configurations rolled over except for the 57.5/42.5 configuration. With these results, the all-wheel braking and steering modification ESC can be implemented and compared.

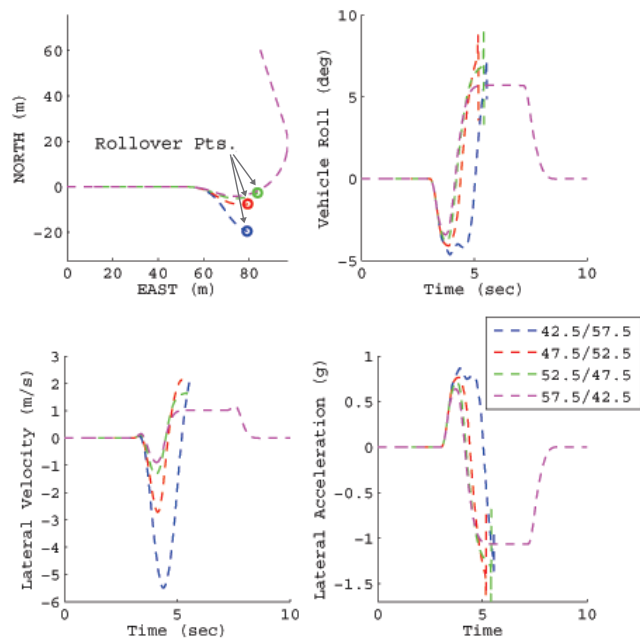


Figure 5.4: The fishhook maneuver with changing WS and no ESC present

Figure 5.5 shows how the ESC system affects the vehicle. As with all of the previous setups, the controller was able to prevent rollover. However, the controller once again reduced the steer angle in a way that would most likely cause a collision in practice. The methods of combining stability and path tracking could be a good avenue for future

research. Simulations show that there is no optimal solution and that some compromises must be made in order to prevent rollover.

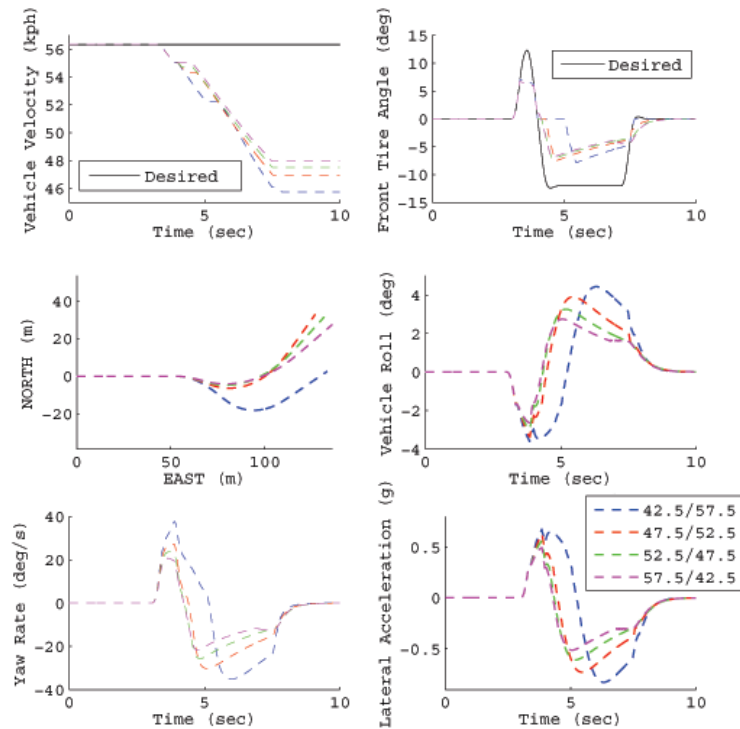


Figure 5.5: The fishhook maneuver with changing WS and all-wheel braking and steering modification

Figure 5.6 shows the independent wheel braking controller with changing WS. This controller once again has a greater ability to keep the desired path. The independent wheel controller was able to prevent rollover for three out of four vehicle configurations. The one setup that rolled (42.5/57.5 WS) is a configuration that simulates an oversteer vehicle with a large rear payload, could not be kept stable during the maneuver. Perhaps with knowledge of some vehicle properties, changes in the vehicle's stability limits and ESC outputs could prevent rollover more often as investigated in the next sections.

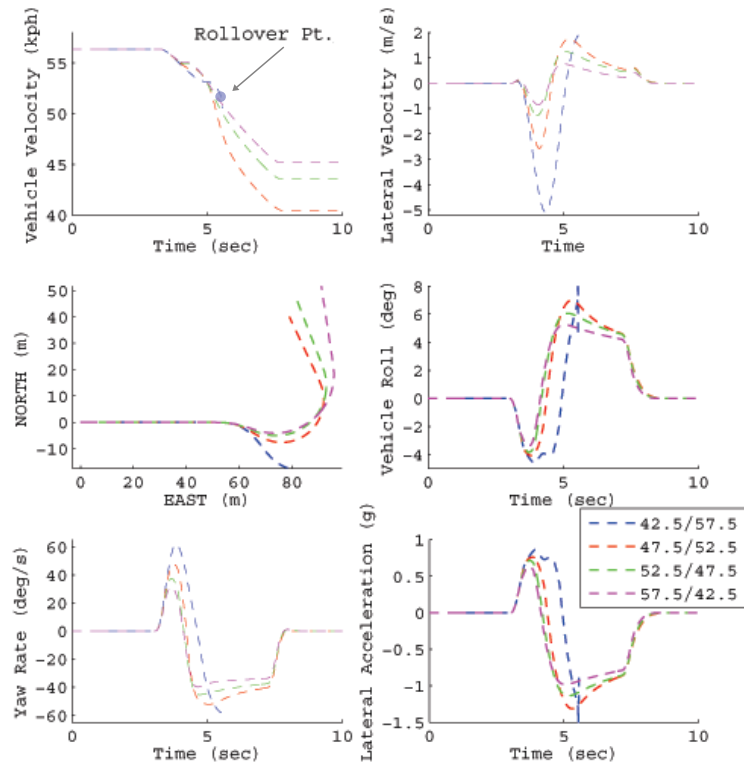


Figure 5.6: The fishhook maneuver with changing WS and independent braking

5.3 Simulation Results for Optimized ESC Limits and Inputs

As previously discussed, a knowledge of key vehicle parameters would allow ESC systems to be altered to more adequately adjust the stability threshold and ESC outputs in order to reduce rollover. The following sections compare the same vehicle configurations in the same NHTSA fishhook maneuver. In these simulations, the values for the maximum lateral acceleration allowed is optimized, as well as the braking forces applied at the wheels.

5.3.1 Varying CG Height With Optimized ESC Controllers

With knowledge of the changing CG height, the ESC system can be adapted to further prevent rollover. Figure 5.7 shows the same simulations performed previously in Figure 5.2, but with an optimized controller for each vehicle setup.

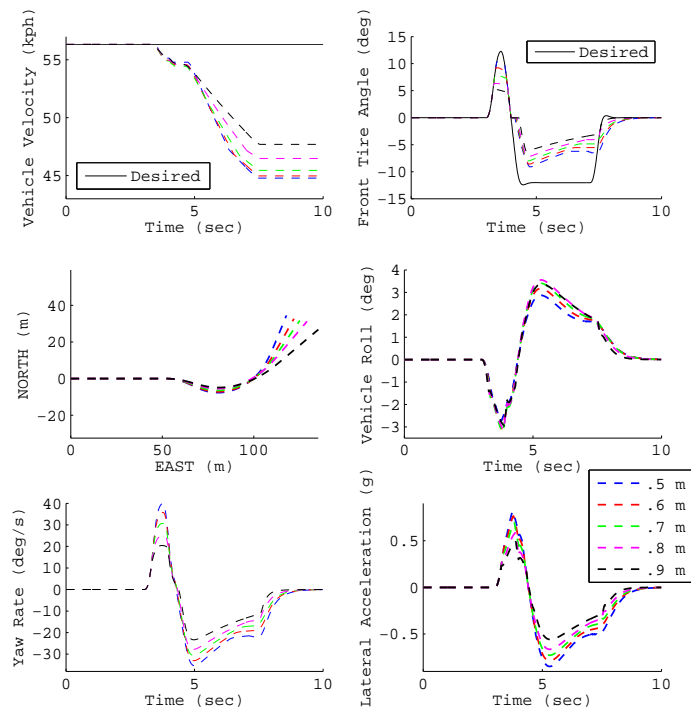


Figure 5.7: CG height changes with an optimized all-wheel braking and steering ESC

This controller once again prevents rollover due to the reduction in yaw rate. In the cases where the CG height is smaller (0.5 and 0.6 m), the controller increases the maximum lateral acceleration and yaw rate allowed before rollover and the braking forces applied by the controller are reduced. With the adjusted stability limits and braking forces, the vehicle is allowed to stay closer to the desired path, and the yaw error is reduced.

The independent braking controller can also be adapted to take knowledge of changing CG heights into effect. Figure 5.8 displays results using the independent braking controller.

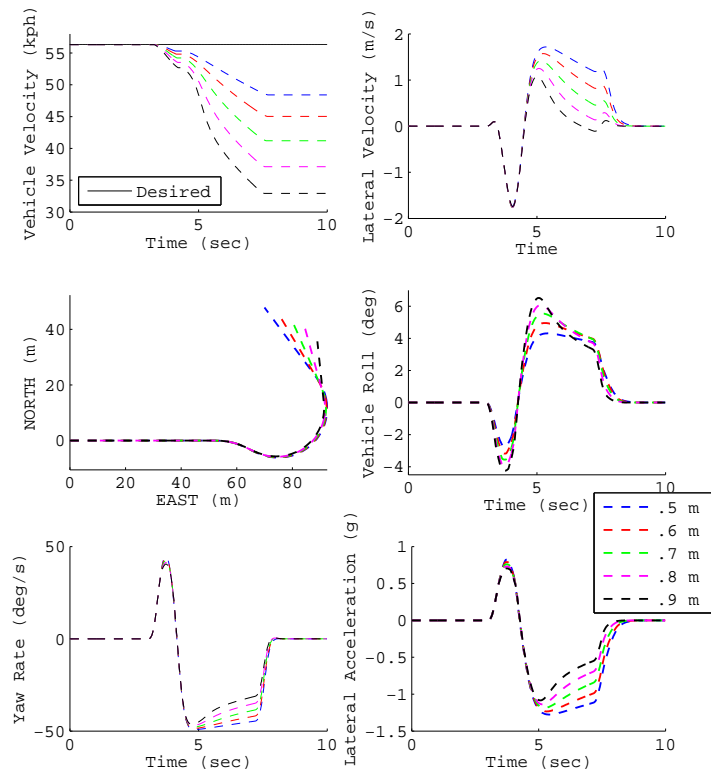


Figure 5.8: CG height changes with an optimized independent braking ESC

The optimized controller manages to keep the vehicle with a CG height of 0.9 stable, despite the fact that it is very close to rollover. Also, the braking forces for the more stable vehicles are reduced to a maximum of 300 N in order to limit the effect of the ESC on the vehicle.

5.3.2 Varying Weight Split With Optimized ESC Controllers

Changes in weight split have been proven to render ESC systems ineffective if the vehicle is very oversteer and the controller gains are not correct. Figure 5.9 shows the fishhook maneuver with the all-wheel braking and steering modification controller. The optimized controller once again manages to keep the vehicles stable by altering the stability limits and braking forces. The 42.5/57.5 WS vehicle is also able to keep more to the desired path than with the standard controller simulated previously in Figure 5.6.

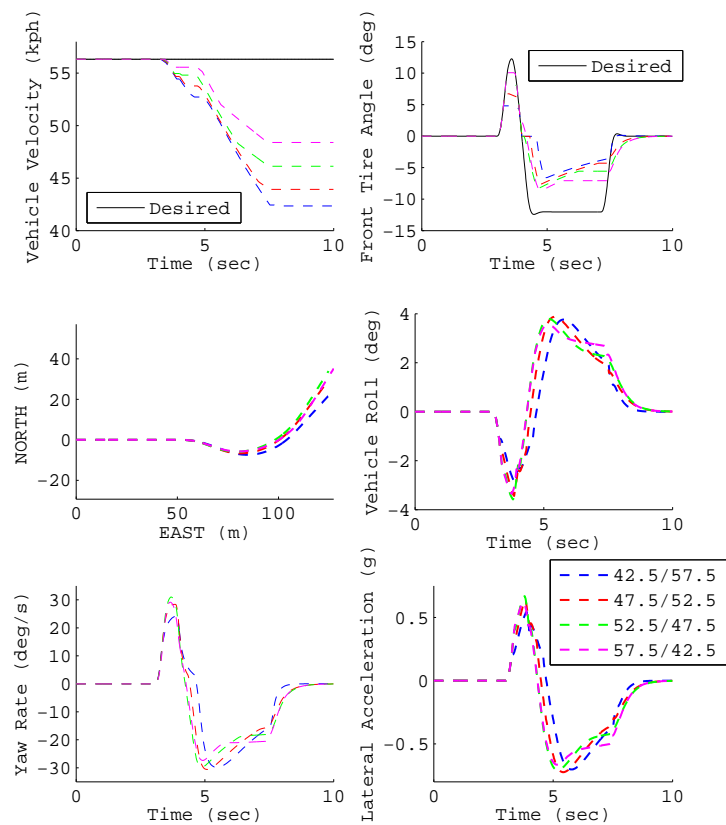


Figure 5.9: WS changes with an optimized all-wheel braking and steering ESC

Figure 5.10 shows a simulation of the optimized independent braking controller in action. This controller is once again able to prevent rollover in all of the cases tested. For the 42.5/57.5 WS case, the vehicle's path is widened and the yaw error is large. However, with the general system applied earlier in the chapter, this vehicle configuration experienced rollover. The knowledge of the weight split allowed the controller to increase its braking forces when it was necessary, and reduce the braking forces when not, resulting in the prevention of rollover.

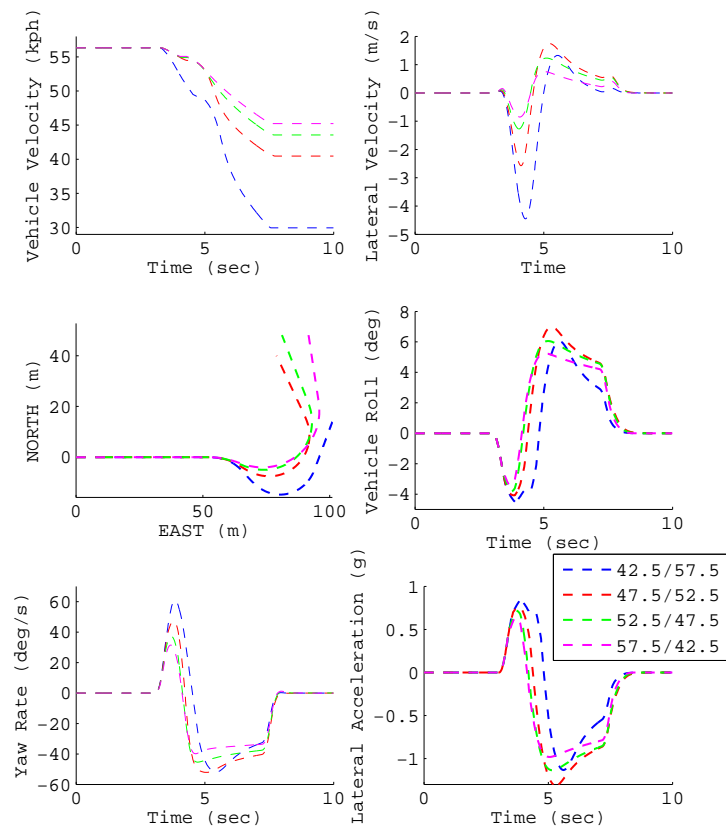


Figure 5.10: WS changes with an optimized independent braking ESC

5.4 Conclusions

The ESC controllers tested in this chapter were subjected to changes in CG height and weight split. With basic limits of lateral acceleration and yaw rate and standard braking forces applied, the stability controllers were able to reduce the occurrence of vehicle rollover most of the time. However, when the controllers were optimized for the vehicle setup, rollover was avoided and path following was improved.

For the all-wheel braking with steering modification controller, the vehicle's stability was greatly improved. However, the vehicle's path error was usually large enough that the implementation in a real vehicle could prove detrimental in the event of an obstacle avoidance maneuver. Perhaps with more research and varied controller gains, the all-wheel braking with steering modification controller could perform better at keeping the desired path, while remaining in a stable region.

The independent braking controller's ability to keep the vehicle's path while reducing the vehicle's lateral acceleration and yaw rate is promising. This type of controller, which is going to be implemented into most new production passenger vehicles, has already proven successful on today's highways. With a knowledge of CG parameters taken from state estimation techniques, vehicle stability controllers can be improved and the number of rollover incidents can be reduced. Simulation results have proven that by optimizing ESC systems to the individual vehicle, specifically providing knowledge of the vehicle's CG location (height and weight split), stability and handling can be greatly improved during evasive maneuvers.

CHAPTER 6
CONCLUSIONS

6.1 Overall Contributions

This thesis demonstrates that with knowledge of a few key vehicle properties, ESC systems can be optimized for better improvement. In order to test the parameters that influence vehicle rollover, a complex vehicle model was created and compared to the CarSim, a commercially available vehicle dynamics software package.

6.1.1 Parameters That Most Influence Rollover

Chapter 3 investigates the key vehicle properties that most affect vehicle rollover. In simulation, it was shown that CG height, track width, understeer gradient, and friction coefficients affect how a vehicle performs during test maneuvers. Simulations in CarSim show that as CG height, understeer gradient, and friction coefficient increase, so does the chance of rollover. Although track width is not a variable property, it was also shown that as the track width is reduced, the chances for rollover increase.

6.1.2 Vehicle Rollover Prediction

Using free body diagrams derived for a four-wheeled vehicle, equations were derived for the prediction of vehicle rollover. Simulation results proved the validity of the modified Static Stability Factor equation. When the CG height or understeer gradient increased or the track width decreased, the maximum lateral acceleration before rollover

allowed by the vehicle was decreased. The Static Stability Factor equation was also modified to include a scale factor for the inclusion of suspension dynamics.

Another rollover prediction formula for the rollover velocity was then created and tested using multiple simulations. Using knowledge of CG height, track width, and radius of turn (or yaw rate), the formula was proven to effectively predict the velocity that a vehicle rolled over in MATLAB and CarSim simulations. Like the SSF, this equation was modified to include a scale factor for weight transfer. The significance of this formula is large because with a few vehicle properties, parameter estimates, and sensor measurements, one can predict if a vehicle will roll.

6.1.3 ESC Development

Chapter 4 consists of the discussion and derivation of seven different types of Electronic Stability Controllers. The stability controllers are modeled in MATLAB and tested for effectiveness. Although only two are examined in Chapter 5, the active torque and the independent braking with steering correction controllers show promise for increased vehicle stability.

6.1.4 Effect of Varying Vehicle Properties on ESC

In Chapter 5, two of the ESC systems were chosen to be tested for robustness to the principal changing vehicle properties. It was shown that the all-wheel braking with steering modification controller can be problematic due to errors in heading, but is very effective in rollover mitigation. An independent wheel braking controller was also examined to test its effectiveness to changing vehicle parameters. This system was

proven in simulation to be a good choice due to its ability to ensure vehicle stability, while remaining close to the desired path.

Chapter 5 also examines the controllers' abilities to adapt to changing vehicle properties. With a prior knowledge of the key vehicle parameters, it was shown that the ESC systems were capable of improving the stability and handling of a vehicle with slight modification of stability limits and ESC outputs.

6.2 Difficulties

In the development of vehicle simulations, small problems arose with the creation of programs in MATLAB. Since every vehicle property must be known for the MATLAB simulations, there were consistency errors when the simulations were first compared to those in CarSim. Due to CarSim's advanced user platform, time to become familiar with the program was required before all of the vehicle parameters could be accurately changed in order to compare to MATLAB simulations.

Another difficulty that arose was the lack of prior knowledge and papers on the development and implementation of complicated ESC systems. Most of the ESC systems, especially the more complicated algorithms, required some adjustment of controller gains and stability limits in order to get the controllers to work properly. However, with time, the ESC development and implementation became successful and accurate testing was performed.

As described in Chapter 3, the effects of understeer gradient were not completely consistent when changes in weight split and cornering stiffness were made. The discrepancies of the empirical results produced some errors with the inclusion of understeer gradient scale factor in rollover prediction formula. Also, a simple, easy to calculate

analytical solution for vehicle rollover velocity and lateral acceleration with the effects of understeer gradient has not been found yet. More work is needed to create a simple, easy to calculate rollover equation that includes the understeer gradient and weight transfer.

6.3 Recommendations for Future Work

While doing this research, it was realized that complicated ESC systems could become a daunting task to take on. In order to fully understand all of the dynamics and characteristics of the active torque distribution and the independent braking with steering controllers, a great deal research needs to be done. Both ESC systems are very promising, some of which are in production vehicles today.

Work is continuing into the inclusion of the understeer gradient effects upon the prediction of rollover velocity and lateral acceleration. It has been shown that the understeer gradient plays a part in the rollover propensity of a vehicle; however, a simple analytical solution that includes its effects could improve the accuracy of the formula.

Although accuracy of the rollover velocity and lateral acceleration equations was proven, testing can also be done to prove the accuracy of the prediction of the other vehicle properties in Equations (3.16), (3.17), (3.18), and (3.19). The velocity and lateral acceleration (SSF) equations were the only ones analyzed due to their importance; however, the prediction of critical CG height, track width, yaw rate, or radius of turn could prove to be useful.

Another good area of future research is state estimation in combination with ESC. With the knowledge of the understeer gradient and the CG height and lateral location, these parameters can be inserted to an adaptable ESC and further optimization would be possible on actual vehicles. The implementation of the ESC algorithms onto a UGV

would prove beneficial and could validate the results of this thesis. To take the ESC systems that require independent braking into account, the brake systems must be independently controlled for each wheel, with the ability to be controlled remotely by computer.

BIBLIOGRAPHY

- [1] L. Blincoe, A. Seay, E. Zaloshnja, T. Miller, E. Romano, S. Luchter, and R. Spicer. The Economic Impact of Motor Vehicle Crashes, 2000. Technical Report DOT HS 809 446, NHTSA, Washington, D.C., May 2002.
- [2] B. L. Boada, M. J. L. Boada, and V. Daz. Fuzzy-Logic Applied to Yaw Moment Control for Vehicle Stability. *Vehicle System Dynamics*, 43(10):753–770, October 2005.
- [3] Sean N. Brennan. Modeling and Control Issues Associated with Scaled Vehicles. Master’s thesis, University of Illinois at Urbana-Champaign, 1999.
- [4] John T. Cameron and Sean Brennan. A Comparative, Experimental Study of Model Suitability to Describe Vehicle Rollover Dynamics for Control Design. In *2005 ASME International Mechanical Engineering Congress and Exposition*, number IMECE2005-80508, Orlando, FL, USA, November 5-11 2005. The Pennsylvania State University.
- [5] Christopher R. Carlson. The Influence of Roll and Weight Transfer on Vehicle Handling. Technical report, Stanford University, April 20 2004. Dynamic Design Lab.
- [6] Christopher R. Carlson and J. Christian Gerdes. Optimal Rollover Prevention with Steer by Wire and Differential Braking. In *2003 ASME International Mechanical Engineering Congress and Exposition*, number IMECE2003 in 41825, Washington D.C., November 16-21, 2003. Stanford University.
- [7] Bo-Chiuan Chen and Huei Peng. Differential-Braking-Based Rollover Prevention for Sport Utility Vehicles with Human-In-The-Loop Evaluations. *Vehicle System Dynamics*, 36(4-5):359389, 2001.
- [8] N. K. Cooperrider, S. A. Hammond, and T. M. Thomas. Testing and Analysis of Vehicle Rollover Behavior. *SAE Paper*, (900366), 2000.
- [9] T. D. Day and J. T. Garvey. Applications and Limitations of 3-Dimensional Vehicle Rollover Simulation. *SAE Paper*, (2000-01-0852), 2000.
- [10] J. C. Dixson. *Tires, Suspension and Handling*. Society of Automotive Engineers, Warrendale, PA, 2 edition, 1996.
- [11] H. Dugoff, P. S. Fancher, and L. Segel. Tire Performance Characteristics Affecting Vehicle Response to Steering and Braking Control Inputs. Technical report, Transportation Research Institute (UMTRI), Washington D.C., 1969.

- [12] H. Dugoff, P. S. Fancher, and L. Segel. An Analysis of Tire Traction Properties and Their Influence on Vehicle Dynamic Performance. *SAE Paper*, (700377), 1970.
- [13] Dustin Edwards. Parameter Identification for Look-Ahead Maneuverability. In *AUVSIs Unmanned Systems North America 2007*. Auburn University, August 2007.
- [14] R. Eger, R. Majjad, and N. Nasr. Rollover Simulation Based on a Nonlinear Model. *SAE Paper*, (980208), 1998.
- [15] J. R. Ellis. The Dynamics of Vehicles During Braking. In *Symposium on the Control of Vehicles*. Institution of Mechanical Engineers, June 1963.
- [16] FARS. Fatality Analysis Reporting System (FARS) Web-Based Encyclopedia. National Center for Statistics and Analysis, National Highway Traffic Safety Administration, U.S. Department of Transportation, <http://www-fars.nhtsa.dot.gov/>.
- [17] Michael Fodor, John Yester, and Davor Hrovat. Active Control of Vehicle Dynamics. In *1998 IEEE Conference*, number 0-7803-5086-3, pages I14-1 – I14-8. Ford Motor Company, 1998.
- [18] Ford. Ford to Make Electronic Stability Control Standard on All Cars and Trucks by End of 2009. *Ford Motor Company Press Release*, September 13 2006.
- [19] Garrick J. Forkenbrock. NHTSA's Light Vehicle Handling and ESC Effectiveness Research Program. In *International Technical Conference on the Enhanced Safety of Vehicles (ESV)*, number 05-0221, Washington D.C., June 2005.
- [20] Garrick J. Forkenbrock and W. Riley Garrott. Testing the Dynamic Rollover Resistance of Two 15-Passenger Vans with Multiple Load Configurations. July 15 2006. NHTSA - DOT Report: DOT HS 809 704. Available at: <http://nhtsa.gov/cars/problems/studies/15PassVans/15-PassVanStabilityControl.pdf>.
- [21] Garrick J. Forkenbrock, Bryan C. O'Harra, and Devin Elsasser. An Experimental Evaluation of 26 Light Vehicles Using Test Maneuvers That May Induce On-Road, Untripped Rollover and a Discussion of NHTSAs Refined Test Procedures - Phases VI and VII of NHTSAs Light Vehicle Rollover Research Program. Final Report DOT HS 809 547, NHTSA/NVS, East Liberty, OH, October 2003.
- [22] Garrick J. Forkenbrock, Bryan C. O'Harra, and Devin Elsasser. A Demonstration of the Dynamic Tests Developed for NHTSA's NCAP Rollover Rating System. (DOT HS 809 705), August 2004. Phase VIII of NHTSA's Light Vehicle Rollover Research Program.
- [23] T. D. Gillespie. *Fundamentals of Vehicle Dynamics*. Society of Automotive Engineers, Warrendale, PA, 1992.

- [24] A. Hac. Rollover Stability Index Including Effects of Suspension Design. *SAE Paper*, (2001-01-0965), 2002.
- [25] Aleksander Hac, Todd Brown, and John Martens. Detection of Vehicle Rollover. *SAE Paper*, (2004-01-1757), 2004.
- [26] Bridget C. Hamblin, Ryan D. Martini, John T. Cameron, and Sean N. Brennan. Low-Order Modeling of Vehicle Roll Dynamics. In *Proceedings of the 2006 American Controls Conference*, pages 4008–4015, Minneapolis, MN, 2006.
- [27] Philip Headley. ESC as a Baseline for Active Safety. In *2005 Enhanced Vehicle Conference*, number Paper Number 05-0332, USA, 2005. Continental Teves.
- [28] Y Hu, C E Neal-Sturgess, and A M Hassan. Simulation of Vehicle Kinematics in Rollover Tests with Quaternions. In *Proc. IMechE Vol. 220 Part D: J. Automobile Engineering*, volume 220, pages 1503–1513, Birmingham, UK, May 2006. Birmingham Automotive Safety Centre, School of Engineering, Department of Mechanical Engineering, University of Birmingham. DOI: 10.1243/09544070JAUTO360.
- [29] Kunsoo Huh, Sunghyon Lim, Jongchul Jung, Daegun Hong, Sangoh Han, Kwangjin Han, Hee Young Jo, and Jae Min Yun. Vehicle Mass Estimator for Adaptive Roll Stability Control. In *SAE 2007 World Congress*, number 2007-01 in 0820, pages 147–152, Detroit, MI, USA, April 16-19 2007. Hanyang University.
- [30] Bjorn Johansson and Magnus Gafvert. Untripped SUV Rollover Detection and Prevention. *43rd IEEE Conference on Decision and Control*, (0-7803-8682-5):5461–5466, December 2004.
- [31] Johanna Spangenberg Jones and Jan Walker. DARPA Finalizes 2007 Urban Challenge Cash Prize Levels. Press Release, December 2006.
- [32] T. M. Klein. A Statistical Analysis of Vehicle Rollover Propensity and Vehicle Stability. *SAE Paper*, (920584), 1992.
- [33] Anders Lie, Claes Tingvall, Maria Krafft, and Anders Kullgren. The Effectiveness of ESC (Electronic Stability Control) in Reducing Real Life Crashes and Injuries. In *2005 Enhanced Vehicle Conference*, number 05-0135, Sweden, 2005. Folksam Research.
- [34] E. K. Liebermann, K. Meder, J. Schuh, and G. Nenninger. Safety and Performance Enhancement: The Bosch Electric Stability Control (ESP). In *2005 Enhanced Vehicle Conference*, number 05-0471, Germany, 2005. Robert Bosch GmbH.
- [35] Jianbo Lu, Dave Messih, Albert Salib, and Dave Harmison. An Enhancement to an Electronic Stability Control System to Include a Rollover Control Function. In *SAE 2007 World Congress*, number 2007-01-0809, pages 15–25, Detroit, MI, USA, April 16-19 2007. Ford Motor Company.

- [36] T. Massel, E. L. Ding, and M. Arndt. Estimation of Vehicle Loading State. In *Proceedings of the 2004 IEEE International Conference on Control Applications*, volume 2, pages 1260–1265, Taipei, Taiwan, September 2-4 2004.
- [37] John McHale. Robots are Fearless. *Military & Aerospace Electronics*, 17(6):26–33, June 2006.
- [38] Bill Milliken and Doug Milliken. *Race Car Vehicle Dynamics*. Society of Automotive Engineers, Warrendale, PA, 1995.
- [39] NHTSA’s NCSA. Traffic Safety Facts 2004. 2005. NHTSA’s National Center for Statistics and Analysis: DOT HS 809 919. Washington DC. Available: <http://www-nrd.nhtsa.dot.gov/pdf/nrd-30/NCSA/TSFAnn/TSF2004.pdf>.
- [40] NHTSA’s NCSA. Traffic Safety Facts 2005. 2006. NHTSA’s National Center for Statistics and Analysis: DOT HS 809 919. Washington DC. Available: <http://www-nrd.nhtsa.dot.gov/pdf/nrd-30/NCSA/TSFANN/TSF2005.pdf>.
- [41] NHTSA. DOT Proposes Anti-Rollover Technology for New Vehicles. *News Release*, September 14 2006.
- [42] H. B. Pacejka, E. Bakker, and L. Lidner. A New Tire Model with an Application in Vehicle Dynamics Studies. *SAE Paper*, (890087), 1989.
- [43] H. B. Pacejka, E. Bakker, and L. Nyborg. Tyre Modelling for Use in Vehicle Dynamics Studies. *SAE Paper*, (870421), 1987.
- [44] Hans B. Pacejka and Egbert Bakker. The Magic Formula Tyre Model. *Vehicle System Dynamics*, 21(1):1–18, 1992.
- [45] Desmond N. Penny. Rollover of Sport Utility Vehicles. *The Physics Teacher*, 42:86–91, February 2004.
- [46] Tom Pilutti, Galip Ulsoy, and Davor Hrovat. Vehicle Steering Intervention Through Differential Braking. In *Proceedings of the American Control Conference*, number TA6 - 10:15, pages 1667–1671, Seattle, WA, USA, June 1995. Ford Research Laboratories.
- [47] John Plumlee. Multi-Input Ground Vehicle Control Using Quadratic Programming Based Control Allocation Techniques. Master’s thesis, Auburn University, August 2004.
- [48] John H. Plumlee, David M. Bevely, and Scott Hodel. Control of a Ground Vehicle Using Quadratic Programming Based Control Allocation Techniques. In *Proceedings in the 2004 American Controls Conference*, 2004.
- [49] Rajesh Rajamani. *Vehicle Dynamics and Control*. Springer, New York, NY, 2006.

- [50] Brendan P. Rivers. US Military Looks at Arming Unmanned Ground Vehicles. *Journal of Electronic Defense*, 29(3):15–16, March 2006.
- [51] Jihan Ryu, Eric J. Rossetter, and J. Christian Gerdes. Vehicle Sideslip and Roll Parameter Estimation using GPS. In *AVEC 2002 6th Int. Symposium on Advanced Vehicle Control*, Hiroshima, Japan, 2002.
- [52] NHTSA 2005 Safercar.gov. Rollover rating system. <http://www.safercar.gov/Rollover/pages/RatSys.htm>, September 2007.
- [53] Insurance Institute For Highway Safety. Electronic Stability Control Could Prevent Nearly One-Third of All Fatal Crashes and Reduce Rollover Risk By as Much as 80%. Technical report, Insurance Institute For Highway Safety, June 13 2006.
- [54] Selim Solmaz, Mehmet Akar, and Robert Shorten. Online Center of Gravity Estimation in Automotive Vehicles using Multiple Models and Switching. In *The Ninth International Conference on Control, Automation, Robotics and Vision (ICARCV) - IEEE*, number 1424403421, 2006. Hamilton Institute, NUI-Maynooth.
- [55] Aldo Sorniotti and Nicolo D’ Alfio. Vehicle Dynamics Simulation to Develop an Active Roll Control System. In *SAE 2007 World Congress*, number 2007-01-0828, Detroit, MI, USA, April 16-19 2007. Politecnico di Torino.
- [56] Alexander Strashny. An Analysis of Motor Vehicle Rollover Crashes and Injury Outcomes. Technical Report DOT HS 810 741, NHTSA Technical Report, Washington, DC, March 2007.
- [57] H. E. Tseng, D. Madau, B. Ashrafi, T. Brown, and D. Recker. Technical Challenges in the Development of Vehicle Stability Control System. In *Proceedings of the 1999 IEEE International Conference on Control Applications*, number 0-7803-5446-X, pages 1660–1666, Hawaii, USA, August 1999.
- [58] Ali Y. Ungoren, Huei Peng, and Danny R. Milot. Rollover Propensity Evaluation of an SUV Equipped with a TRW VSC System. In *2000 Society of Automobile Engineers, Inc.*, number 2001-01-0128, 2000.
- [59] Randall Whitehead, William Travis, David M. Bevly, and George Flowers. A Study of the Effect of Various Vehicle Properties on Rollover Propensity. In *SAE International*, number 2004-01-2094. Auburn University, 2004.
- [60] Randall J. Whitehead. A Study of the Properties That Influence Vehicle Rollover Propensity. Master’s thesis, Auburn University, 2005.
- [61] Randall J. Whitehead, Benjamin Clark, and D. M. Bevly. ESC Effectiveness During Property Variations on Scaled Vehicles. In *2005 ASME International Mechanical Engineering Congress and Exposition*, number IMECE2005 in 82558, Orlando, FL, November 5-11 2005.

- [62] Jim R. Wilde, Gary J. Heydinger, Dennis A. Guenther, Thomas P. Mallin, and Andrew M. Devenish. Experimental Evaluation of Fishhook Maneuver Performance of a Kinetic Suspension System. *SAE Paper*, (2005-01-0392), 2005.
- [63] Jangyeol Yoon and Kyongsu Yi. A Rollover Mitigation Control Scheme Based on Rollover Index. In *2006 American Control Conference*, number 1-4244-0210-7, Minneapolis, MN, June 14-16 2006.

APPENDICES

APPENDIX A

VEHICLE NOMENCLATURE

a	Length between CG and front contact patch
a_y	Lateral Acceleration
b	Length between CG and rear contact patch
B	Shock Damping (f/r)
CG	Center of Gravity
d	Length from rc to CG
δ	Steer Angle
F_b	Damping Force (f/r)
F_k	Spring Force (f/r)
F_y	Tire Lateral Force (fL, fR, rL, rR)
F_z	Tire Vertical Force (fL, fR, rL, rR)
H_{CG}	CG Height
H_{rc}	RC Height (f/r)
K_{ARB}	Anti-Roll Bar Stiffness (f/r)
K_s	Spring Stiffness (f/r)
M	Sprung Mass (f/r)
m	Unsprung Mass (f/r)
MT	Total Mass
M_{arb}	Anti-roll Bar Moment (f/r)
ϕ	Roll Angle
r	Yaw Rate
rc	Roll Center (f/r)
R_y	Lateral Reaction Force (fL, fR, rL, rR)
R_z	Vertical Reaction Force (fL, fR, rL, rR)
S	Length between L and R springs/dampers (f/r)
tw	Track Width (f/r)
V	Vehicle Velocity
V_x	Vehicle Longitudinal Velocity
V_y	Vehicle Lateral Velocity
f = front r = rear L = Left R = Right	

APPENDIX B

VEHICLE PROPERTIES

Typical SUV Properties - Taken From a 2000 Chevrolet Blazer

Wheelbase:	L	2.72 <i>m</i>
Front Track Width:	TW_f	1.45 <i>m</i>
Rear Track Width:	TW_r	1.40 <i>m</i>
CG Height (Sprung Mass):	H_{CG}	0.6 <i>m</i>
RC Height:	H_{RC}	0.4 <i>m</i>
Unsprung Mass Height:	H_m	0.25 <i>m</i>
Vehicle Mass:	MT	2150 <i>kg</i>
Sprung Mass:	M	1720 <i>kg</i>
Unsprung Mass:	m	430 <i>kg</i>
Steering Ratio	SR	18
Standard Weight Split	WS	55/45 (<i>f/r</i>)
Dist. from CG to Front Contact Patch	a	1.22 <i>m</i>
Dist. from CG to Rear Contact Patch	b	1.5 <i>m</i>
Moment of Inertia	I_z	3800 <i>kg * m²</i>
Mass Moment of Inertia about x-axis	I_x	1243 <i>kg * m²</i>
Tire Cornering Stiffness per Tire	C_α	60000 <i>N/rad</i>
Stiffness of Front Springs	k_f	72500 <i>N/m</i>
Stiffness of Rear Springs	k_r	67000 <i>N/m</i>
Distance between Front springs	S_{k_f}	0.7747 <i>m</i>
Distance between Rear springs	S_{k_r}	0.9906 <i>m</i>
Distance between Front dampers	S_{b_f}	0.7747 <i>m</i>
Distance between Rear dampers	S_{b_r}	0.762 <i>m</i>
Force from Front Anti-Roll Bar per Tire	F_{ARB_f}	750 <i>N/degree</i>
Force from Rear Anti-Roll Bar per Tire	F_{ARB_r}	550 <i>N/degree</i>

APPENDIX C

ESC CONTROLLER DESCRIPTION

C.1 Stability Threshold Stages

The stability thresholds defined in MATLAB simulations consist of single and two-stage levels. The single stage controllers consist of one preset value of lateral acceleration or yaw rate that limits the acceptable level of the two vehicle properties. Figure C.1 depicts the single stage controller regulations. Once the magnitude of the lateral acceleration or yaw rate exceeds the maximum acceptable level, the controller is applied and stability is improved.

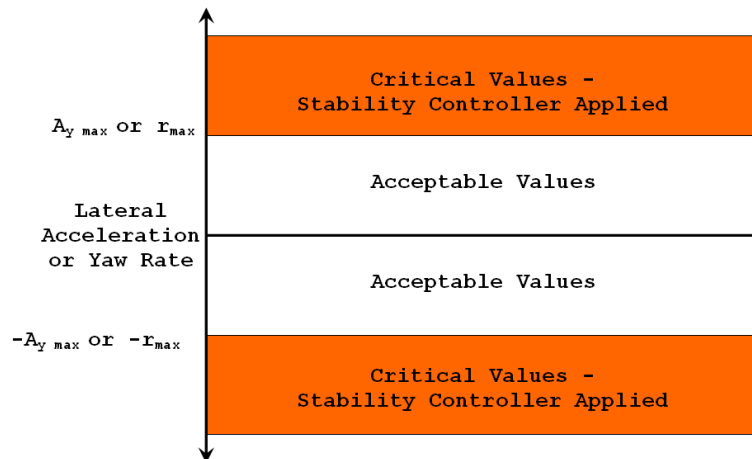


Figure C.1: The single stage controller

The two stage controller has more options. With two predefined levels of lateral acceleration and yaw rate, a “warning” and “critical” level can be established. When the critical level is exceeded, the controller applies the maximum amount of braking torque or steering modification. However, between the warning level and critical level,

there are several options. For example, possible choices for braking levels include a step value, a linear increase from zero or another point, or even a nonlinear increase with increasing values of lateral acceleration or yaw rate. The possibilities of the controller types are endless. Figure C.2 depicts the double stage controller regulations.

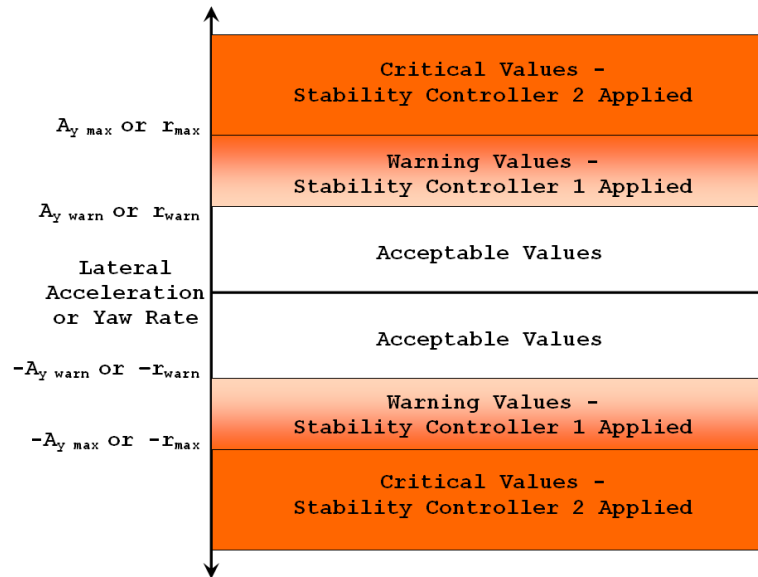


Figure C.2: The two stage controller

C.2 ESC Types and Inputs

The controllers implemented in MATLAB were created to be inserted into the vehicle model described in Chapter 2. All of the controllers modeled had inputs of lateral acceleration and yaw rate. These vehicle properties were used because the measurements are easily measured with an accelerometer and gyroscope, sensors that can be relatively inexpensive to install. The more complex controllers also use measurements of independent wheel velocities and steer angle.

Table C.1 - ESC Types:
Power Reduction
All-Wheel Braking
Independent Wheel Braking
Active Torque Distribution
Steering Modification
Steering Modification with All-Wheel Braking
Independent Wheel Braking with Steering Control

C.3 Power Reduction

With the vehicle modeled in MATLAB, the power reduction controller limits the power applied to the wheels. Since the rolling resistance and air drag were not included in the vehicle model, the power reduction is modeled as a slight braking force. Although the effects of air drag and rolling resistance are not necessarily linear, the assumption is adequate for testing purposes, since the vehicle usually finishes the maneuver before a noticeable velocity change occurs.

The controller works as follows: if the absolute value of the lateral acceleration or yaw rate measured is greater than the preset limit, then the controller adds a slight braking force to all of the wheels. This braking torque was found from previous data with a vehicle performing coast down tests. A linear fit for the deceleration was made, and the braking force (i.e. power reduction) was found by varying the braking forces in simulation until the behavior matched the experimental data.

Figure C.3 shows the braking torques applied for a power reduction controller. For example, when the lateral acceleration exceeded a set limit (0.3 g), the controller simulated a power reduction with a braking torque of 50 N-m.

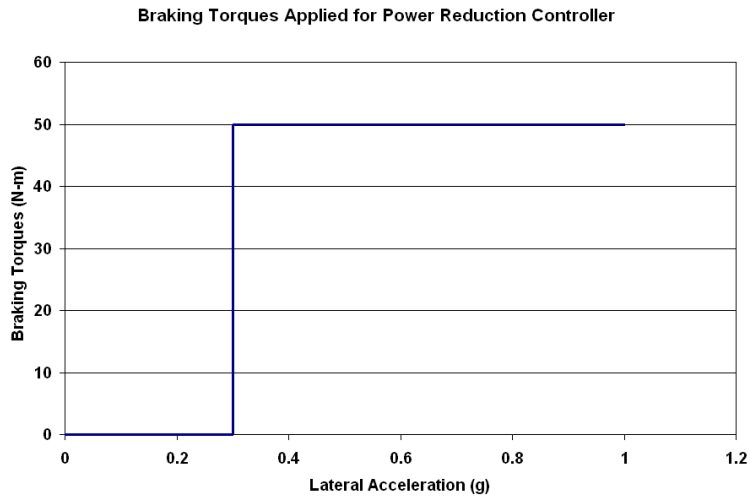


Figure C.3: The braking torques applied to simulate a power reduction

C.4 All-Wheel Braking

The all-wheel braking controller is somewhat similar to the power reduction controller, except for differences in the braking forces applied. Several different options were modeled in MATLAB simulations for the braking forces applied. The constant braking controllers are comprised of single and multi-stage limits, with varying braking forces.

The basic all-wheel controller was almost identical to the step input in the power reduction controller; however, the braking force applied was greater. This not only added the effects of wind and rolling resistance, but it also incorporated an actual braking force on the vehicle.

To further improve the controller's performance, a second stage of the controller was added. By setting two limits of lateral acceleration and yaw rate, the controller can apply different braking torques depending on the threat of stability loss. Figure C.4 shows an example of a multi-stage controller with two limits incorporated. When the

vehicle reaches a warning lateral acceleration (0.3 g), a braking torque of 200 N-m is applied. If the lateral acceleration reaches the second defined value (0.45 g), a maximum braking torque of 450 N-m is applied. This level was once again found using previous test data where hard braking occurred.

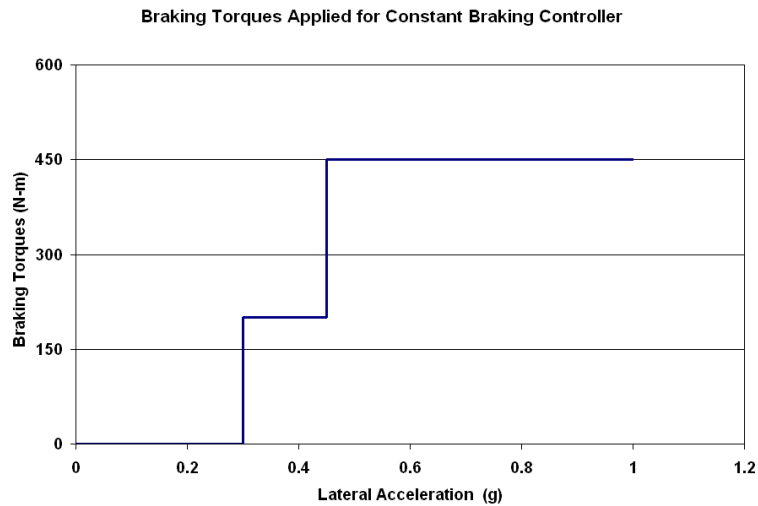


Figure C.4: The braking torques applied to simulate a multi-step braking controller

In order to increase the controller's ability to improve stability, the braking torques can be altered using the values of lateral acceleration. Figure C.5 shows how the variable braking torques can be applied to the all-wheel braking controller. Here the controller applies the 200 N-m braking torque when the lower limit is breached, but once that level is exceeded, the braking torque grows depending on the magnitude of the lateral acceleration of the vehicle. This increase continues until the maximum defined level of lateral acceleration or yaw rate is achieved and the maximum braking torque is applied (450 N-m).

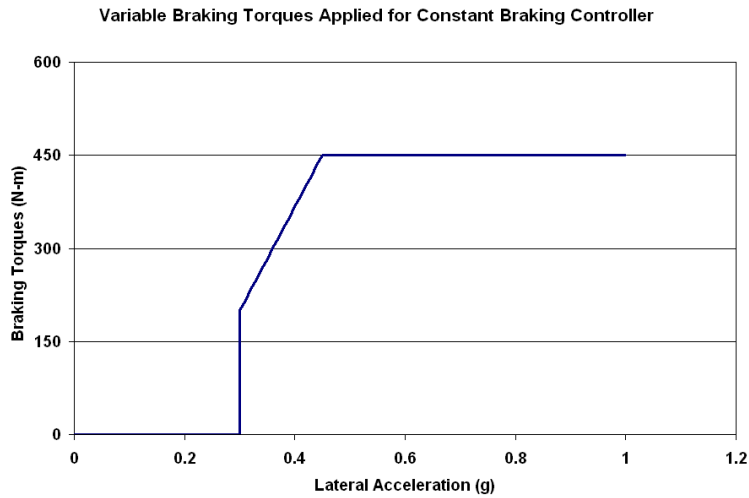


Figure C.5: The braking torques applied to simulate a variable braking controller

C.5 Independent Wheel Braking

The independent wheel braking controller modeled in MATLAB used the variable braking torques shown in Figure C.5; however, the brakes are applied to independent wheels (or sides) of the vehicle. The derivation of the brake steer moment is described in Section 4.7.1. The longitudinal braking forces applied by the wheels are calculated by dividing the braking torque by the tire’s effective radius ($F_x = \tau/R_{eff}$). If this force is greater than the lateral force allowed by the tire model, the maximum lateral force becomes that allowed by the tire model and some sliding occurs.

If the vehicle is understeer ($K_{us} > 0$) and the stability threshold is compromised, braking torques are applied to the inner wheels. In the oversteer case ($K_{us} < 0$), outer wheel braking is applied to increase stability. For the neutral steer case, inner wheel braking is also applied, in order to reduce errors in yaw rate. Figure C.6 shows a vehicle performing the fishhook maneuver with the independent wheel braking controller applied.

When the vehicle exceeds the stability limit, the braking torques are applied to the inner wheels since it is understeer.

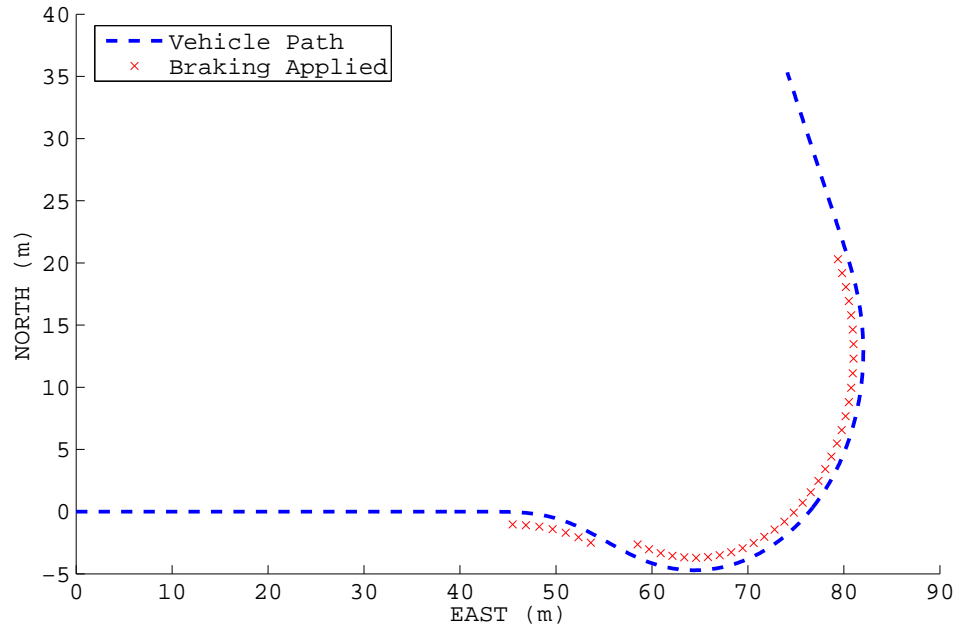


Figure C.6: The fishhook maneuver with braking times with independent wheel braking

C.6 Active Torque Distribution

The active torque distribution controller is similar to the independent wheel braking controller; yet, a positive longitudinal force is applied to the wheels that are not being braked during evasive maneuvers. In the simulations presented in this thesis, the engine torques applied were constant (200 N-m) when the stability threshold was exceeded. This was chosen for simplicity, although the effectiveness of the controller could probably improve with more research and modification.

C.7 Steering Modification

The steering modification controller required a compromise between stability and path following. There is no perfect amount of steering modification allowed by the controller, yet a value must be chosen that reduces the unsafe level of lateral acceleration and yaw rate, while not deviating far from the path.

The controller modeled in MATLAB once again uses a two stage stability threshold. Once the first stability threshold is crossed (past the warning lateral acceleration or yaw rate), the steering controller simply holds the steer angle until the driver's steer angle input is reduced. If the lateral acceleration or yaw rate continues to increase past the second stability threshold, the controller then actively reduces the steer angle by a preset percentage. The setting this percentage was done by trial and error to see what compromise between stability and path deviation is acceptable. Figures C.7 and C.8 show the performance of the steering modification controller when the second stage of the controller reduces the steer angle by 0.1% for each time interval (0.01 sec). The path of the vehicle is close to that of one without the controller, but the stability of the vehicle is compromised.

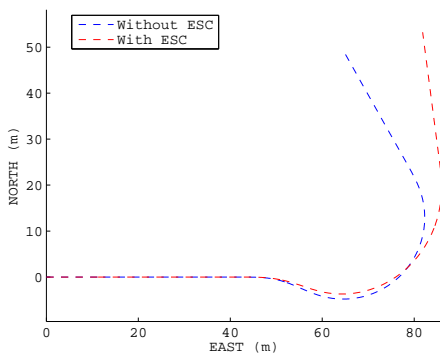


Figure C.7: Position

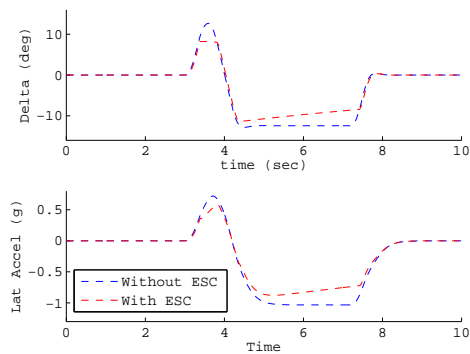


Figure C.8: δ & Lateral Accel.

Figures C.9 and C.10 show the performance of the steering modification controller when the second stage of the controller reduces the steer angle by 0.5% for each time interval (0.01 sec). With this controller output, the stability of the vehicle is more guaranteed, but the vehicle's path is not close to the desired path.

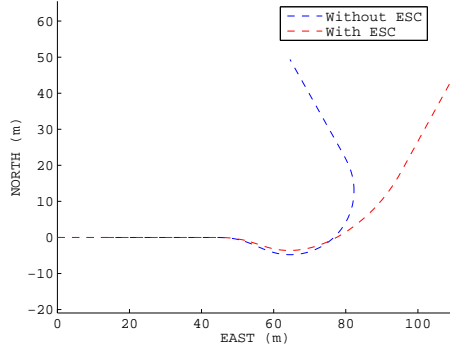


Figure C.9: Position

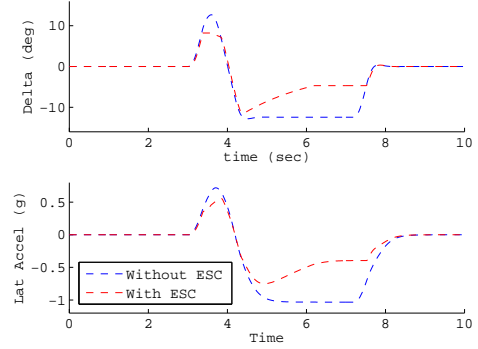


Figure C.10: δ & Lateral Accel.

As seen in the previous figures, the compromise between stability and path following is a difficult one. For the simulations in this thesis, the controller was given a steer angle reduction of 0.3% per time interval once the second stability index was compromised. This value was chosen because it successfully reduces the lateral acceleration and yaw rate of the vehicle while staying somewhat close to the path.

C.8 Steering Modification with All-Wheel Braking

The steering modification with all-wheel braking controller is simply a combination of the two previously-described controllers. Once the first stability threshold is crossed, the steer angle is held constant and a medium brake force is applied on all of the wheels. Similarly, if the second threshold is entered, the vehicle applies a large braking force and the steer angle is reduced by 0.3% per time interval.

The gains of the controller (braking torques and steering modification) could be adjusted to possibly improve the stability of the vehicle, although the all-wheel braking aspect of the controller is somewhat limited, since it does not induce a brake steer moment that can reduce the vehicle's yaw rate error.

C.9 Independent Wheel Braking with Steering Control

The independent wheel braking with steering modification controller is the most complex of the controllers described in this thesis. This controller uses the two-stage stability threshold, similar to the basic independent wheel braking controller; however, if the lateral acceleration and yaw rate are less than the maximum allowed value before the second stability threshold, the controller modifies the steer angle while individually braking particular wheels to slow the vehicle and improve path following. This is made possible with the knowledge of the vehicle's yaw rate, lateral acceleration, velocity, and driver steering input.